

**Physiological characterization of native
mechanotransduction channels in identified sensory
neurons**

Inaugural-Dissertation
to obtain the academic degree
Doctor rerum naturalium (Dr. rer. nat.)
submitted to the Department of Biology, Chemistry, Pharmacy
of Freie Universität Berlin

by
Oscar Sánchez Carranza
from State of Mexico, Mexico

Berlin, 2021

The present work was carried out under the supervision of Prof. Dr. Gary R. Lewin from April 2016 to January 2021 at the Max Delbrück Center for Molecular Medicine in the Helmholtz Association.

1st reviewer: Prof. Dr. Gary R. Lewin

2nd reviewer: Prof. Dr. Oliver Daumke

Date of defense: 15th of June 2021

Declaration of independence

I hereby declare that I have written this thesis independently and have not used any sources or aids than those indicated.

The work has not been submitted in the same or a similar version to any other examination authority.

Place, date

Signature

Table of contents

1.	SUMMARY	1
1.1.	Zusammenfassung.....	3
2.	INTRODUCTION	5
2.1.	Piezo channels.....	5
2.2.	Biophysical properties and modulation of PIEZO channels	8
2.2.1.	Mechanosensitivity and inactivation properties of PIEZO channels.....	9
2.2.2.	Ion selectivity of PIEZO channels	12
2.2.3.	Voltage modulation of PIEZO channels	13
2.2.4.	PIEZO channels are modulated by STOML3	14
2.2.5.	Chemical regulation of PIEZO channels.....	14
2.3.	Sensory mechanotransduction and the role of PIEZO2 in light touch.....	15
2.4.	Mechanotransduction of PIEZO2 in Nociception.....	18
2.5.	Mechanotransduction of PIEZO2 in Proprioception	20
2.6.	Mechanotransduction of PIEZO2 in non-sensory systems.....	21
2.7.	Genetic diseases related to mutations in PIEZO2.....	23
2.7.1.	Loss of function mutations.....	23
2.7.2.	Gain-of-function mutations.....	23
3.	AIMS OF THIS WORK	29
4.	MATERIAL AND METHODS.....	33
4.1.	Molecular biology.....	33
4.1.1.	Preparation of DNA plasmids	33
4.1.2.	Site-directed mutagenesis.....	33
4.2.	Cell culture.....	33
4.2.1.	Cultured cell lines	33
4.2.2.	DRG culture	34
4.2.3.	hiPSCs-CMs culture.....	34

4.3.	Animals.....	35
4.3.1.	Piezo2 ^{R2756H} and Piezo2 ^{R2756K} mice.....	35
4.3.2.	Piezo2 ^{-/-}	35
4.3.3.	Piezo2 ^{CKO}	36
4.4.	Genotyping.....	36
4.5.	Preparation of pillar arrays.....	36
4.6.	Electrophysiology.....	37
4.6.1.	Whole-cell patch clamp.....	37
4.6.2.	High Speed Pressure Clamp.....	38
4.7.	von Frey experiments.....	38
4.8.	Calcium imaging.....	40
4.9.	Statistical analysis.....	40
5.	RESULTS.....	43
5.1.	Characterization of N2a ^{Piezo1^{-/-}} cell line with pillar arrays.....	43
5.2.	Biophysical properties of pathogenic mutations of Piezo2.....	43
5.3.	Voltage sensitivity of mutations related to GS, DA5 and MWS.....	50
5.4.	Physiological characterization of Piezo2 ^{R2756H} and Piezo2 ^{R2756K} mice.....	55
5.5.	Characterization of MA currents in DRG neurons from Piezo2 ^{R2756H} and Piezo2 ^{R2756K} mice.....	57
5.5.1.	Characterization of MA currents in mechanoreceptors from Piezo2 ^{R2756H} and Piezo2 ^{R2756K} mice.....	58
5.5.2.	Characterization of MA currents in nociceptors from Piezo2 ^{R2756H} and Piezo2 ^{R2756K} mice.....	62
5.5.3.	Mechanical nociception in Piezo2 <i>KI</i> mice increases <i>in-vivo</i>	65
5.6.	Native MA currents in DRG neurons from Piezo2 ^{-/-} mice.....	67
5.7.	Native MA currents in DRG neurons from Piezo2 ^{CKO} mice.....	70
5.8.	Modulation of PIEZO channels by the STOML3 protein.....	72
5.9.	Role of PIEZO1 in Cardiomyocytes.....	74
6.	DISCUSSION.....	81

6.1.	Mutations in the R2765 in PIEZO2 are GoF mutations	81
6.2.	<i>KI</i> Piezo2 mice resembles clinical features of DA5, GS and MWS patients.....	83
6.3.	Piezo2 <i>KI</i> DRG neurons are more sensitive to mechanical stimuli.....	84
6.4.	GoF mutations in Piezo2 increase sensitivity to stimulus-evoked pain-like behaviour	86
6.5.	Mechanotransduction in Piezo2 ^{-/-} and Piezo2 ^{CKO} mice.....	87
6.6.	PIEZO channels are sensitized by STOML3 in membrane patches.....	89
6.7.	PIEZO1 is essential for mechanotransduction in hiPSC-CMs	90
7.	CONCLUSIONS.....	93
8.	APPENDIX.....	97
8.1.	List of figures.....	97
8.2.	List of tables.....	101
8.3.	Abbreviations	103
9.	REFERENCES.....	107
10.	ACKNOWLEDGMENTS.....	119

1. Summary

The mechanosensitive PIEZO2 ion channel is involved in touch and pain sensation. Interestingly, in humans, point mutations in the *PIEZO2* gene cause Gordon Syndrome (GS), Distal Arthrogryposis Type 5 (DA5) and Marden-Walker Syndrome (MWS). Patients with these diseases share some clinical features, including congenital contractures of the feet and hands, short stature and scoliosis. However, the biophysical impact of some PIEZO2 mutations, and how they contribute to the observed phenotype, have not been characterized in detail. Using patch-clamp recordings in combination with elastomeric pillar arrays, we show that pathogenic mutations that cause GS, DA5 and/or MWS change the biophysical properties of Piezo2. Recently, we demonstrated that PIEZO channels are also modulated by voltage and have apparent open probabilities of ~10% at physiological membrane potentials. To test if the pathological mutations alter the voltage sensitivity of Piezo2 channels, we generated a stretch-sensitive chimeric channel combining the N-terminal domain of Piezo1 and the pore forming part of Piezo2 and performed tail current protocols with high-speed pressure-clamp (HSPC). We show that these mutations dramatically change the voltage sensitivity of the chimeric channels and thereby increase the apparent open probability. Additionally, two *knock-in* mice carrying the mutations Piezo2^{R2756H} and Piezo2^{R2756K} were generated to study the native mechanically activated (MA) currents from dorsal root ganglia neurons. We observed that in sensory neurons, the mutations R2756H and R2756K cause a sensitization of MA channels, making the neurons more sensitive to respond to lower pillar deflections and change the biophysical properties of the endogenous MA currents. Finally, we carried out von-Frey *in-vivo* experiments and found that pathogenic mutations in Piezo2 make mice more sensitive to stimulus-evoked pain-like behaviour. Our data demonstrates that pathological PIEZO2 mutations are gain-of-function mutations and sensitize the response to nocifensive stimuli.

1.1. Zusammenfassung

Der mechanosensitive Ionenkanal PIEZO2 ist am Tast- und Schmerzempfinden beteiligt. Interessanterweise verursachen Punktmutationen im *PIEZO2*-Gen im Menschen das Gordon-Syndrom (GS), distale Arthrogryposis Typ 5 (DA5) und das Marden-Walker-Syndrom (MWS). Von diesen Krankheiten betroffene Menschen zeigen gemeinsame klinische Merkmale, wie zum Beispiel angeborene Kontrakturen der Hände und Füße, kleinen Wuchs und Skoliose. Nichtsdestotrotz wurden die biophysikalischen Auswirkungen einiger PIEZO2-Mutationen und wie sie zum beobachteten Phänotyp beitragen bisher nicht im Detail untersucht. Mittels Patch-Clamp-Ableitungen in Verbindung mit der elastomerischen Pillar-Array-Technik zeigen wir, dass pathogene Mutationen, welche GS, DA5 und/oder MWS hervorrufen, die biophysikalischen Eigenschaften von Piezo2 verändern. Vor Kurzem haben wir nachgewiesen, dass PIEZO-Kanäle auch durch Spannung gesteuert werden und eine Kanalverfügbarkeit von ~10 % unter physiologischen Membranpotentialen aufweisen. Um zu testen, ob die pathologischen Mutationen die Spannungssensitivität der Piezo2-Kanäle verändern, haben wir einen berührungsempfindlichen, chimärischen Kanal aus der N-terminalen Domäne von Piezo1 und dem porenbildenden Teil von Piezo2 erstellt und diesen mit Tail-Current-Protokollen und der High-Speed-Pressure-Clamp-Technik (HSPC) untersucht. Wir zeigen hier, dass diese Mutationen die Spannungsempfindlichkeit des chimärischen Kanals drastisch verändern und damit die Kanalverfügbarkeit erhöhen. Außerdem haben wir zwei *knock-in*-Mauslinien, die die Mutationen Piezo2^{R2756H} und Piezo2^{R2756K} tragen, erzeugt, um die nativen, mechanisch aktivierten (MA) Ströme in Neuronen aus Spinalganglien zu untersuchen. Wir haben beobachtet, dass die Mutationen R2756H und R2756K in sensorischen Neuronen zu einer Sensibilisierung der MA-Kanäle führen, somit die Neuronen empfindlicher auf feine, mechanische Stimulationen reagieren und die biophysikalischen Eigenschaften der endogenen MA-Ströme verändert werden. Abschließend haben wir von-Frey-Experimente *in vivo* durchgeführt und herausgefunden, dass pathogene Mutationen in Piezo2 Mäuse empfindlicher für mechanischen Schmerz machen. Unsere Daten zeigen, dass pathologische PIEZO2-Mutationen *gain-of-function*-Mutationen sind und die Antwort auf schmerzauslösende Reize verstärken.

2. Introduction

2.1. Piezo channels

Mechanotransduction is the process by which mechanical stimuli are translated into electrical signals. Ion channels play an important role in transforming the physical information into chemolectrical signals because they can sense stimuli within milliseconds (Poole et al., 2014). Although it is well known that mechanically activated (MA) ion channels are essential for mechanotransduction, the identification and characterization of these molecules has been challenging. In 2010, however, two mechanosensitive ion channels were identified: the PIEZO1 and PIEZO2 channels (Bertrand Coste et al., 2010).

PIEZO1 and PIEZO2 (encoded by the *Piezo1/FAM38A* and *Piezo2/FAM38B* genes, respectively) belong to the evolutionary conserved family of mechanosensitive PIEZO ion channels (B. Coste et al., 2010). PIEZO channels are structurally different to any other known proteins and are very large compared to other ion channels (more than 2500 amino acids in human and mouse PIEZO proteins). Recent cryo-electron microscopy (cryo-EM) reconstitutions of mouse Piezo1 and Piezo2 revealed that a functional PIEZO channel is composed of three identical subunits (homotrimeric channel) and each subunit consists of 38 transmembrane domains (TM) (Ge et al., 2015; Guo & MacKinnon, 2017; Saotome et al., 2018; L. Wang et al., 2019; Zhao et al., 2018). Even though the structure of the TMs 1-12 of PIEZO1 was not resolved, sequence analysis suggests that the structure and arrangement is similar to that of PIEZO2.

The homotrimeric channel resembles a three-bladed propeller that in detergent micelles forms a dome shape of 18-24 nm of diameter and 6-9 nm of depth (Guo & MacKinnon, 2017; L. Wang et al., 2019) (**Figure 2.1**). The propeller is constituted of three peripheral blades (TM1-TM36); three intracellular beams that run nearly parallel to the membrane and support the proximal TM25-TM38; the anchor domain, a three-helix wedge that connects TM36 with TM37 and may help to stabilize the integrity of the ion-conducting pore (Zhao et al., 2016); and the central pore module that is formed by a trimer of the outer helix (OH or TM37), the central cap, the inner helix (IH or TM38) and the C-terminal domain (CTD) from all three subunits. The OH and IH are intervened by the Cap, a flexible extracellular domain between the OH and IH that allows the flow of cations and ensures ion conduction by opening the transmembrane gate of the channel (L. Wang et al., 2019; Zhao et al., 2016). The three IH enclose the hydrophobic transmembrane pore which is highly conserved across species (L. Wang et al., 2019; Zhao et al., 2018). The CTD makes the connections between the inner helices and the intracellular side and supports the central axis. All these domains that form the propeller-like channel are crucial for the gating of

the channel. It has been shown that deletion of these domains or point mutations on the different components of the channel result in a loss of mechanosensitivity of the channel, suggesting that the gating of the channel is a complex process in which movement of the domains and interdomain interactions need to be synchronized for a proper mechanical activation.

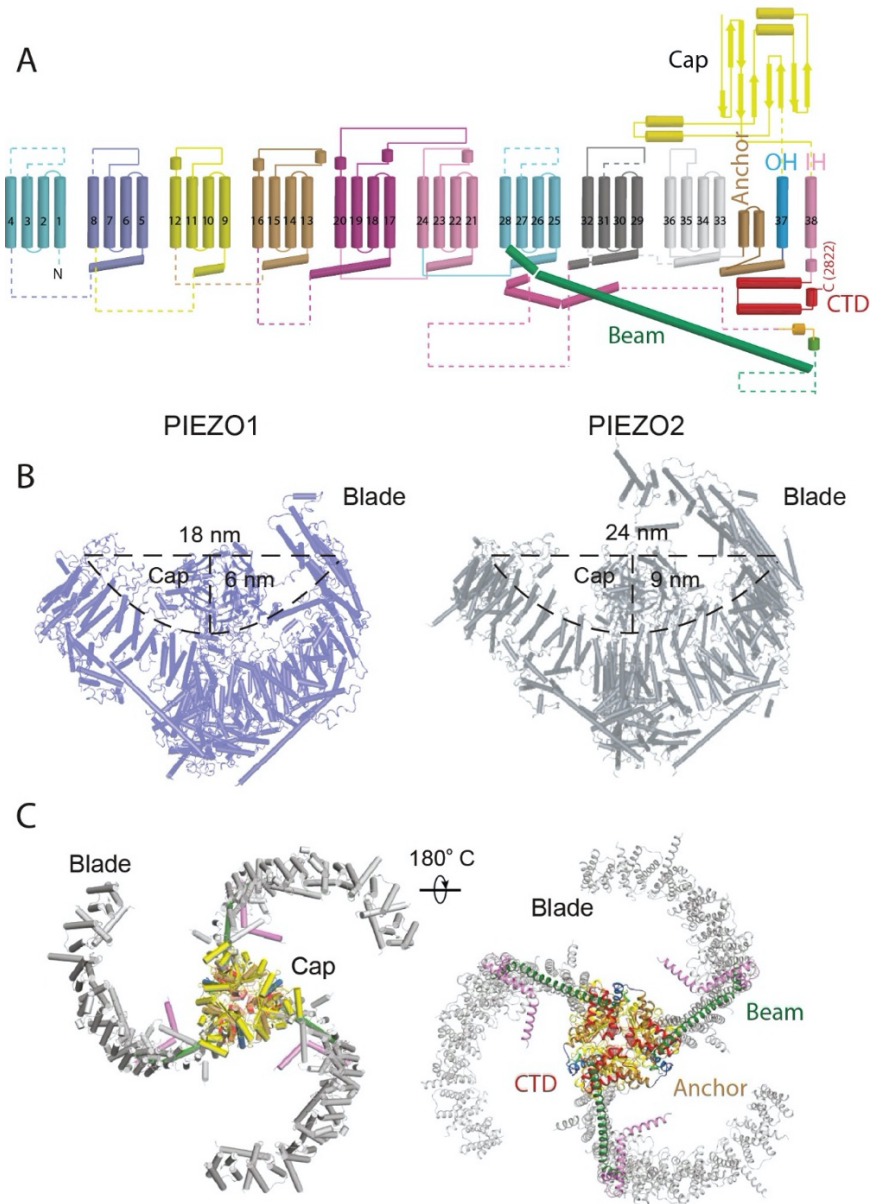


Figure 2.1. Structure of PIEZO channels

A. Topological model of the 38-transmembrane-helix of a PIEZO monomer. Helices are shown as cylinders. Dashed lines indicate the non-resolved regions. The beam, anchor domain, Cap, outer helix (OH), inner helix (IH) and C-terminal domain (CTD) are shown. (Modified from (L. Wang et al., 2019)); **B.** Side view of the homotrimeric model of PIEZO1 (left) (PDB ID: 4RAX, (Guo & MacKinnon, 2017)) and PIEZO2 channels (right) (PDB ID: 6KG7, (L. Wang et al., 2019)). The length and depth of the dome-shape is indicated for both trimeric channels. **C.** Top (left) and bottom (right) views of homotrimeric PIEZO channels. Note the three-bladed propeller shape. The cap domain is shown at the top view. The beam, anchor and CTD can be seen from the bottom view (Modified from (L. Wang et al., 2019)).

The mechanical activation of the trimeric channel leads to inward currents with fast inactivation either in the heterologous system or in the native environment (Coste et al. 2010; Moroni et al. 2018; Poole et al. 2014; Woo et al. 2014, 2015). Deletion of either *piezo1* or *piezo2* in mice results in embryonic or post-natal lethality, respectively (Dubin et al., 2012; Nonomura et al., 2017; Ranade, Qiu, et al., 2014), demonstrating their essential biological function. Even though the channels share some structural and biophysical properties, the understanding of the expression and their contribution to biological processes is still in progress. To date, it is known that PIEZO1 is highly expressed in red blood cells, lung, bladder and pancreas, while PIEZO2 was found to be expressed in dorsal root ganglia (DRG) neurons, skin, bladder and lung. Thus, PIEZO channels play multiple roles in different organs.

The mechanosensitive PIEZO1 channel plays an important role in sensing mechanical forces in blood flow and is required for the development of the cardiovascular and lymphatic systems (J. Li, Hou, Tumova, Muraki, Bruns, Ludlow, Sedo, Hyman, Mckeown, et al., 2014; Lukacs et al., 2015; Ranade, Qiu, et al., 2014), red blood cells homeostasis (Cahalan et al., 2015; Zarychanski et al., 2012), blood pressure (Zeng et al., 2018), smooth muscle cells (Retailleau et al., 2015), chondrocytes (Servin-Vences et al., 2017), neural differentiation (Pathak et al., 2014) and bone formation (Sun et al., 2019; Zhou et al., 2020). Additionally, loss-of-function (LoF) or gain-of-function (GoF) mutations in PIEZO1 in humans lead to xerocytosis and lymphatic dysplasia (Albuisson et al., 2013; Andolfo et al., 2013; Bae et al., 2013; Lukacs et al., 2015; Zarychanski et al., 2012). GoF mutations in PIEZO1 increase the sensitivity of the channel to mechanical stimuli (Bae et al., 2013), slow inactivation resulting in an increase of calcium permeation (Albuisson et al., 2013; Bae et al., 2013; S. Ma et al., 2018; Zarychanski et al., 2012) and modulate the voltage sensitivity increasing the apparent channel availability (Moroni et al., 2018).

PIEZO2 is expressed in DRG neurons (B. Coste et al., 2010) and is important for sensing fine touch and pain in humans and mice (Maksimovic et al., 2014; Murthy, Loud, et al., 2018; Poole et al., 2014; Szczot et al., 2018; S. Woo, Ranade, et al., 2014) as well as proprioception (Assaraf et al., 2020; Chesler et al., 2016; Florez-Paz et al., 2016; Haliloglu et al., 2017; Mahmud et al., 2017; S.-H. Woo et al., 2015). Piezo2 is expressed in airway-innervating sensory neurons and is involved in the regulation of respiration in mice (Nonomura et al., 2017), urination (Marshall et al., 2020) and, in synergy with Piezo1, is essential for bone formation (Zhou et al., 2020). PIEZO2 LoF mutations in humans (*see below; section 2.7*) result in somatosensory and proprioceptive deficits, congenital contractures and scoliosis (Chesler et al., 2016; Delle Vedove et al., 2016; Haliloglu et al., 2017; Mahmud et al., 2017; Yamaguchi et al., 2019). To date, there is only one study that shows that mutations in PIEZO2 (I802F and del2727E) are GoF mutations that result

in Distal Arthrogryposis Type 5 (DA5) and perhaps musculoskeletal pain (B. Coste et al., 2013). Other missense mutations in PIEZO2 are considered to be (putative) GoF mutations, however the biophysical properties and consequences of these mutations have not been investigated (Alisch et al., 2016; S. Li et al., 2018; Mcmillin et al., 2014; Okubo et al., 2015; Zapata-Aldana et al., 2019).

2.2. Biophysical properties and modulation of PIEZO channels

The mechanical activation and biophysical properties of PIEZO channels including inactivation properties, voltage modulation, pore properties and regulatory proteins have been intensely studied in the last decade. Different methods compatible with patch-clamp recordings, such as high-speed pressure clamp (HSPC), indentation and pillar arrays techniques have been developed to study the biophysical properties of MA ion channels, including PIEZO proteins (**Figure 2.2**). HSPC consists of applying reproducible pressure stimuli either to a single patch of membrane in the outside-out or inside-out patch-clamp configuration or to the whole cell (cell attached patch-clamp configuration) (**Figure 2.2A**). The indentation technique uses a piezoelectric-driven blunt glass pipette that “pokes” the membrane of cells. MA currents are studied during whole-cell recordings and mechanosensitive currents can be recorded at relatively large deflection (~ 500 nm – ~ 10 μ m) (**Figure 2.2B**). The pillar arrays technique uses elastomeric pili that are deflected with a controlled piezoelectric device and applies local mechanical displacement. Similar to the indentation technique, the pillar arrays method allows the study of mechanosensitive ion channels during whole-cell recordings, but requires smaller deflections (down to ~ 10 nm) to activate MA currents (**Figure 2.2C**). (Poole et al., 2014, 2015; Ranade et al., 2015; Wu et al., 2016).

In 2010, Coste *et al.* showed that MA currents from a mouse neuroblastoma cell line (N2a cells) and mouse DRG neurons are mediated by mouse Piezo1 and Piezo2 (mPiezo1 and mPiezo2), respectively (B. Coste et al., 2010). They found that both proteins are non-selective cationic channels and that MA currents were sensitive to ruthenium red and gadolinium when applied extracellularly and stimulating the cells with a glass probe (indentation technique). Additionally they showed that both channels display rapidly adapting currents in heterologous systems and that Piezo2 is required for fast inactivating currents in DRG neurons (B. Coste et al., 2010). Later on, when characterizing the biophysical properties of PIEZO1 from *Homo sapiens* (*H. sapiens*, hPIEZO1), *Dario rerio* (*D. rerio*, DrPiezo1) and *Drosophila melanogaster* (*D. melanogaster*, DmPiezo1), it was found that the mechanosensitivity of PIEZO channels is conserved in humans,

non-mammalian vertebrates and invertebrates (Bertrand Coste et al., 2012; Moroni et al., 2018) (Table 2.1).

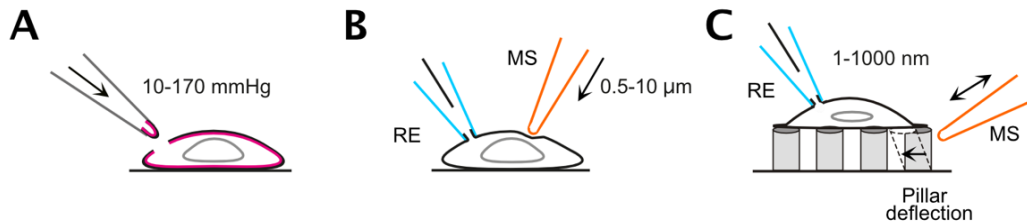


Figure 2.2. Mechanotransduction techniques

Cartoons of HSPC in the outside-out configuration (A), indentation (B) and pillar arrays (C) methods used to study MA ion channels. Note that for the indentation and pillar arrays assays, patch clamp recordings are made in the whole cell configuration. RE, recording electrode; MS, mechanical stimulator. Modified from (Servin-Vences et al., 2017)

2.2.1. Mechanosensitivity and inactivation properties of PIEZO channels

Consistent with their different physiological roles, PIEZO channels are activated differently by mechanical stimuli and have different biophysical properties. In contrast to PIEZO1, PIEZO2 is poorly gated by membrane stretch, whereas both channels are equally responsive to membrane indentation and to substrate deflection (Moroni et al., 2018; Poole et al., 2014; L. Wang et al., 2019). Moreover, PIEZO1 channels inactivate more slowly than PIEZO2 (Table 2.1, 2.3).

Recent studies suggested that differences in stretch-sensitivity and inactivation properties relied on the N-terminal (including TM1-TM36 and anchor domains) and C-terminal regions (including the OH, Cap, IH and C-terminal domains) of PIEZO channels, respectively. When fusing the N-terminal region of mPiezo1 with the C-terminal region of the poorly stretch-sensitive mPiezo2 (mP1/mP2 channel), it was found that the chimeric channel was newly stretch-sensitive. The mP1/mP2 channel showed stretch-gated currents with inactivation kinetics similar to those observed when overexpressing PIEZO2 in a heterologous system and slower kinetics compared to PIEZO1 inactivation (Moroni et al., 2018). Moreover, when deleting the extracellular loops between TM15-16 and TM19-20 of PIEZO1, it was found that mutant channels lost most of their mechanosensitive properties. Similar results were found when mutating L1342 and L1345 (located in the beam domain) in PIEZO1 (Zhao et al., 2018). Thus, it had been concluded that the stretch or mechanical sensitivity of PIEZO channels is transmitted by the N-terminal region of the channel and the inactivation properties were governed by the pore region.

Research from different groups has tried to dissect the N-terminal and C-terminal regions to determine which residues regulate the biophysical properties of PIEZO channels. As mentioned above, PIEZO channels are involved in different biological processes and this knowledge has come up, in part, by the discovery of human disorders related to these channels. Interestingly, in 2013, two studies showed that mutations in PIEZO1 and PIEZO2 channels lead to hereditary xerocytosis (HX) and distal arthrogyrosis type 5 (DA5), respectively (Bae et al., 2013; B. Coste et al., 2013). HX is an autosomal dominant disease that causes dehydration of red blood cells and results in haemolytic anaemia (Bae et al., 2013; Zarychanski et al., 2012). DA5 is an autosomal dominant human disorder characterized by distal limb contractures, ptosis and in some cases lung disease (B. Coste et al., 2013; Mcmillin et al., 2014). In both studies it was shown that mutations causing HX and DA5 are gain of function mutations and change the biophysical properties of the channels.

Bae et al. (2013) found that M2225R and R2456H mutations in hPIEZO1 cause HX (Bae et al., 2013). Intriguingly, M2225 sits in the Cap domain, while R2456 is in the IH of the channel (Guo & MacKinnon, 2017; Saotome et al., 2018). Both mutants showed slower inactivation kinetics and mutants R2456H and R2456K (an artificial mutation included in this study) had decreased sensitivity to pressure pulses in a heterologous system (**Table 2.1**). Additionally, hPIEZO1 mutants displayed a pronounced latency to activation in the presence of pressure stimuli (Bae et al., 2013). By recording single channel activity directly in red blood cells from a patient with the mutation R2456H, it was found that this mutation increases the channel open probability at -50 mV (even in the absence of mechanical stimuli) compared to erythrocytes from healthy patients, where spontaneous ion-channel activity was not detected (Andolfo et al., 2013).

Table 2.1. Biophysical properties of PIEZO1 channels.

nd, not determined; RA, rapidly adapting; IA, intermediate adapting; SA, slowly adapting currents.

	(B. Coste et al., 2010)	(Bertrand Coste et al., 2012)	(Bae et al., 2013)	(Albuisson et al., 2013)	(Poole et al., 2014)	(Moroni et al., 2018)
Species	Mouse	Fly	Human	Human	Mouse	Zebra fish
τ_{inact} (ms)	15.3 ± 1.6	6.2 ± 0.3	~ 16	8.6 ± 0.4	RA: 2.3 ± 0.4 IA: 16 ± 2.2 SA: nd	~ 350
Conductance (pS)	22.9 ± 1.4	3.3 ± 0.3	nd	nd	nd	nd
E_{rev} (mV)	~ 6	~ 0	nd	7.2	nd	~ 0
P_{50} (mmHg)	28.1 ± 2.8	31.2 ± 2.8	43 ± 0.7	nd	nd	51.0 ± 2.7
Method	HSPC and indentation	HSPC and indentation	HSPC and indentation	Indentation	Pillar arrays	HSPC
Cell system	N2a cells	HEK293T	HEK293T	HEK293T	HEK293	N2a ^{Piez1^{-/-}} cells

Table 2.2. Biophysical properties of PIEZO1 mutants related to human diseases
nd, not determined. E2496ELE indicates a duplication of leucine (L) 2495 and glutamate (E) 2496.

	<i>(Bae et al., 2013)</i>	<i>(Bae et al., 2013)</i>	<i>(Bae et al., 2013)</i>	<i>(Albuisson et al., 2013)</i>			
Species	Human	Human	Human	Human	Human	Human	Human
Mutation	M2225R	R2456H	R2456K (artificial)	R1358P	A2020T	T2127M	E2496ELE
Structural domain	Cap domain	IH	IH	Beam	TM34	Anchor domain	CTD
τ_{inact} (ms)	~ 20	~ 50	~ 150	13.8 ± 1.5	12.2 ± 0.5	11 ± 0.7	15 ± 1.1
E_{rev} (mV)	nd	nd	nd	3	6.8	6	5.4
P_{50} (mmHg)	45 ± 0.6	30 ± 0.6	35 ± 1.1	nd	nd	nd	nd
Method	HSPC and indentation	HSPC and indentation	HSPC and indentation	Indentation	Indentation	Indentation	Indentation
Cell system	HEK293T	HEK293T	HEK293T	HEK293T	HEK293T	HEK293T	HEK293T

The mutations I802F and E2727del (deletion of the residue E2727) in hPIEZO2 lead to DA5 (B. Coste et al., 2013). I802 is located in TM16 while E2727 is found in the CTD (L. Wang et al., 2019). Similar to what has been observed in hPIEZO1 mutants, the E2727del mutant displayed slower inactivation kinetics, while I802 showed similar inactivation properties to wildtype hPIEZO2 (Table 2.4) (B. Coste et al., 2013).

Taking these observations from PIEZO mutants together, it was assumed that the N-terminal region was responsible for efficient stretch-sensitivity and that the C-terminal region (including the cap, IH and CTD) of the channel plays a crucial role in maintaining inactivation, latency and deactivation properties of PIEZO channels. However, recent studies showed that mechanosensitivity and inactivation kinetics are not governed only by residues in the N- or C-terminal region, respectively.

Table 2.3. Biophysical properties of PIEZO2 channels
nd, not determined; RA, rapidly adapting; IA, intermediate adapting; SA, slowly adapting currents.

	<i>(B. Coste et al., 2010)</i>	<i>(B. Coste et al., 2013)</i>	<i>(Eijkelkamp et al., 2013)</i>	<i>(Poole et al., 2014)</i>	<i>(Taberner et al., 2019)</i>
Species	Mouse	Human	Human	Mouse	Mouse
τ_{inact} (ms)	6.8 ± 0.7	6.2 ± 0.6	4.4 ± 0.8	RA: 1.2 ± 0.4 IA: 29 ± 10 SA: nd	2.8 ± 0.1
E_{rev} (mV)	6.3 ± 0.4	~ 0	9.7 ± 1.6	nd	11.9 ± 1.2
Method	Indentation	Indentation	Indentation	Pillar arrays	Indentation
Cell system	N2a cells	HEK293T	HEK293T	HEK293	N2a ^{Piezol^{-/-}} cells

Table 2.4. Biophysical properties of PIEZO2 mutants related to human diseases

	(B. Coste <i>et al.</i> , 2013)	(B. Coste <i>et al.</i> , 2013)
Species	Human	Human
Mutation	I802F	E2727del
Structural domain	TM16	CTD
τ_{inact} (ms)	~ 6	~ 20
E_{rev} (mV)	~ 0	~ 0
Method	Indentation	Indentation
Cell system	HEK293T	HEK293T

When deleting the Cap region of PIEZO channels completely or partially, it was found that both PIEZO1 or PIEZO2 showed completely abolished mechanosensitivity (L. Wang *et al.*, 2019). A similar effect was observed when mutating P2536 and E2537 residues (located in the CTD) of mPiezo1, where MA currents were substantially reduced (Zheng, Gracheva, *et al.*, 2019). Moreover, in 2013, Albuissou *et al.* showed that R1358P, A2020T and T2121M mutations in PIEZO1 (located in the beam domain, TM34 and anchor domain, respectively and all in the N-terminal region) displayed slower inactivation kinetics (Albuissou *et al.*, 2013) (**Table 2.2**). Interestingly, when mutating residues that form beam-CTD or IH-CTD interactions in PIEZO2 (interdomain-interactions), it was found that mutant channels displayed higher mechanical thresholds when stimulating with the indentation technique, but showed similar inactivation kinetics (Taberner *et al.*, 2019). Thus, these results showed that mechanotransduction properties and inactivation kinetics are ruled by different residues located in the N- and C-terminal regions.

2.2.2. Ion selectivity of PIEZO channels

Recently, based on cryo-EM structures and functional analysis, it was shown that truncated Piezo1 channels that contained only the C-terminal region recapitulates single channels permeation of the full-length channel (Nosyreva *et al.*, 2020). Thus, it is established that the C-terminal region that includes the OH, CAP, IH and CTD trimerizes to form the central pore module (Zhao *et al.*, 2016, 2018) (**Figure 2.3**).

The IH forms the transmembrane pore of PIEZO channels. Interestingly, in PIEZO1, IH lacks negatively charged residues, while in PIEZO2, E2757 is the only negatively charged residue (L. Wang *et al.*, 2019; Zhao *et al.*, 2018). E2757 in PIEZO2 controls ion-permeation properties. When neutralizing E2757 to Alanine (E2757), PIEZO2 channels exhibited a reduction of ~50% in the permeability to Ca^{2+} relative to Cs^{+} and decreased single-channel conductance of about 30%, compared to wild type channels (L. Wang *et al.*, 2019).

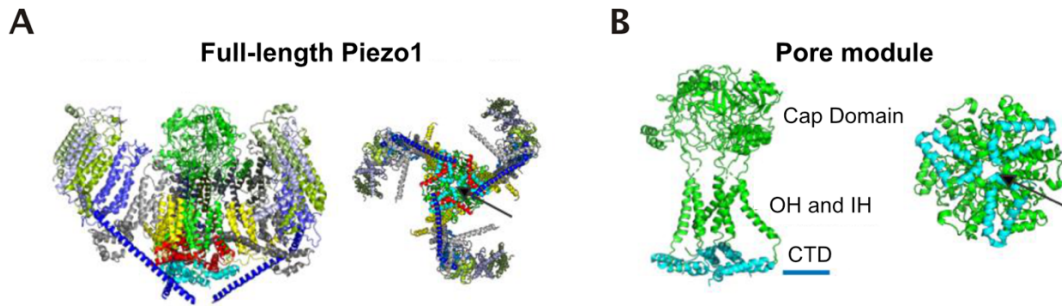


Figure 2.3. Pore module of Piezo1

Cryo-EM structure of full-length Piezo1 (A) and pore module (B). Side (*left*) and intracellular views (*right*) are shown for both structures. Structural organization of PIEZO2 channels is similar according to available cryo-EM data (L. Wang et al., 2019). Modified from (Nosyreva et al., 2020).

Additionally, residues E2769 and E2770 of PIEZO2 (E2495 and E2496 of PIEZO1) that form an IH-CTD linker, form a negatively charged environment that controls ion conduction. Neutralization of these residues by Alanine resulted in reduced MA currents and changed the reverse potential of the channel, indicating alterations of ion selectivity. (Zhao et al., 2016) Thus, residues in the IH and IH-CTD linker, are crucial for the ion-conduction pathway.

2.2.3. Voltage modulation of PIEZO channels

Similar to different stretch-activated ion channels, PIEZO channels are voltage modulated (Bockenhauer et al., 2001; Maingret et al., 2002; Martinac et al., 1987; Moroni et al., 2018; Schewe et al., 2016). PIEZO channels are non-selective cationic ion channels that display outward rectification and fast inactivation properties at negative potentials. Strikingly, inactivation of mammalian PIEZO channels is voltage dependent, the channels display slower or non-inactivation at positive holding voltages than at negative voltages. (B. Coste et al., 2010, 2013; Eijkelkamp et al., 2013; Moroni et al., 2018; Wu et al., 2017). However, Piezo channels from *D. rerio* and *D. melanogaster* show none or weak inactivation both at negative or positive voltages (Moroni et al., 2018).

When dissecting the voltage dependence of the inactivation of PIEZO channels, it was claimed that a single lysine located in the IH of mPiezo1 (K2479) is necessary to confer this biophysical property (Wu et al., 2017). However, even though this lysine is conserved among hPIEZO1, mPiezo2, hPIEZO2 and DrPiezo1, it is not conserved in DmPiezo1 (**Figure 2.4**). Thus, discrepancies in voltage dependence of the inactivation kinetics and evolutionary analysis indicate that there should be more residues involved in regulating this biophysical property of PIEZO channels.

		IH																				
hPiezo1	2439	I	M	G	L	Y	V	S	I	V	L	V	I	G	K	F	V	R	G	F	F	S
mPiezo1	2466	I	V	G	L	Y	V	S	I	V	L	V	V	G	K	F	V	R	G	F	F	S
hPiezo2	2670	I	M	G	L	Y	A	S	V	V	L	V	I	G	K	F	V	R	E	E	F	S
mPiezo2	2740	I	M	G	L	Y	A	S	V	V	L	V	I	G	K	F	V	R	E	E	F	S
DrPiezo1	2455	I	M	G	L	Y	V	S	V	V	L	V	I	G	K	F	V	R	G	F	F	S
DmPiezo1	2437	I	I	G	L	Y	T	T	F	V	L	L	A	S	R	E	M	K	S	E	I	G

Figure 2.4. Sequence comparison between IH of PIEZO channels

Residues forming the IH of PIEZO channels. In the red square is shown the conserved Lysine in human and mouse Piezo1 and Piezo2, and in DrPiezo1. Note that the Lysine in DmPiezo1 is not conserved. Amino acid alignment was done using ESPrnt 3.0 (Robert & Gouet, 2014).

In addition to the voltage dependence of inactivation, the open probability of PIEZO channels is regulated by voltage. Recently, it was found that depolarized voltages increase the apparent open probability of PIEZO channels. Moreover, the voltage modulation of PIEZO1 is altered in GoF mutations related to HX (when testing the homologous mutations in the mPiezo1 channel). Mutations that cause HX in humans, increase the open probability of PIEZO1 up to ~7 fold and shift the gating of the channel to more depolarized voltages. (Moroni et al., 2018). All these observations indicate that PIEZO channels are strongly regulated by voltage, a crucial property that could play a role to their physiological function in different mechanosensory systems.

2.2.4. PIEZO channels are modulated by STOML3

PIEZO channels can be modulated by other transmembrane proteins such as stomatin-like protein 3 (STOML3). STOML3 is an integral membrane protein that modulates mechanosensation of PIEZO channels by increasing their sensitivity to mechanical stimuli and preventing desensitization of PIEZO channels to repeated mechanical stimuli (Poole et al., 2014; Qi et al., 2015). Stoml3 protein is highly expressed in DRG neurons and increases the stiffness of the plasma membrane through recruiting cholesterol which facilitates the gating of Piezo2 channels (Qi et al., 2015; Wetzel et al., 2007). Interestingly, about 65% of sensory neurons from global *knockout* mice lacking Stoml3 (*Stoml3^{-/-}*) lost poking induced MA currents (Qi et al., 2015; Wetzel et al., 2007). Thus, the current picture is that Stoml3 sensitize PIEZO channels perhaps by controlling membrane stiffness around the channel protein.

2.2.5. Chemical regulation of PIEZO channels

Chemical regulation of ion channels has been crucial to study their role in physiology. To date, it is known that Yoda1 specifically modulates PIEZO1, but not PIEZO2. Yoda1 induces Ca^{2+} influx in cells expressing PIEZO1 channels. When analysing the effect of Yoda1 on PIEZO1 currents (using patch-clamp methods) it was found that Yoda1 increases the open probability of

the channels and the mechanical threshold for gating (Syeda et al., 2015). Yoda1 has become a valuable tool to investigate the contribution of PIEZO1 channels in different biological processes (Cahalan et al., 2015; Chubinskiy-Nadezhdin et al., 2019; Davies et al., 2019; Lai et al., 2020).

2.3. Sensory mechanotransduction and the role of PIEZO2 in light touch

The skin is equipped with specialized mechanoreceptors that allow animals to detect and perceive tactile stimuli down to nanometer-scale movements (Poole et al., 2014, 2015). Skin movement (e.g., stretching or indentation) is transformed into electrical signals (mechanotransduction) via the gating of mechanically-activated (MA) ion channels at mechanoreceptor terminals (Lechner & Lewin, 2013). Mechanotransduction of innocuous touch in the skin primarily occurs in sensory neurons that have their cell bodies in the dorsal root ganglia (DRG) and cutaneous end-organs such as Merkel cells and Meissner's corpuscles (Abraira & Ginty, 2013; K. O. Johnson, 2001; Lewin & Moshourab, 2004). The mechanoreceptor afferent neurons have pseudounipolar axons that innervate almost all organs of the body (Poole et al., 2015), including Merkel cells and Meissner's corpuscles, as well as hair follicles (**Figure 2.5**) (Abraira & Ginty, 2013; K. O. Johnson, 2001; Lechner & Lewin, 2013).

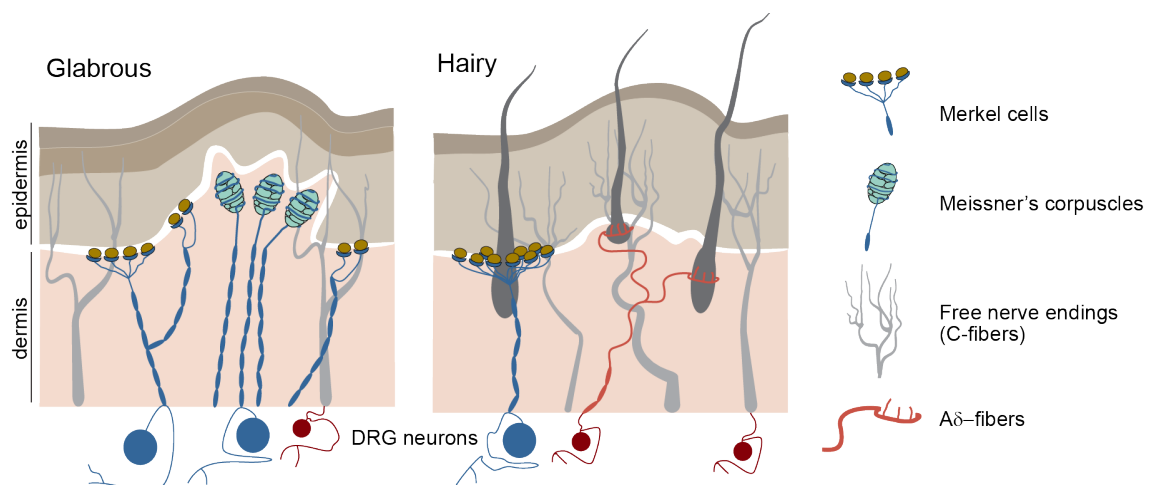


Figure 2.5. Mechanotransduction in mammalian skin

In glabrous skin (right), mechanotransduction of innocuous touch is mediated by large size DRG neurons (blue DRG neurons) and end organs such as Merkel cells and Meissner's corpuscles. Merkel cell-neurites complex is located in the basal layer of the epidermis. Meissner's corpuscles are situated in the dermis. Noxious touch is detected in glabrous skin by free nerve endings (C-fibers). In hairy skin (left), light touch is also detected by Merkel cells. Noxious responses are sensed by C- and A δ -fibers.

Mechanosensitive channels form the machinery of mechanotransduction in the somatic sensory neurons that sense touch and pain (Poole et al., 2015). Recently, there has been significant progress in identifying MA channels in vertebrates that are involved in mechanotransduction in the somatosensory system and non-sensory systems (Beaulieu-Laroche et al., 2020; B. Coste et

al., 2010; Jia et al., 2020; Murthy, Dubin, et al., 2018; Patkunarajah et al., 2020; Servin-Vences et al., 2017).

PIEZO2 channels are expressed in a large subset of DRG neurons and transduce mechanical stimuli into MA currents (B. Coste et al., 2010). In the skin, PIEZO2 is localised at the nerve terminals of sensory neurons that innervate hairy and glabrous skin. Additionally, Piezo2 is expressed in non-neuronal Merkel cells in both hairy and glabrous skin (**Figure 2.6**). (Abraira & Ginty, 2013; García-Mesa et al., 2017; Ikeda et al., 2014; K. O. Johnson, 2001; Maksimovic et al., 2014; Ranade, Woo, et al., 2014; S. Woo, Ranade, et al., 2014).

Merkel cells are innervated by A β slowly adapting type 1 afferents (SA1) that, when mechanically activated by small amplitude ramp and hold stimuli, show a dynamic phase characterised by a high-frequency firing at the beginning of the stimulus, and a static phase characterised by sustained firing with variable intervals between spikes during the hold phase (Abraira & Ginty, 2013; K. O. Johnson, 2001; Kenneth O. Johnson et al., 2000; Maksimovic et al., 2014). Interestingly, in 2013 and 2014 two independent groups showed that both Merkel cells and SA1 afferents contribute to light touch where Piezo2 plays a crucial role, but contribute differently to the biphasic responses previously described in SA1 responses (Ikeda et al., 2014; Maksimovic et al., 2014; Ranade, Woo, et al., 2014; S. Woo, Ranade, et al., 2014).

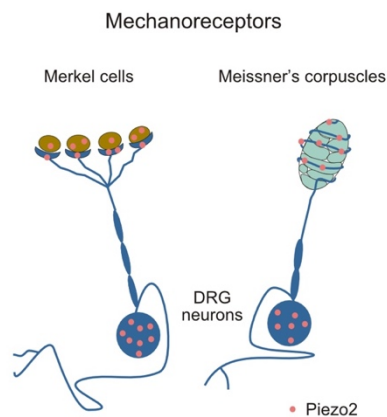


Figure 2.6. Expression of PIEZO2 in mechanoreceptors

Cartoon representation of Merkel cells- and Meissner's corpuscles-neuron complexes. The expression of PIEZO2 is shown in pink dots.

Merkel cells are intrinsically mechanosensitive and displayed rapidly adapting mechanosensitive currents when stimulated directly *in-situ* in hair follicles from rats (Ikeda et al., 2014) and directly *in-vivo* in isolated cells from mice (Maksimovic et al., 2014; S. Woo, Ranade, et al., 2014). With genetic tools it was shown that MA currents in Merkel cells in rodents were Piezo2-dependent

(Ikeda et al., 2014; Maksimovic et al., 2014; S. Woo, Ranade, et al., 2014). Additionally, genetically modified mice lacking Merkel cells in the epidermis, showed truncated SA1 firing during the static phase when recording touch-dome afferents, showing longer variable intervals between spikes that were completely abolished during a sustained mechanical stimulus (Maksimovic et al., 2014). A similar effect was observed in touch-dome afferents when deleting *piezo2* in intact epidermal tissue (Maksimovic et al., 2014). Thus, Merkel cells are mechanotransducers that tune SA1 responses of A β sensory fibers and contribute to keep sustained responses and high frequency firing in a Piezo2-dependent way.

By carrying out *ex-vivo* skin nerve recordings from hairy skin in mice where *piezo2* was specifically deleted in sensory neurons (Piezo2^{CKO}), Ranade *et al.* (2014) observed that deletion of *piezo2* resulted in the loss of mechanosensitivity in around 50% of A β fibers (Ranade, Woo, et al., 2014). Additionally, they showed that the dynamic and static phases of SA1 fibers recorded from Piezo2^{CKO} mice were almost abolished (Ranade, Woo, et al., 2014). These findings suggested that Piezo2 mediates mechanosensitivity to DRG neurons in *ex vivo* preparations and contributes to the biphasic SA1 responses of A β sensory fibers. *In vivo* von Frey experiments in Piezo2^{CKO} showed that these animals had an increased threshold in paw withdrawal to innocuous stimuli compared to wildtype mice, supporting a role for Piezo2 in touch sensation (Ranade, Woo, et al., 2014).

The current model is that Piezo2 is required for the Merkel cell-neurite complex in skin that encodes high spatial resolutions to sense curvatures, textures and edges and light touch (Ikeda et al., 2014; K. O. Johnson, 2001; Kenneth O. Johnson et al., 2000; Maksimovic et al., 2014; Ranade, Woo, et al., 2014; S. Woo, Lumpkin, et al., 2014; S. Woo, Ranade, et al., 2014). However, the fact that not all responses in SA1 fibers were abolished in Piezo2^{CKO} animals suggests that there must be other ion channels that are crucial for sensory mechanotransduction.

Meissner's corpuscles are also involved in light touch, and some evidence indicates that Piezo2 might also be involved in mechanotransduction in these end organs (Ranade, Woo, et al., 2014). Meissner's corpuscles are innervated by A β rapidly adapting type I afferents (RA1). RA1 afferents are more sensitive to dynamic skin deformation than SA1 but are insensitive to static stimuli (Abraira & Ginty, 2013; K. O. Johnson, 2001). RA fibers are important for giving feedback signals about movement of objects in contact with the hand. Thus, RA1 afferents play a role in sensing gentle force and providing a fine sensorimotor control. (Abraira & Ginty, 2013; K. O. Johnson, 2001; Neubarth et al., 2020). Interestingly, Piezo2 is also expressed in the afferents that innervate

Meissner's corpuscles in glabrous skin (García-Mesa et al., 2017; Ranade, Woo, et al., 2014), however the contribution of Piezo2 to RA1 firing activity has not been characterized in detail.

In humans, LoF mutations in PIEZO2 resulted in loss of touch sensation in patients (Chesler et al., 2016; Delle Vedove et al., 2016; Haliloglu et al., 2017; Mahmud et al., 2017; Yamaguchi et al., 2019). When quantified, it was observed that patients with LoF mutations in PIEZO2 had reduced sensitivity to vibration stimuli in glabrous and hairy skin (Chesler et al., 2016). However some patients showed normal vibration senses (Haliloglu et al., 2017). Additionally, two patients showed diminished sensory nerve conductance velocities (37 ms^{-1}) related to A β fibers (Delle Vedove et al., 2016). When comparing punctate-touch detection, in some patients a doubling of the threshold for sensing mechanical stimuli was observed in glabrous skin compared to control individuals, but not in hairy skin (Chesler et al., 2016; Szczot et al., 2018), while in some others the results were inconsistent (Haliloglu et al., 2017; Yamaguchi et al., 2019). Altogether, the observations suggest that even though there is an evolutionarily conserved role of PIEZO2 channels for sensing light touch in mammals, the inconsistencies among patients support the idea that there must be more mechanosensitive ion channels involved in light-touch sensation in humans.

2.4. Mechanotransduction of PIEZO2 in Nociception

In addition to mechanoreceptors and end-organs involved in sensing light touch, the skin is also equipped with additional afferent neurons that help vertebrates to sense pain after noxious mechanical stimuli such as a pinprick and blunt pressure. The sensory afferents that detect noxious mechanical stimuli are called nociceptors (Abdo et al., 2019; Abraira & Ginty, 2013; Lewin & Moshourab, 2004). Nociceptor endings are found in the epidermis of glabrous and hairy skin and are divided broadly into A δ - and C-fibers that transduce noxious responses such as pinprick and blunt pressure, respectively (**Figure 2.5**) (Abraira & Ginty, 2013; Lewin & Moshourab, 2004; Murthy, Loud, et al., 2018). As for the transduction of light touch, noxious mechanical stimuli are detected by sensory neurons via the activation of MA channels.

As it was previously mentioned, *PIEZO2* is expressed in a large subset of DRGs, including small-sized neurons that express transient receptor potential cation channels V1 (TRPV1), a marker for nociceptors, suggesting that PIEZO2 plays a role in sensing noxious responses (B. Coste et al., 2010; Usoskin et al., 2014). Recently, three independent groups showed that PIEZO2 is involved in pain sensation and is required for mechanical allodynia, abnormal sensory processing caused by nerve injury or inflammation process that results in hypersensitivity to innocuous mechanical

stimuli, in mice and humans (Eijkelkamp et al., 2013; Murthy, Loud, et al., 2018; Szczot et al., 2018).

By performing voltage-clamp recordings from DRGs where *Piezo2* expression was conditionally deleted (*Piezo2*^{CKO}), Murthy *et al.* showed that the proportion of isolated nociceptors insensitive to mechanical stimuli was higher compared to wildtype (Murthy, Loud, et al., 2018). Additionally, *ex vivo* skin nerve preparation experiments from the hairy skin of mutant mice showed that even though all A δ - and C-fibers responded to mechanical stimuli, the mechanical threshold for A δ - fibers was higher in *Piezo2*^{CKO} mice than in wildtype mice (Murthy, Loud, et al., 2018; Ranade, Woo, et al., 2014) and a reduced firing activity was observed in both fibers when applying 400 mN of mechanical force (Murthy, Loud, et al., 2018). Finally, by performing von Frey tests *in vivo* experiments it was shown that *Piezo2*^{CKO} mice exhibit impaired nocifensive behavior compared to wild type, showing fivefold higher withdrawal threshold to mechanical stimuli (Murthy, Loud, et al., 2018). All these data showed that *Piezo2* is expressed in A δ - and C-fibers contributes partially to punctate and blunt pain in mice (**Figure 2.7**).

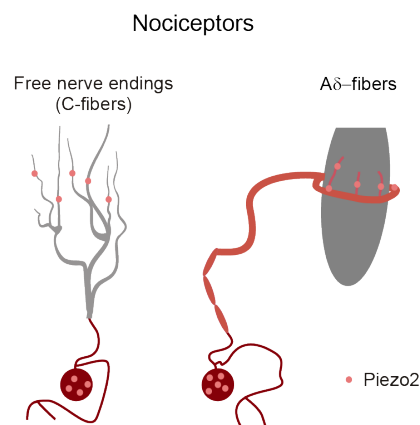


Figure 2.7. Expression of PIEZO2 in nociceptors

Cartoon representation of C- and A δ -fibers. The expression of PIEZO2 is shown in pink dots.

Mechanical hyperalgesia can be induced in mice and humans by causing cutaneous inflammation when administering compounds that activate nociceptors or by causing a trauma to the sensory nerves, such as the sciatic nerve, in the peripheral nervous system (Richner et al., 2011; Wetzel et al., 2017). Capsaicin, the pungent component in hot chili peppers activates TRPV1 in nociceptors and generates neurogenic inflammation and mechanical hyperalgesia (Caterina et al., 1997; Murthy, Loud, et al., 2018; Szczot et al., 2018). By injecting capsaicin intradermally in mice, it was shown that *Piezo2*^{CKO} animals did not exhibit mechanical hyperalgesia nor had a reduced nocifensive behavior compared to wildtype (Murthy, Loud, et al., 2018). The spared nerve injury

(SNI) method was used to cause direct damage to the sciatic nerve axons and cause allodynia in mice. Murthy SE., *et al.* found that Piezo2^{CKO} animals did not developed allodynia when stimulating with a brush stroke compared to wildtype animals and had reduced hyperalgesia after nerve injury (Murthy, Loud, *et al.*, 2018). Thus, Piezo2 contributes partially to allodynia and to nerve-injury-induced hyperalgesia.

There are discrepancies whether PIEZO2 is required for detection of noxious mechanical stimuli in humans. Some patients with LoF *PIEZO2* mutations had normal pinprick, pressure pain and pinch threshold on glabrous skin but impaired difficulties detecting light touch (Chesler *et al.*, 2016; Haliloglu *et al.*, 2017; Szczot *et al.*, 2018). However, some other patients showed decreased pain sensation when stimulated with noxious mechanical stimuli (in some cases data was inconsistent) (Behunova *et al.*, 2019; Mahmud *et al.*, 2017; Yamaguchi *et al.*, 2019). Additionally, some patients with GoF mutations in Piezo2 showed musculoskeletal pain, however another patient was suspected to have high threshold pain sensation (B. Coste *et al.*, 2013). These contradictions do not allow us to conclude whether in humans PIEZO2 is necessary for detection of noxious mechanical stimuli. However, similar to what was observed in mice, PIEZO2 contributes to pain sensation in humans (Szczot *et al.*, 2018).

2.5. Mechanotransduction of PIEZO2 in Proprioception

Proprioception is the sense of body and limb position and movement that requires specialized sensory neurons, proprioceptors. Proprioceptors are sensory neurons that convey information about stretch and tension in muscles and tendons. They are crucial for conscious sensation of limb position and movement as well as unconscious sensations (i.e. knee jerk reflex), and the sense of balance (Proske & Gandevia, 2012; S.-H. Woo *et al.*, 2015). In mammals, proprioceptors have their cell bodies in the dorsal root ganglia (DRG) and innervate two types of mechanoreceptors in skeletal muscles peripherally, muscle spindles (MS) and Golgi tendon organs (GTO) (Bewick & Banks, 2014; Proske & Gandevia, 2012).

In mice and humans, PIEZO2 is an important ion channel to sense length and tension within the skeletal muscle fibers via proprioceptors (Assaraf *et al.*, 2020; Chesler *et al.*, 2016; Florez-Paz *et al.*, 2016; Haliloglu *et al.*, 2017; Mahmud *et al.*, 2017; S.-H. Woo *et al.*, 2015). In mice, Piezo2 co-expresses in 81% of parvalbumin positive sensory neurons (Palv⁺), a marker for proprioceptors, and is present in their peripheral sensory endings (MS and GTO proprioceptive sensory endings, where mechanotransduction starts) (Arber *et al.*, 2000; S.-H. Woo *et al.*, 2015). Additionally, deletion of Piezo2 in proprioceptors or caudal DRG neurons in Piezo2^{CKO} mice resulted in ablation of most of RA currents when stimulating the soma with the poking technique (Florez-

Paz et al., 2016; S.-H. Woo et al., 2015), suggesting that Piezo2 is a major mechanotransducer molecule in proprioceptors. Moreover, Piezo2^{CKO} mice showed abnormal postnatal limb positioning or impaired body coordination (Florez-Paz et al., 2016; S.-H. Woo et al., 2015), consistent with *ex-vivo* experiments where muscle afferent activity was highly reduced in Piezo2^{CKO} compared to wildtype animals (S.-H. Woo et al., 2015).

In humans, although the expression of human PIEZO2 in proprioceptors and skeletal system has not been described, LoF or putative-GoF mutations in PIEZO2 lead to proprioceptive deficits. Particularly, patients with LoF mutations in PIEZO2 showed impaired limb coordination when closing eyes, pseudoathetosis (spontaneous movements of outstretched arms) and/or hypotonia (low muscle tone, probably due to modified behavior of MS and GTO) (Behunova et al., 2019; Chesler et al., 2016; Delle Vedove et al., 2016; Haliloglu et al., 2017; Mahmud et al., 2017; Yamaguchi et al., 2019). On the other hand, patients with putative-GoF mutations developed psychomotor delay during childhood (Alisch et al., 2016) and lack of tendon reflexes (Zapata-Aldana et al., 2019). Additionally, patients with mutations in PIEZO2 developed scoliosis and hip dysplasia, a phenotype that was recently associated with Piezo2 expression in the proprioceptive system (Assaraf et al., 2020). Together, the evidence showed that in mice Piezo2 is the principal mechanotransducer in proprioceptive neurons and the fact that patients with mutations in PIEZO2 develop proprioceptive deficits, indicates that PIEZO2 channels are fundamental for mammalian proprioception.

2.6. Mechanotransduction of PIEZO2 in non-sensory systems

Since its discovery, it was known that PIEZO2 is highly expressed in sensory neurons, lungs, colon and bladder (Bertrand Coste et al., 2010). It was not until 2017, however, that the contribution of this channel in lung physiology was described (Nonomura et al., 2017). The respiratory system experiences constant mechanical forces during breathing and respiratory volume must be controlled to prevent over-expansion of the lungs. Airway-innervating sensory neurons (including vagal and dorsal neurons) innervate pulmonary neuroepithelial cells, that control the depth of respiration. Interestingly, global ablation of *Piezo2* in airway-sensory neurons in mice cause respiratory distress in neonates, resulting in death within 24 h after birth due to respiratory failure (Nonomura et al., 2017). On the other hand, in adult mice where *piezo2* was deleted (Piezo2^{CKD}) in airway-innervating sensory neurons, they breathed in excessively deeply compared to wildtype animals, despite having normal breathing frequency (Nonomura et al., 2017). These observations suggest that Piezo2 in mice is essential to control effective breathing in new-borns and maintain normal respiration in adults.

Humans with inactive variants of *PIEZO2* are able to survive, however, patients show respiratory distress afterbirth (Behunova et al., 2019; Chesler et al., 2016; Delle Vedove et al., 2016) and reduced lung inflation during childhood (Haliloglu et al., 2017). Additionally, patients with GoF and putative GoF mutations in *PIEZO2* showed respiratory distress after birth (Alisch et al., 2016), and restrictive lung disease (B. Coste et al., 2013; Okubo et al., 2015), shortness of breath (B. Coste et al., 2013; Okubo et al., 2015) and respiratory problems during adulthood (Zapata-Aldana et al., 2019). Therefore, the role of *PIEZO2* as a mechanotransducer in the respiratory system appears conserved in mammals.

The gastrointestinal tract responds to mechanical movement which results in serotonin release. The cells specialized for secreting serotonin in response to mechanical stimuli in the gastrointestinal tract are enterochromaffin cells (EC) which constitute the largest population of epithelial enteroendocrine cells (Alcaino et al., 2018; F. Wang et al., 2017). *PIEZO2* is expressed in mouse and human ECs (F. Wang et al., 2017) and *knock-down* with siRNA, or conditional *knock-out* or pharmacologically block of *PIEZO2* in these cells result in ablation of rapidly inactivating mechanosensitive currents and in inhibition of stretch-induced serotonin release (Alcaino et al., 2018; F. Wang et al., 2017). Further studies using *in vivo* genetic models will allow us to understand better the role of *PIEZO2* in the gastrointestinal tract. So far, humans with mutations in *PIEZO2* have not been reported to suffer from gastrointestinal problems, and little is known about the role of *PIEZO* in human gastrointestinal pathophysiology.

Urination is the process of voiding urine from the bladder. During this process mechanotransduction is involved as bladder filling is detected to initiate to micturition. The urinary tract is composed by layers of epithelial cells, among them the umbrella cells which have been proposed to act as mechanosensors to initiate micturition (de Groat, W. C. & Yoshimura, 2009; Marshall et al., 2020). Additionally, the bladder is innervated by sensory neurons from DRGs which respond to chemical and mechanical stimuli (de Groat, W. C. & Yoshimura, 2009). *PIEZO2* is expressed in umbrella cells and sensory neurons innervating the bladder, suggesting its importance in regulating mechanotransduction during urination (Marshall et al., 2020). Interestingly, deletion of *piezo2* either in umbrella cells or sensory neurons in mice, resulted in longer and irregular intervals between bladder contractions and higher bladder pressure for urination, suggesting that *Piezo* is essential to regulate urination during bladder filling and relaxation processes (Marshall et al., 2020). Additionally, in humans, *PIEZO2*-deficient patients showed decreased voiding frequency and sensation of incomplete voiding (Marshall et al., 2020). Thus, *PIEZO2* is necessary to coordinate urination in mammals.

2.7. Genetic diseases related to mutations in PIEZO2

2.7.1. Loss of function mutations

In mice, global deletion of *piezo2* (*Piezo2*^{-/-}) results in post-natal lethality (Dubin et al., 2012; Nonomura et al., 2017). Interestingly, biallelic LoF mutations in humans do not always cause lethality, but lead to distal arthrogryposis with impaired proprioception and touch (DAIPT) (**Table 2.5**) (Behunova et al., 2019; Chesler et al., 2016; Delle Vedove et al., 2016; Mahmud et al., 2017; Yamaguchi et al., 2019).

In 2016, Chesler *et al.* reported the first cases of biallelic LoF variants in *PIEZO2* causing human disorders (Chesler et al., 2016). They described the molecular etiopathology of one patient with two non-sense mutations in *PIEZO2* (R1575* and R1685*) and a patient with a non-sense mutation and a missense mutation (R1685* and R1685P, respectively). These patients showed altered touch and proprioception sensations. In addition patients had congenital hip dysplasia, limb contractures and progressive scoliosis. When overexpressing the mouse *Piezo2* construct carrying the R1575*, R1685* and R1685P variants in HEK293 cells, no mechanically activated currents were recording, concluding that patients carrying these mutations are LoF mutations (Chesler et al., 2016).

Impaired proprioception and altered touch and -in some cases- pain sensations in *PIEZO2*-deficient patients are consistent with the phenotypes observed in *Piezo2*^{CKO} mice (Eijkelkamp et al., 2013; Florez-Paz et al., 2016; Murthy, Loud, et al., 2018; Ranade, Woo, et al., 2014; Szczot et al., 2018; S. Woo, Ranade, et al., 2014). Additionally, similar to what was observed in *Piezo2*^{CKO} and/or *Piezo2*^{-/-} mice, patients showed progressive scoliosis (Behunova et al., 2019; Chesler et al., 2016; Delle Vedove et al., 2016; Haliloglu et al., 2017; Mahmud et al., 2017; Yamaguchi et al., 2019), some patients developed respiratory problems (Behunova et al., 2019; Chesler et al., 2016; Delle Vedove et al., 2016; Haliloglu et al., 2017) and urinary complications (Marshall et al., 2020). All these observations give rise to the idea that *PIEZO2* function is largely conserved in mice and humans.

2.7.2. Gain-of-function mutations

The first and only genotyping and phenotyping characterization of GoF mutations in *PIEZO2* was done by Coste *et al.* (B. Coste et al., 2013). They found that mutations in I802F and E2727del in *PIEZO2* resulted in faster channel recovery from inactivation when mechanically activated and E2727del mutation showed slower inactivation kinetics in vitro. Patients with these mutations developed distal arthrogryposis type 5 (DA5), a group of arthrogryposis that affects

progressively congenital joint contractures including hand and feet, results in scoliosis, short stature, ocular abnormalities, ptosis, pulmonary dysfunction and an increase in resting muscle tone, particularly in the chest. Recent studies showed that in addition to I802F and E2727del mutations other PIEZO2 variants were found in DA5 patients, however the physiological consequences of these mutations have not been characterized. (**Table 2.6**) (B. Coste et al., 2013; Mcmillin et al., 2014; Okubo et al., 2015; Zapata-Aldana et al., 2019).

Other human disorders have been linked to mutations in PIEZO2: Gordon Syndrome (GS) and Marden-Walker syndrome (MWS). GS and MWS belong to distal arthrogyriposis congenital disorders and the symptoms are similar to those of DA5 patients, GS and MWS individuals develop congenital joint contractures that affect the hands and feet, scoliosis and show short stature. However, unlike DA5 patients, some patients with GS and MWS develop cerebellar malformations and cleft palate (**Table 2.6**). The R2756H PIEZO2 mutation was commonly found in patients with GS, while mutations R2756C and W2417C were found in patients with MWS. (Alisch et al., 2016; Mcmillin et al., 2014; Seidahmed et al., 2020). The genetic and phenotypic overlap among GS, DA5 and MWS patients indicates the contribution of PIEZO2 in a shared developmental process that might include the development of skeletal muscle (Assaraf et al., 2020; Mcmillin et al., 2014).

In comparison to LoF mutations studies, the effect of GoF mutations in the somatosensory system has barely been addressed. Two DA5 patients reported altered pain sensation (Chesler et al., 2016) and a third one showed normal sensory nerve conduction. Moreover, mutations in PIEZO2 causing GS, MWS and novel variants related to DA5 are considered to be GoF mutations, however, to date there is no physiological evidence that supports that claim.

Table 2.5 Clinical features associated with LoF mutations in PIEZO2
nd, not determined; ID, intracellular domain; ED, extracellular domain

	(Chesler et al., 2016)	(Delle Vedove et al., 2016)	(Mahmud et al., 2017)	(Haliloglu et al., 2017)	(Behunova et al., 2019)	(Yamaguchi et al., 2019)
Total of patients	2	10	3	1	1	1
Mutation (amino acids)	R1575*; R1685* R1685*; R1685P	L1874*, P1007*, S517*, del exons 6-7	S903*	R462*	R26*	V1391*
Structural domain	ID; ID ID; ID	ID, ED, ED	ID	ID	ED	ED
Functional phenotype	not functional	unreported	unreported	unreported	unreported	unreported
Short stature	nd	8/10 1/10 nd	yes	no	no	yes
Altered touch sensation	yes	1/10 9/10 nd	yes	inconsistent	nd	yes
Altered pain sensation	no	nd	yes	no	inconsistent	inconsistent
Impaired proprioception	yes	yes	yes	yes	yes	yes
Congenital hip dysplasia	yes	1/10 1/10 nd	nd	yes	no	yes
Congenital contractures in limbs	yes	8/10 1/10 nd	yes	yes	yes	yes
Scoliosis	yes	9/10 1/10 nd	yes	yes	yes	yes
Absent/reduced deep tendon reflexes	yes	9/10 1/10 nd	yes	nd	yes	yes
Pulmonary disease	no	6/10 4/10 nd	nd	no	yes	no

Table 2.6 Clinical characteristics associated with PIEZO2 mutations
nd, not determined; ns, not specified; DA1, Distal Arthrogryposis type 1; ED, extracellular domain.

	(B. Coste et al., 2013)	(B. Coste et al., 2013)	(Mcmillin et al., 2014)	(Mcmillin et al., 2014)	(Mcmillin et al., 2014)	(Mcmillin et al., 2014)	(Okubo et al., 2015)	(Alisch et al., 2016)	(S. Li et al., 2018)	(Zapata-Aldana et al., 2019)	(Seidahmed et al., 2020)
Disease	DA5	DA5	GS	GS	DA5	MWS	DA5	GS	DA1	DA5	MWS
Total of patients	2	1	14	1	51	1	4	3	4	4	1
Mutation (amino acids)	I802F	E2727del	R2686H	W2746*	M712V, M998T, T2221I, S2223L, T2356M, R2686H, R2718L, R2718P, E2727del, S2739P	R2686C	A1486P	R2686H	R2718Q	S2690R	W2417C
Structural domain	TM16	CTD	IH	CTD	TM14, TM19, ED, ED, Anchor, IH, CTD, CTD, CTD, CTD	IH	Beam	IH	CTD	IH	OH
Functional phenotype	Faster recovery from inactivation	Faster recovery from inactivation and slower inactivation kinetics	unreported	unreported	unreported	unreported	unreported	unreported	unreported	unreported	unreported
Short stature	2/2	yes	8/14 4/14 nd	yes	18/51 7/51 nd	no	Yes	3/3	3/4 1/4 nd	3/4	ns
Altered touch sensation	Nd	nd	nd	nd	nd	nd	nd	nd	nd	nd	nd
Altered pain sensation	2/2	nd	nd	nd	nd	nd	nd	nd	no	nd	nd
Ptosis	2/2	yes	4/14	yes	24/51	yes	4/4	2/3 1/3 nd	no	no	yes
Congenital contractures in limbs	yes	yes	yes	yes	yes	yes	yes	yes	yes	yes	yes
Scoliosis	1/2	no	6/14	yes	20/51 4/51 nd	yes	2/4	0/3	no	1/4	yes
Cleft palate	Nd	nd	11/14	yes	no	yes	no	1/3	no	0/4	yes
Muscle tone	1/2	yes	ns	ns	ns	ns	nd	nd	no	4/4	nd
Pulmonary disease	2/2	yes	no	no	13/51 6/51 nd	no	2/4 2/4 nd	nd	nd	1/4 3/4 nd	nd
Cerebellar malformations	nd	nd	3/14	no	1/51 42/51 nd	yes	nd	nd	nd	nd	yes

3. Aims of this work

In isolated sensory neurons based on their inactivation kinetics, three types of mechanically activated (MA) currents have been identified: rapidly adapting (RA), intermediate adapting (IA) and slowly adapting (SA) currents (B. Coste et al., 2010; Hu & Lewin, 2006). The currents with an inactivation time constant (τ_{inact}) <5 ms are classified as RA currents, while those with a $\tau_{\text{inact}} = 5-50$ ms are considered IA and those with a $\tau_{\text{inact}} >50$ ms are SA (Poole et al., 2014).

Recently, two new mechanically gated channels were discovered: the PIEZO1 and PIEZO2 channels. PIEZO channels are non-selective cation channels, ruthenium red (RR) sensitive and both lead to RA currents (Bertrand Coste et al., 2010). In the Lewin lab, in collaboration with the Patapoutian group (Scripps USA) it was shown that in mice, the conditional deletion of the Piezo2 channel (*Piezo2^{CKO}*) leads to a silencing of the major transducer of mechanically activated currents in isolated sensory neurons (Ranade, Woo, et al., 2014). Thus, the model is that the deletion of *piezo2* gene in mice leads to the silencing of the main native mechanically gated current in sensory neurons.

Interestingly, it has been shown that in humans missense mutations in *PIEZO2* lead to different congenital diseases, such as DA5, GS and MWS (Alisch et al., 2016; B. Coste et al., 2013; S. Li et al., 2018; Mcmillin et al., 2014; Okubo et al., 2015; Seidahmed et al., 2020; Zapata-Aldana et al., 2019). However, the biophysical effects of these mutations and the impact that they have on the observed phenotype have not been examined. We studied the effect of pathogenic mutations by overexpressing the m*Piezo2* cDNA carrying the mutations in N2a^{*Piezo1*^{-/-}} cells, a cell line that lacks endogenous Piezo1-mediated ion currents (Moroni et al. 2018). With pillar arrays and HSPC techniques, we compared the biophysical properties between the mutants and the wild type channel. Recently in our group, we demonstrated that PIEZO channels are voltage modulated and that pathogenic mutations in Piezo1 that cause Xerocytosis in humans increase the open probability of the channel (Moroni et al., 2018). Using HSPC method, we studied the tail currents from the channels carrying the pathogenic mutations. For this aim, we used a stretch-sensitive chimeric channel combining the N-terminal domain of Piezo1 and the pore forming part of Piezo2 (mP1/mP2) (Moroni et al., 2018). The tail current protocol allowed us to determine if the voltage sensitivity in the chimeric channel that has the pore of Piezo2 is also affected.

Moreover, we generated *knock-in* (*KI*) mice carrying mutations that cause DA5 and GS (*Piezo2*^{R2765H} and *Piezo2*^{R2756K} mice) with CRISPR-Cas9 method. We studied the native MA

currents from mechanoreceptors and nociceptors of DRG neurons to see if the pathogenic mutations cause an effect in the biophysical properties of this type of currents.

Based on the previous studies where a hypersensitisation of PIEZO1 was observed in pathogenic mutations in this channel (Bae et al., 2013), we tested *in-vivo* whether Piezo2^{R2765H} and Piezo2^{R2756K} mice are hypersensitive to mechanical nociception with von Frey technique.

Another aim of this project was to measure the properties of mechanosensitive currents in sensory neurons with the pillar arrays technique and to compare their biophysical properties in Piezo2 wild type (Piezo2^{+/+}), global Piezo2 *knockout* (Piezo2^{-/-}) and Piezo2^{CKO} mice. One hypothesis was that the pillar deflection would not trigger mechanically gated currents in Piezo2^{-/-} and or Piezo2^{CKO} DRG neurons, as it was previously reported in the Piezo2^{CKO} mice, with the soma indentation technique (Ranade, Woo, et al., 2014). An alternative hypothesis was that mechanically induced currents would still be present in Piezo2^{-/-} and or Piezo2^{CKO} DRG neurons, but currents would have different biophysical properties compared to Piezo2^{+/+} neurons. The last hypothesis was supported by studies where it was shown that with the pillar arrays method it is possible to measure high-threshold mechanosensitive currents not detectable with the indentation technique in sensory neurons and chondrocytes (Poole et al., 2014; Servin-Vences et al., 2017).

Previously, it has been described that Stoml3 protein is necessary for mechanotransduction in mice (Wetzel et al. 2007) and regulates the deflection-gated activity of Piezo channels (Poole et al. 2014). However, it was not clear whether the effect is directly or indirectly through the interaction with cytoplasmic or extracellular matrix components. Here, we co-expressed the stretch-sensitive chimeric mP1/mP2 (Moroni et al. 2018) and PIEZO1 channels with STOML3 in N2a^{Piezo1^{-/-}} cells and performed HSPC in the outside-out configuration. We expected to see a sensitization of the channels when co-expressed with STOML3 at membrane configuration.

Finally, previous studies have shown that PIEZO1 is important for mechanotransduction in the circulatory system. Electrophysiological recordings from cardiomyocytes (CMs) indicate that these cells express endogenously stretch-sensitive ion channels (Guharay & Sachs, 1984). Interestingly, PIEZO1 is expressed in human CMs and is upregulated in heart failure in neonatal rats (Liang et al., 2017; Wong et al., 2018). However, a direct electrophysiological characterization of PIEZO1 in CMs was lacking. We hypothesized that stretch-sensitive currents from CMs are mediated by PIEZO1. In collaboration with Maria Bikou, from AG Hübner (MDC, Berlin), human induced pluripotent stem cells (hiPSCs) were differentiated into cardiomyocytes (hiPSC-CMs) and with CRISPR-Cas9 technology, a cell line lacking *PIEZO1* was generated (hiPSC-

CMs^{PIEZOKO}). With HSPC, we studied the biophysical properties of stretch-sensitive currents from both wild type and hiPSC-CMs^{PIEZO1KO}.

4. Material and methods

4.1. Molecular biology

4.1.1. Preparation of DNA plasmids

DNA constructs containing Piezo1, Piezo2 variants and Stoml3 were purified from transformed bacteria grown in large-scale bacterial culture (50 mL Midiprep, PureYield™ Plasmid Midiprep System, Promega). The midpreps were made according to the manufacture's protocol. DNA quantification was measured using a NanoDrop 2000 (ThermoFisher Scientific).

4.1.2. Site-directed mutagenesis

Insertion of point mutations in mPiezo2 and the chimeric channel mP1/mP2 were carried out using the Q5® Site-Directed Mutagenesis Kit (NEB, Inc) according to the manufacture's indications. Specific primers for each mutant were used at 0.5 µM (See Table 4.1). Additionally, Polymerase chain reactions (PCR) mix contained 5 ng of template DNA and 1X of Q5 Hot Start High-Fidelity Master Mix. PCR products were used as template for bacteria transformation and ampicillin resistant colonies were chosen and grown in large-scale bacterial culture (as previously described) for DNA purification. DNA plasmids were sequenced to verify the insertion of point mutations.

Table 4.1. PCR primers used for site-directed mutagenesis.

mPiezo2 and mP1/mP2 chimeric channels were used as template DNA. Primer sequences are listed as 5'-3'. Point mutations are highlighted in bold.

Mutant	Forward primer	Reverse primer
R2756H	GAA ATT TGT TCA TGA GTT CTT CAG	CCA ATT ACA AGG ACA ACA G
R2756C	GAA ATT TGT TTG TGA GTT CTT CAG	CCA ATT ACA AGG ACA ACA G
R2756K	GAA ATT TGT TAA AGA GTT CTT CAG TGG G	CCA ATT ACA AGG ACA ACA G

4.2. Cell culture

4.2.1. Cultured cell lines

N2a^{Piezo1^{-/-}} cells (Moroni et al., 2018) were used for the characterisation of the biophysical properties of the mutants of mPiezo2 and the chimeric channel mP1/mP2. Recently we showed that these cells lack stretch- and deflection-gated currents (Moroni et al., 2018; Patkunarajah et al., 2020). Cells were cultured in 45% DMEM-Glutamax (gibco, ThermoFisher SCIENTIFIC),

45% Opti-MEM (gibco, ThermoFisher SCIENTIFIC), 10% fetal calf serum (PAN Biotech GMBH) and 1% penicillin and streptomycin (Sigma-Aldrich) media.

Wildtype N2a cells (N2a^{Wt}) were used as control to show endogenous deflection-gated currents and were cultured as described above.

N2a^{Piezol^{-/-}} cells were transiently transfected using FuGeneHD (Promega, Madison). Briefly, a mix of 100 μ L of Opti-MEM, 3 μ L of FuGeneHD and 1 μ g of DNA was incubated for 10 min at room temperature. The mix was added to Na2^{Piezol^{-/-}} cells cultured in 30 mm x 15 mm Petri dishes and 900 μ L of media containing 50% DMEM-Glutamax and 50% Opti-MEM was added for an overnight transfection. Electrophysiological recordings were made 18-24 h post-transfection. At least four transfections were made for each set of experiments.

4.2.2. DRG culture

DRG neurons were collected from all the spinal segments (or dorsal if indicated) in plating medium on ice (DMEM-F12 (Invitrogen) supplemented with L-Glutamine (2 μ M, Sigma-Aldrich), Glucose (8 mg/ml, Sigma Aldrich), Penicillin (200 U/mL)-Streptomycin (200 μ g/mL) and 10 % fetal horse serum). The DRGs were treated with Collagenase IV (1 mg/ml, Sigma-Aldrich) for 1 h when working with adult mice or 15 min when working with embryos (E18.5) and pups (6 weeks old, P6), at 37°C and then washed three times with Ca²⁺- and Mg²⁺-free PBS. The samples were incubated with trypsin (0.05%, Invitrogen, Karlsruhe) for 15min, at 37°C. After the enzymatic treatment, the collected tissue was triturated with a pipette tip and plated in a droplet of plating medium on the elastomeric pillar arrays precoated with laminin (4 μ g/cm², Invitrogen) as described in Poole K., *et al.* for the pillar arrays experiments (*see preparation of pillar arrays section*) (Poole et al., 2014). Cells were cultured overnight, and the electrophysiology experiments were performed after 18-24 h of the dissection.

4.2.3. hiPSCs-CMs culture

In collaboration with Maria Bikou (AG, Hübner, MDC, Berlin), hiPSCs were induced by to differentiate towards cardiomyocytes using a chemically defined, xeno-free protocol (Burrige et al., 2014). At day 0 (d0), media was changed to CDM3 (RPMI 1640 medium (Life Technologies), 500 μ g/mL *Oryza sativa*-derived recombinant human albumin (Sigma-Aldrich) and 213 μ g/mL L-ascorbic acid 2-phosphate (Sigma-Aldrich)) containing 3 μ M CHIR99021, a GSK3B inhibitor, (TOCRIS). After 48 h, on day 2 (d2) media was changed to CDM3 containing 2 μ M Wnt-C59, WNT inhibitor, (TOCRIS). Media was changed with CDM3 every other day at day 4 (d4) and day 6 (d6). Contracting cells could be observed from day 8 (d8) or day 9 (d9). After day 10 (d10)

CDM3 medium was replaced with CDM3-L (without glucose) in order to metabolically select cardiomyocytes (Tohyama et al., 2013). From d20 to d30 CDM3 was replaced with CDM3 to enhance maturation and the media was changed every other day.

4.3. Animals

All experiments with mice were done in accordance with protocols reviewed and approved by the German Federal authorities (State of Berlin).

4.3.1. Piezo2^{R2756H} and Piezo2^{R2756K} mice

Constitutive *KI* mice were generated using CRISPR-Cas9 technology by the ingenious targeting laboratory (USA). For each mutant, gRNAs (guide RNAs) and ssDNA (single-stranded DNA) donors were designed (**Table 4.2**) and injected into fertilized embryos (F0 mutant animals or founders). F0 embryos were transferred into pseudopregnant mice. Founders were bred with wild type background animals (C57B1/6) to generate F1 mice.

Table 4.2. gRNA and ssDNA donor sequences used to insert point mutations in Piezo2

Sequences are listed as 5'-3'. gRNA for Piezo2^{R2756H} is shown as complementary and reverse direction. Point mutations of ssDNA are highlighted in bold.

<i>KI</i> mutant	gRNA	ssDNA
Piezo2 ^{R2756H}	TGG AAG CTC TTC AAA	TGC TGT CTC TTT CAG TAT CAT GGG ATT GTA TGC ATC TGT TGT CCT TGT AAT TGG GAA ATT TGT TCA TGA GTT CTC AGT GGG ATC
	CAT GAT GG	TCT CAT TCC ATC ATG TTT GAA GAG CTT CCA AAT GTG GAC AGA ATC TTG AAG TTG TGC ACA GAT ATA TTC CTC GTG AGG GAG ACA
Piezo2 ^{R2756K}	TTG TTC GTG AGT TCT	ACC ATC TTC ATC ATT TTC TCC TTG CTG TCT CTT TCA GTA TCA TGG GAT TGT ATG CAT CTG TTG TCC TTG TAA TTG GGA AAT TTG TTA
	TCA GTG GG	AGG AGT TCT CAG TGG GAT CTC TCA TTC CAT CAT GTT TGA AGA GCT TCC AAA TGT GGA

4.3.2. Piezo2^{-/-}

Piezo2^{+/-} mice (Nonomura et al., 2017; Ranade, Woo, et al., 2014) were mated to generate Piezo2^{-/-} mice (Piezo2^{KO}). The females were monitored for 7 days to observe the presence or absence of vaginal plug during mating. The day when the vaginal plug was observed was considered as the embryonic day 0.5 (E0.5). The females were sacrificed at E18.5 in a 100% CO₂

chamber. The embryos were collected and put in PBS on ice before DRG extraction, as described in Lechner et al., (2009) (Lechner et al., 2009). A piece of the tail was cut for genotyping.

4.3.3. Piezo2^{CKO}

Hoxb8^{+Cre} (Witschi et al., 2010) mice were mated with Piezo2^{+/-} to generate Hoxb8^{+Cre};Piezo2^{+/-} animals. In parallel Piezo2^{fl/fl} mice (S. Woo, Ranade, et al., 2014) were mated with Ai14^{fl/fl} mice (Madisen et al., 2010) to generate Piezo2^{fl/fl}; Ai14^{fl/fl}. Subsequently, Hoxb8^{+Cre}; Piezo2^{+/-} were mated with Piezo2^{fl/fl}; Ai14^{fl/fl} animals to generate Piezo2^{CKO} (Hoxb8^{+Cre}; Piezo2^{-fl}; Ai14^{+fl}). Hoxb8^{+/+}; Piezo2^{-fl}; Ai14^{+fl} were used as control animals (Piezo2^{Ctrl}) (**Figure 5.26**).

4.4. Genotyping

To genotype Piezo2^{R2756H}, Piezo2^{R2756K} and mice, a biopsy of every animal was taken after weaning pups from their parents. To genotype Piezo2^{KO} and Piezo2^{CKO} animals, a piece of tail was taken from E18 embryos and P6 pups, respectively. Tissues were incubated overnight at 55° C while shaking at 800 rpm in a lysis buffer containing (in mM) 200 NaCl, 100 Tris pH 8.5, 5 EDTA, 0.2% of SDS and Prot K (10 mg/mL, Carl Roth).

PCRs were performed using supernatant of the lysis preparation as DNA template (20-100 ng), 1X Taq PRC buffer, 2 mM MgCl₂, 0.2 mM dNTPs, 1.25U Taq-polymerase (ThermoFisher Scientific) and 0.5 mM of forward- and reverse-specific primers targeting *piezo2* (**Table 4.3**). PCR protocols were established according to the manufacturer.

For Piezo2^{R2756H} and Piezo2^{R2756K} genotyping, enzyme restriction assays were performed to differentiate between different possible genotypes. Inserted point mutations generated digesting sites that allow us to identify wildtype, heterozygous and homozygous animals from each *KI* mice. PCR products were incubated overnight with BspI and MseI restriction endonucleases (NEB Inc.) for Piezo2^{R2756H} and Piezo2^{R2756K}, respectively (**See table 4.3**). Amplified and digested DNA fragments were observed by gel electrophoresis.

4.5. Preparation of pillar arrays

Pillar arrays were prepared as previously described (Patkunarajah et al., 2020; Poole et al., 2014; Servin-Vences et al., 2017). Briefly, silanized negative masters were used as templates. Negative masters were covered with polydimethylsiloxane (PDMS, sylgard 184 silicone elastomer kit, Dow Corning Corporation) mixed with a curing agent at 10:1 ratio (elastomeric base:curing agent) and incubated for 30 min. Glass coverslips were placed on the top of the negative masters containing PDMS and baked for 1h at 110° C. Pillar arrays were carefully peeled from the negative

masters. The resulting radius- and length-size of individual pilus within the array was 1.79 μm and 5.8 μm , respectively. While the elasticity and the spring constant of each pilus was 2.1 MPa and 251 pN-nm, respectively, as previously reported (Patkunarajah et al., 2020; Poole et al., 2014; Servin-Vences et al., 2017). Before use for cell culture, pillar arrays were plasma cleaned with a Femto low-pressure plasma system (Deiner Electronic GmbH) and coated with EHS laminin (20 $\mu\text{g}/\text{mL}$) or Fibronectin from bovine serum (200 $\mu\text{g}/\text{mL}$).

Table 4.3. PCR primers used for genotyping transgenic mice

The expected size (in base pairs, bp) is also shown. Note that for biopsies from *Piezo2*^{R2756H} and *Piezo2*^{R2756K} mice the expected size of the bands after the enzymatic digestion is shown.

Mice line	Forward primer	Reverse primer	Expected size (bp)
<i>Piezo2</i> ^{R2756H}	GAA AGA GCT ACT TTG	CCT GTC AGA AGA GAA	<i>Piezo2</i> ^{+/+} : 499
	AAA GGA GTA TGT GC	ATG GTT GCC	<i>Piezo2</i> ^{R2756H/+} : 499, 174, 325
			<i>Piezo2</i> ^{R2756H/R2756H} : 174, 325
<i>Piezo2</i> ^{R2756K}	GAA AGA GCT ACT TTG	CCT GTC AGA AGA GAA	<i>Piezo2</i> ^{+/+} : 499
	AAA GGA GTA TGT GC	ATG GTT GCC	<i>Piezo2</i> ^{R2756K/+} : 383, 210, 173, 69, 47
			<i>Piezo2</i> ^{R2756K/R2756K} : 210, 173
<i>Piezo2</i> ^{KO} for wt allele	CTC AGA CTT GGA GAT CCT GTA GC	CCC TAC CCA CCC ATT CCC ATT TT	140
<i>Piezo2</i> ^{KO} for mutant allele	CTC AGA CTT GGA GAT CCT GTA GC	CTT CCT GAC TAG GGG AGG AGT A	392
<i>Piezo2</i> ^{Cre}	GGG GTC TCT AAT GGA TGC AA	AAC CAG CGT TTT CGT TCT GC	1200
<i>Piezo2</i> ^{fl}	CTC AGA CTT GGA GAT CCT GTA GC	GAC TCA GAT TTT CCA CAT GGG G	258
Ai14 for wt allele	AAG GGA GCT GCA GTG GAG TA	CCG AAA ATC TGT GGG AAG TC	297
Ai14 for mutant allele	CTG TTC CTG TAC GGC ATG G	GGC ATT AAA GCA GCG TAT CC	196

4.6. Electrophysiology

4.6.1. Whole-cell patch clamp

Whole-cell patch clamp experiments were made from DRG neurons and transiently transfected N2a^{Piezo1^{-/-}} cells using pulled and heat-polished borosilicate glass pipettes (Harvard apparatus, 1.17 mm x 0.87 mm) with a resistance of 3-6 M Ω . The pipettes were pulled using a DMZ puller (Germany), and filled with a solution containing (in mM): 110 KCl, 10 NaCl, 1 MgCl₂, 1 EGTA and 10 HEPES. For recordings in DRG neurons QX-314 (Alomone Labs) at 0.001 mM was added. The pH was adjusted to 7.3 with KOH. The extracellular solution contained (in mM): 140 NaCl, 4 KCl, 2 CaCl₂, 1 MgCl₂, 4 Glucose and 10 HEPES. The pH was adjusted to 7.4 with NaOH. Pipette and membrane capacitance were compensated using the auto-function of Patchmaster (HEKA, Elektornik GmbH, Germany) and series resistance was compensated to minimize

voltage errors. Currents were evoked by mechanical stimuli (see below) at a holding potential of -60 mV.

For pillar arrays experiments, a single pilus was deflected using a heat-polished borosilicate glass pipette (mechanical stimulator) driven by a MM3A micromanipulator (Kleindiek Nanotechnik, Germany) as described in (Poole et al., 2014). Only cells on the top of pili were stimulated. Pillar deflection stimuli were applied in the range of 0-1000 nm, larger deflections were discarded. For quantification and comparison analysis, the data was binned by the magnitude of the stimuli (1-10, 11-50, 51-100, 101-250, 251-500, 501-1000 nm) and calculated the mean of the current amplitudes within each bin for every cell. Bright field images (Zeiss 200 inverted microscope) were collected using a 40x objective and a CollSnapEZ camera (Photometrics, Tucson, AZ) before and after the pillar stimuli to calculate the pillar deflection. The pillar movement was calculated comparing the light intensity of the center of each pilus before and after the stimuli with a 2D-Gaussian fit (Igor Software, WaveMetrics, USA).

4.6.2. High Speed Pressure Clamp

HSPC (Ala Scientific) experiments were carried out in excised outside-out patched pulled from transiently transfected N2a^{Piezo1KO} cells and ihPSC-CMs. Recording pipettes had a final resistance of 6-8 MΩ. Positive pressure pulses were applied through the recording electrode. Pressure steps protocol consisted in ranging stimuli from 10 to 170 mmHg, in 20 mmHg steps while holding the patch potential at -60 mV. Tail currents protocol consisted on applying depolarized prepulses ranging from 0 to 140 mV followed by a repolarizing voltage step to -60 mV in the continuous presence of pressure. Recording solutions consisted in symmetrical ionic conditions containing (in mM): 140 NaCl, 10 HEPES, 5 EGTA adjusted to pH 7.4 with NaOH (Moroni et al. 2018). Currents were recorded at 10 KHz and filtered at 3 KHz using an EPC-10 USB amplifier (HEKA, Elektornik GmbH, Germany) and Patchmaster software.

Currents and the biophysical parameters were analyzed using FitMaster (HEKA, Elektornik GmbH, Germany).

4.7. von Frey experiments

Calibrated von Frey (Semmes-Weinstein) filaments (Aesthesio®, USA) were used to test the 50% paw withdrawal threshold (50% PWT) in mice to mechanical nocifensive responses *in-vivo*. The “up-down method” was used to calculate the 50% PWT. The “up-down method” determines the weight of stimulus that triggers a response 50% of the times it is applied (Chaplan et al., 1994; Christensen et al., 2020; Dixon, 1980). Testing was carried out during the light phase.

Mice (7-12 weeks old) were placed in plastic cages with a metal grid floor bottom that allowed access to paw stimulation. Animals were habituated for two consecutive days during week one for 20 min. During week two (experimental week), mice were placed in the plastic cages for ~20 min (accommodation) before the behavioral test. In all cases, the accommodation process finished until cage exploration stopped. Each animal was tested at least twice on different days. Mid-plantar right and left hind paws were stimulated for approximately 1-3 s with von Frey filaments in the range of 0.008, 0.02, 0.04, 0.07, 0.16, 0.4, 0.6, 1.0, 1.4 and 2 g. Von Frey filaments were presented perpendicular to hind paws at intervals of 3-5 min. A positive response was considered when the paw was withdrawn.

To test the 50% PWT, positive or negative responses to different stimulations were traced. Testing started with the 0.4 g filament. In the absence of paw withdrawal (negative response, O), a stronger stimulus was presented. When observing paw withdrawal (positive response, X) a weaker stimulus was tested. Following a breaking point (e.g., XO or OX; Figure 4.1 A, B respectively) four more stimuli were applied resulting in a pattern of negative or positive responses (e.g., XO/XXOX or OX/OOXO; **Figure 4.1 A and B**, respectively).

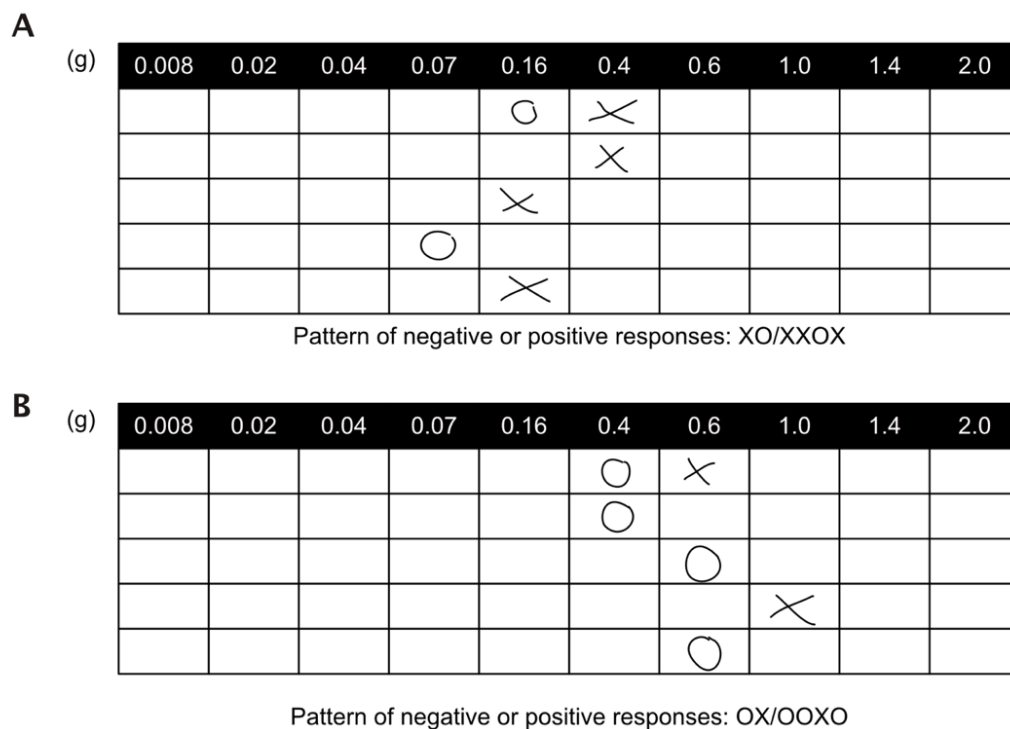


Figure 4.1. XO-response patterns

The 0.4 g filament was used to start the experiment. After a break point (e.g., XO (A) or OX (B)) four additional stimuli were applied resulting in a pattern of negative or positive responses (e.g., XO/XXOX (A), OX/OOXO (B)).

XO-response patterns of each animal were uploaded on https://bioapps.shinyapps.io/von_frey_app/ as indicated by (Christensen et al., 2020) to calculate the 50% PWT as previously described (Chaplan et al., 1994; Dixon, 1980):

$$50\% \text{ PWT (g)} = (10^{[X_f + k\delta]}) / 10,000$$

Where X_f is the value (in log units) of the last von Frey filament tested; k is the value provided by Chaplan statistic table for XO-response patterns (Chaplan et al., 1994); δ is the mean difference (in log units) between stimuli. 50% PWT values were thus calculated by taking the average of measurements to paw withdrawals on different days from each mouse. Progressive nociceptive responses were calculated during three consecutive weeks.

4.8. Calcium imaging

hiPSC-CMs^{wt} and hiPSC-CMs^{PIEZOKO} were cultured on Matrigel™ and loaded with Cal-520 (5 mM, CAL520® AM, AAT Bioquest, Inc). Cells were perfused with extracellular solution (in mM: 140 NaCl, 4 KCl, 2 CaCl₂, 1 MgCl₂, 4 glucose, 10 HEPES, adjusted to pH 7.4 with NaOH) at room temperature. Images were acquired with an Olympus BX51WI microscope equipped with a DG4 (Sutter Instruments) and a CoolSNAP ES camera (Visitron). Image acquisition and analysis were done using MetaFluro (Molecular Devices). Every image was taken in cycles of 3 s. The baseline of the fluorescence (F_0) was established by taking the average of the first 10 cycles. Ionomycin (1 μ M) was used to normalize the maximum signal of Cal-520. Data was plotted using the formula: $\Delta F/F_0 = (F - F_0)/F_0$.

4.9. Statistical analysis

All data analyses were performed using GraphPad Prism and all data sets were tested for normality. Parametric data sets were compared using a two-tailed, Student's t -test. Nonparametric data sets were compared using a Mann-Whitney test. To compare more than two groups, One-way ANOVA was used. Categorical data were compared using Fisher's exact or χ^2 tests.

5. Results

5.1. Characterization of N2a^{Piezo1^{-/-}} cell line with pillar arrays

Piezo1 channels were first identified and characterised in N2a cells, a neuroblastoma cell line (Bertrand Coste et al., 2010). To investigate the effect of pathogenic mutations in PIEZO2 it was necessary to use a cell line that lacks MA currents. Recently, in our lab the N2a^{Piezo1^{-/-}} cell line was generated (Moroni et al., 2018). By the time this work was developing, it was known that N2a^{Piezo1^{-/-}} cells did not show MA currents evoked with HSPC or indentation (Moroni et al., 2018). However, it was not clear whether N2a^{Piezo1^{-/-}} cells expressed deflection-sensitive currents.

The pillar array technique (**Figure 5.1**) was used to characterise the deflection-sensitive currents from N2a^{Wt} and N2a^{Piezo1^{-/-}} cells. As expected, all N2a^{Wt} cells that were tested expressed endogenously deflection-gated currents, presumably evoked from the activation of Piezo1 channels. Three types of MA currents were observed: RA, IA and SA currents (**Figure 5.2A**). The deflection threshold of the deflection-sensitive currents was 223 ± 44.65 nm (mean \pm s.e.m.). Interestingly, 10 out of 19 N2a^{Piezo1^{-/-}} cells tested lacked any deflection-sensitive currents in a range of 1 - 1000 nm (**Figure 5.2B**), and those that presented MA currents responded to less than 5% of the deflection stimuli in comparison to ~40% from N2a^{Wt} cells (**Figure 5.2C**; Student's t test; **** P<0.0001). In addition, when binning the peak currents of MA currents (see methods) from N2a^{Wt} and N2a^{Piezo1^{-/-}} cells we observed that N2a^{Piezo1^{-/-}} cells lost most of their deflection-gated currents, consistent with what was reported in Patkunarajah *et al.* 2020 (Patkunarajah et al., 2020). These data demonstrate that N2a^{Piezo1^{-/-}} cells largely lack endogenously MA currents and are a good model to study the biophysical properties of heterologously expressed pathogenic Piezo2 channels.

5.2. Biophysical properties of pathogenic mutations of Piezo2

GoF mutations in hPIEZO2 lead to different human diseases such as GS, DA and MWS (Alisch et al., 2016; B. Coste et al., 2013; Y. Ma et al., 2019; Mcmillin et al., 2014; Zapata-Aldana et al., 2019). We focused on studying the mutations occurring at R2756 of mPiezo2 (R2686 in hPIEZO2) because this Arg is highly conserved among PIEZO channels in different species (**Figure 5.3**). Interestingly, mutations in the homologous Arg of hPIEZO1 (R2456) causes human diseases such as HX and lymphatic dysplasia (Albuisson et al., 2013; Andolfo et al., 2013; Bae et al., 2013; Cahalan et al., 2015; Lukacs et al., 2015; Zarychanski et al., 2012). Mutations related to Xerocytosis change the biophysical properties of PIEZO1 by slowing the inactivation of the channel to mechanical stimuli and altering the voltage modulation of PIEZO1 by increasing the

apparent open probability of the channel (Albuisson et al., 2013; Bae et al., 2013; Moroni et al., 2018). However, the biophysical impact of mutations in R2686 of hPIEZO2 (R2756 in mPiezo2), and how they contribute to the observed phenotype in patients, have not been characterised in detail.

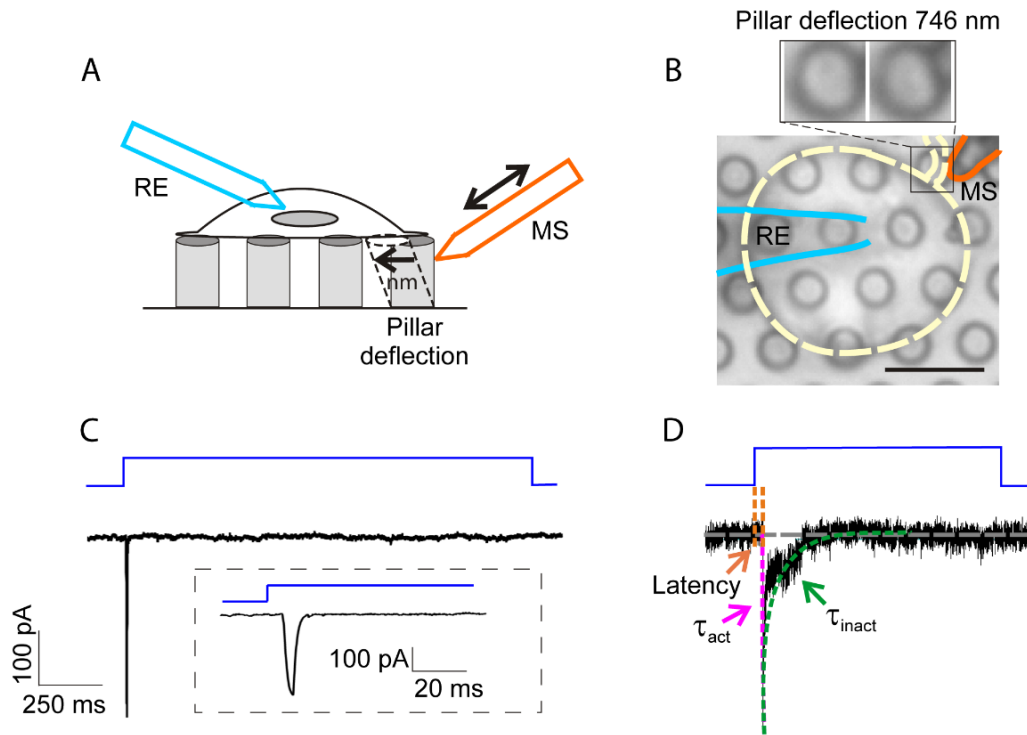


Figure 5.1. Pillar deflection

A. Schematic representation of the pillar deflection method. The cells were plated on the top of pillar arrays and a single pilus was deflected with a mechanical stimulator (MS). The MA currents were recorded with the patch-clamp technique at a holding potential of -60 mV. **B.** Bright field image of an embryonic DRG neuron cultured on laminin-coated pillar arrays. A pilus under the neurite of the cell was chosen and was mechanically deflected with the MS. In the insert, the position of a single pilus is shown before and after the deflection. The pillar deflection was calculated according to Poole et al. 2014. Bar scale, 10 μm . **C.** A representative recording of a RA current evoked after the mechanical stimulation (pillar deflection 746 nm). An amplification of the current peak is shown in the insert. **D.** Biophysical properties of deflection-gated currents. The latency is defined as the time interval between the mechanical stimulation and the activation of the MA ion channels. Activation and inactivation time constants (τ_{act} and τ_{inact} , respectively) are also shown. RE, recording electrode.

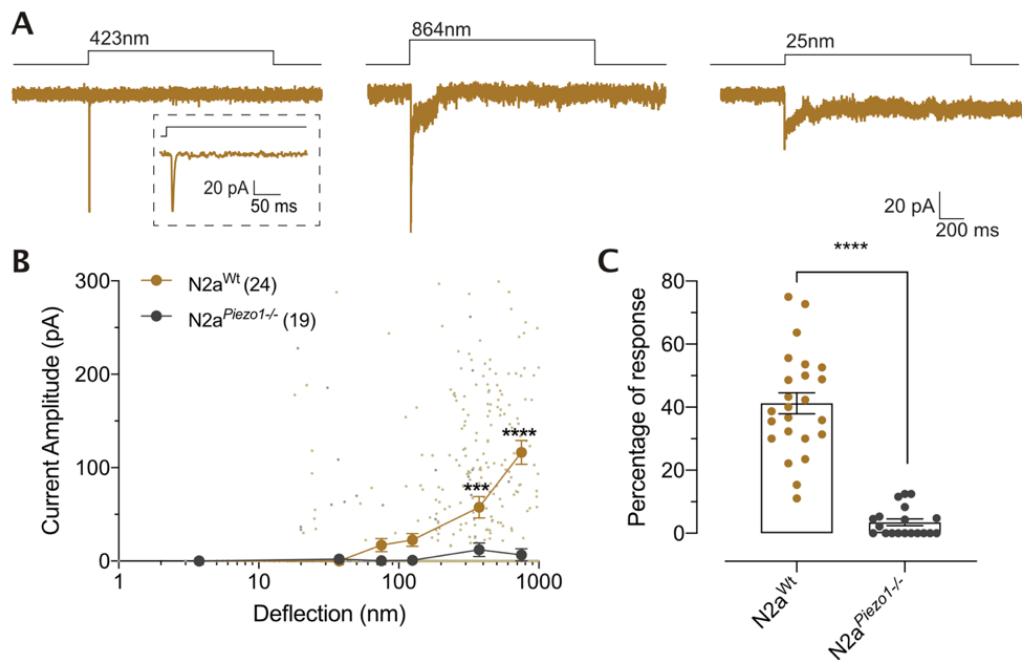


Figure 5.2. Characterization of the MA currents in N2a^{Piezo1-/-} cell with pillar arrays technique

A. Representative traces of the three different types of MA currents from Na2^{Wt} cells. Rapidly adapting (RA), intermediate adapting (IA) and slowly adapting (SA) currents were observed. The insert is an amplification of the RA trace showed. The deflection stimuli applied are indicated for each trace. **B.** Stimulus-response plot of the deflection sensitive currents from N2a^{Wt} (gold) and N2a^{Piezo1-/-} (gray) cells. Each small circle represents the value of individual peak currents. Recordings from each cell were binned according to the size of the stimuli (see methods) and the current amplitudes were averaged within each bin, then across the cells. Big circles were plotted as mean \pm s.e.m. (Two-way ANOVA, Sidak's multiple comparison test; *** $P=0.0005$, **** $P<0.0001$). **C.** Percentage of response to deflection stimuli (41.21 ± 3.32 and 3.47 ± 1.05 % for N2a^{Wt} and N2a^{Piezo1-/-}, respectively). The total amount of stimuli was considered as 100%. Note that the percentage of response of responsive N2a^{Piezo1-/-} cells is very low compared to the control. Each dot represents the percentage of individual cells. The data were plotted as mean \pm s.e.m. (Student's t test; **** $P<0.0001$). Experiments were made in parallel with Dr. Wei Zhong.

To investigate the biophysical consequences of these mutations, homologous pathological mutations of hPIEZO2 (R2686) were inserted in the mouse clone (R2756). The mutations reside on the TM38 or Inner Helix (IH) which is part of the pore-forming region of the channel (L. Wang et al., 2019) (**Figure 5.3**). Mutations R2756H and R2756C were inserted as they had been associated with GS, DA and MWS (Alisch et al., 2016; Mcmillin et al., 2014). Previous studies showed that the artificial mutation R2456K in hPIEZO1 cause a larger effect on the inactivation and voltage modulation of the channel than R2756H (Albuisson et al., 2013; Bae et al., 2013; Moroni et al., 2018). Therefore, even though PIEZO2 R2686K mutation have not been reported in humans, mPiezo2 R2756K mutant was included in this study.

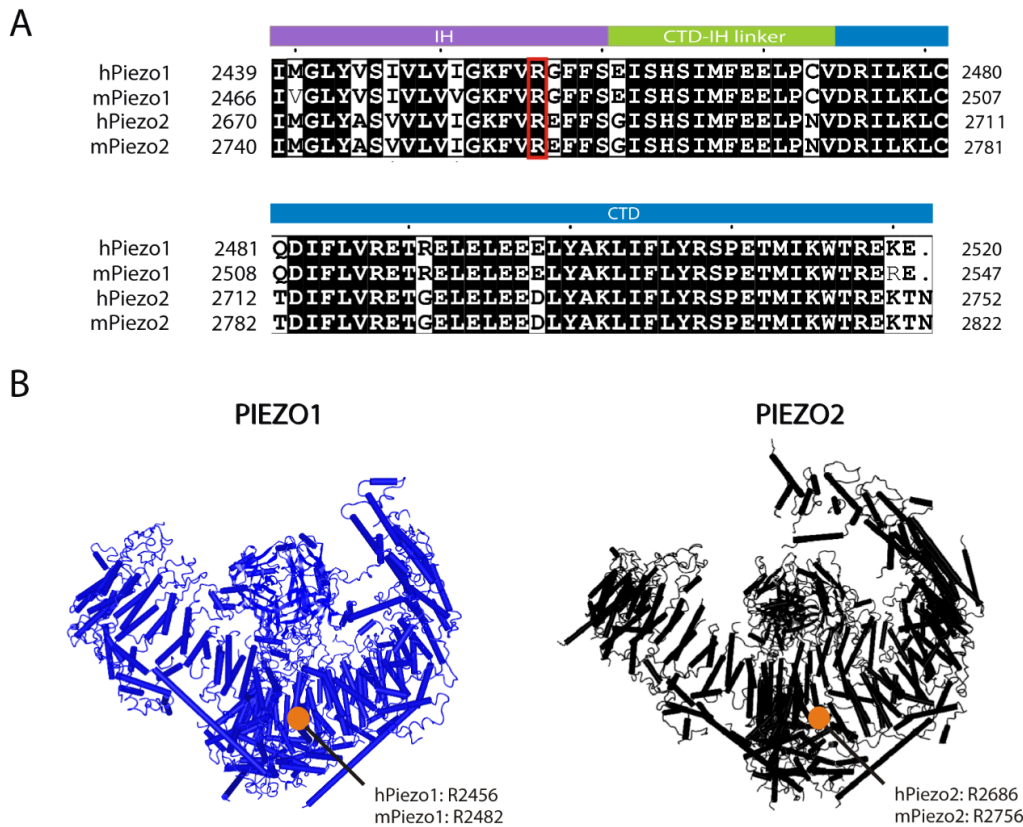


Figure 5.3. Amino acid residue alignment of the C-terminal domain of PIEZO channels

A. Sequence comparison between PIEZO channels. Note that the Arg (R, in red square) in PIEZO1 involved in Xerocytosis is conserved in PIEZO2 channels. Conserved amino acids are black-shaded. The domains showed in this figure were labelled as showed in Zhao et al. 2018. Amino acid alignment was done using ESPrpt 3.0 (Robert & Gouet, 2014). **B.** Atomic model of the trimeric PIEZO1 (left) (PDB ID: 4RAX (Guo & MacKinnon, 2017)) and PIEZO2 channels (right) (PDB ID: 6KG7 (L. Wang et al., 2019)). The red and green dots indicate the position of the Arg related to Xerocytosis and to GS, MWS and DA5, respectively. IH, Inner Helix; CTD-IH linker, C-Terminal Domain-Inner Helix linker; CTD, C-Terminal Domain.

First, the expression of mPiezo2 in N2a^{Piezo1^{-/-}} cells was established. With the pillar array technique, deflection-gated currents were recorded in the range of 1-1000 nm with very rapid inactivation kinetics in all the cells tested (n=14, **Figure 5.4**). The rapidly adapting currents observed are consistent with the biophysical properties of Piezo2 (B. Coste et al., 2013; Moroni et al., 2018; Taberner et al., 2019). As in previous studies, when binning the data according to the size of the stimuli, bigger currents were observed when larger stimuli were applied (**Figure 5.4 A, B**). This type of current was mostly absent in GFP-transfected cells where only 6 out of 12 cells responded to mechanical stimuli. Moreover, GFP-transfected cells responded to less than 3% of the deflection-stimuli in comparison to ~40% in mPiezo2-transfected cells (**Fig. 5.4 C**; Student's t test; **** P<0.0001). Thus, mPiezo2 is successfully expressed in N2a^{Piezo1^{-/-}} cells and its expression is associated with deflection-gated currents.

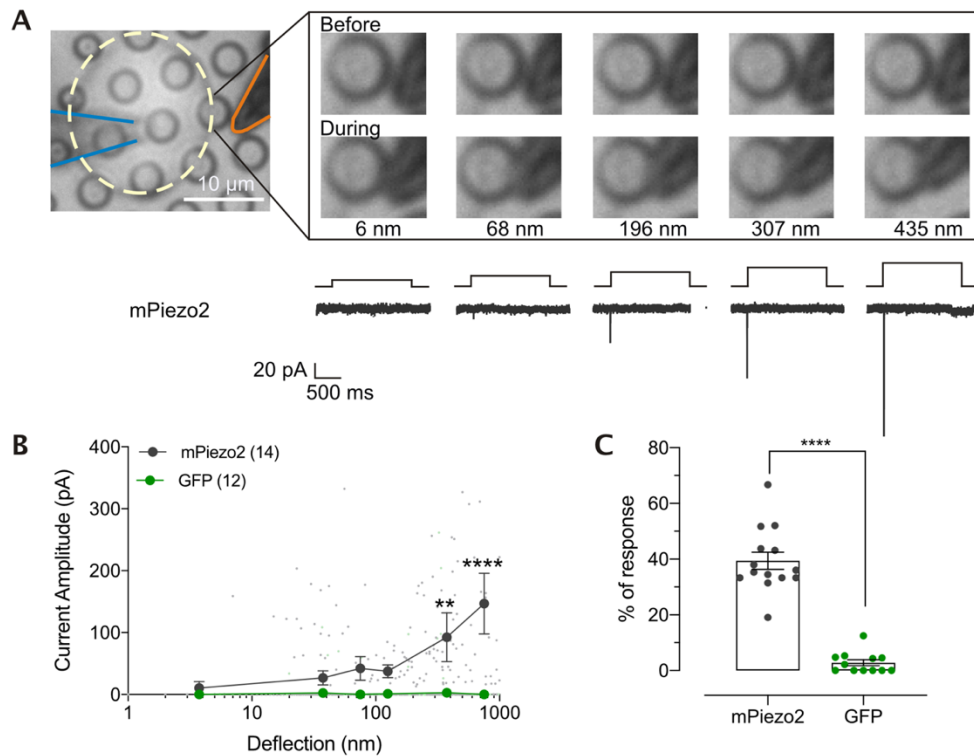


Figure 5.4. Expression of mPiezo2 channels in $N2a^{Piezo1-/-}$ cells lead to deflection-gated currents

A. Bright-field picture of a mPiezo2-transfected $N2a^{Piezo1-/-}$ cell cultured on pillar arrays. The insert shows an amplification of the stimulated pilus and the sequential stimuli applied with their corresponding deflection-gated inward current (grey traces). The representative traces correspond to RA currents. Note that the larger the deflection, the larger the MA current. **B.** Stimulus-response plot of the deflection sensitive currents from mPiezo2-transfected $N2a^{Piezo1-/-}$ (gray, mPiezo2) and GFP-transfected $N2a^{Piezo1-/-}$ (green, GFP) cells. Each small circle represents the value of individual peak currents. Recordings from each cell were binned according to the size of the stimuli (see methods) and the current amplitudes were averaged within each bin, then across the cells. The big circles were plotted as mean \pm s.e.m. (Two-way ANOVA, Sidak's multiple comparison test; ** $P=0.002$, **** $P<0.0001$). **C.** Percentage of response to deflection stimuli (39.39 ± 3.08 and 2.8 ± 1.09 % for mPiezo2- and GFP-transfected $N2a^{Piezo1-/-}$ cells, respectively). The total amount of stimuli was considered as 100%. Note that the percentage of response of responsive GFP-transfected $N2a^{Piezo1-/-}$ cells is very low compared to the control. Each dot represents the percentage of individual cells. The data were plotted as mean \pm s.e.m. (Student's t test; **** $P<0.0001$).

When overexpressing mPiezo2 variants in $N2a^{Piezo1-/-}$ and plotting the deflection-current amplitude relationship, no differences were observed between mPiezo2 wildtype, R27556H and R2756C mutants (**Figure 5.5 A**). Additionally, similar values were obtained when comparing the maximum peak current (I_{max}) (**Figure 5.5 B**) and the percentage of response to deflection-stimuli (**Figure 5.5 C**) from each cell between all mPiezo2 variants, suggesting that the channels were similarly expressed in the heterologous system. However, the R2756K variant showed more sensitive MA currents in the range of 51-100 and 101-250 nm (Mann Whitney test * $P=0.46$ and ** $P=0.008$, respectively) compared to the wildtype channel. Strikingly, current saturation occurred in the R2756K mutant within the stimulus range of this study, allowing us to determine the Half-maximal activation of approximately 76 nm by using a Boltzmann sigmoidal fit (**Figure 5.5**). Moreover, when examining the deflection threshold which is defined as the smallest

stimulus necessary to gate MA currents, cells overexpressing the R2756K mutant required ~5 times lower deflections to evoke mechanosensitive currents (210.6 ± 62.6 and 42.23 ± 12.4 nm for mPiezo2 and R2756K channels, respectively). Thus, the substitution of the R2756 by a lysine results in a five-fold increase of sensitivity to deflection-stimuli in mPiezo2.

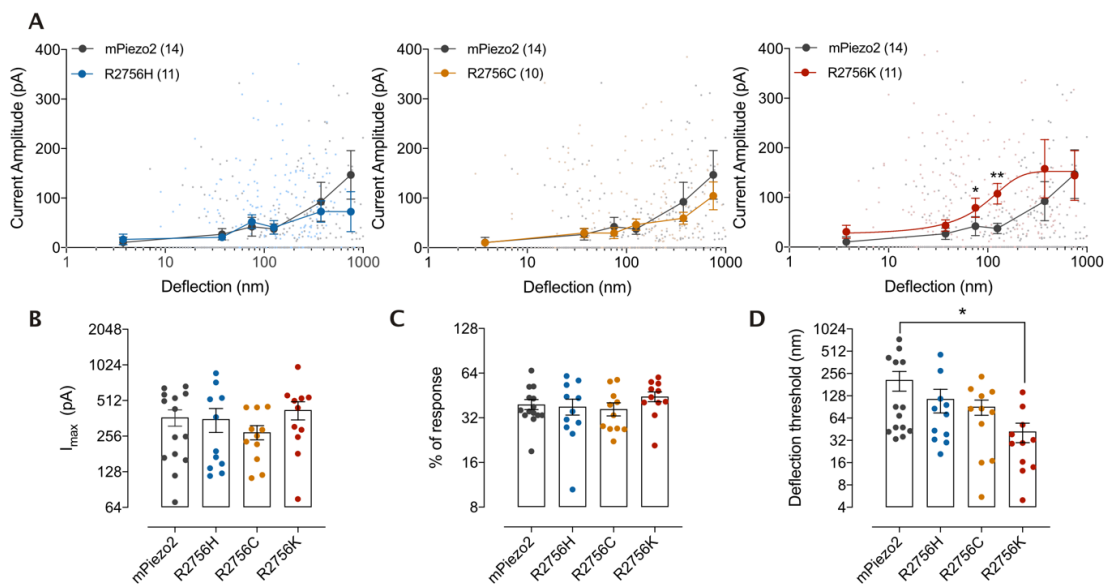


Figure 5.5. Mutations in R2756 of mPiezo2 increase the deflection sensitivity of the channel

A. Stimulus-response plot of the deflection sensitive currents from $N2a^{Piezo1-/-}$ cells expressing mPiezo2 (pink) and the mutants R2756H (orange), R2756C (blue) and R2756K (green). Each small circle represents the value of individual peak currents. Recordings from each cell were binned according to the size of the stimuli (see methods) and the current amplitudes were averaged within each bin, then across the cells. The big circles were plotted as mean \pm s.e.m. (Mann Whitney test $*P=0.46$, $**P=0.008$; two-way ANOVA indicates that the deflection-current amplitude relationship overall is not different between mutants and mPiezo2; n.s., $P>0.05$). **B.** Amplitude current was conserved in all the mutants. I_{max} (maximum peak current); each dot represents the I_{max} of individual cells. (368.8 ± 57.88 , 356.3 ± 81.26 , 276 ± 38.21 and 426.1 ± 74.49 pA for mPiezo2, R2756H, R2756C and R2756K, respectively; mean \pm s.e.m.; Kruskal-Wallis test; n.s., $P>0.5$). **C.** Percentage of response to deflection stimuli. The total amount of stimuli was considered as 100%. Each dot represents the percentage of individual cells. Data was plotted as mean \pm s.e.m. (Kruskal-Wallis test; n.s., $P>0.5$). **D.** Deflection threshold was increased in mPiezo2 mutants. Each dot represents the threshold of individual cells (mean \pm s.e.m.; Kruskal-Wallis test, $*P=0.01$).

Even though most of the recorded currents from mPiezo2-transfected cells were RA currents (83%), a minor proportion were classified as IA and SA currents (12 and 5%, respectively) (Figure 5.6 B). Strikingly, when evoking deflection-gated currents of R2756H, R2756C and R2756K mutants, the three types of currents were also recorded, however the proportion of IA slightly increased in mPiezo2 mutants (27, 25 and 18% in R2756H, R2756C and R2756K, respectively) (Figure 5.6 A, B). The latency of the currents, which is defined as time interval between the mechanical stimulus and the activation of the current, was longer in R2756H and R2756C mutants (Table 4). In addition, the τ_{act} and τ_{inact} of the R2756H mutant were slower than mPiezo2 wildtype (Fig. 5.6 C, Table 5.1). This finding suggests that mutations in the R2756 of mPiezo2 (R2686 in hPIEZO2) change the biophysical properties of the channel.

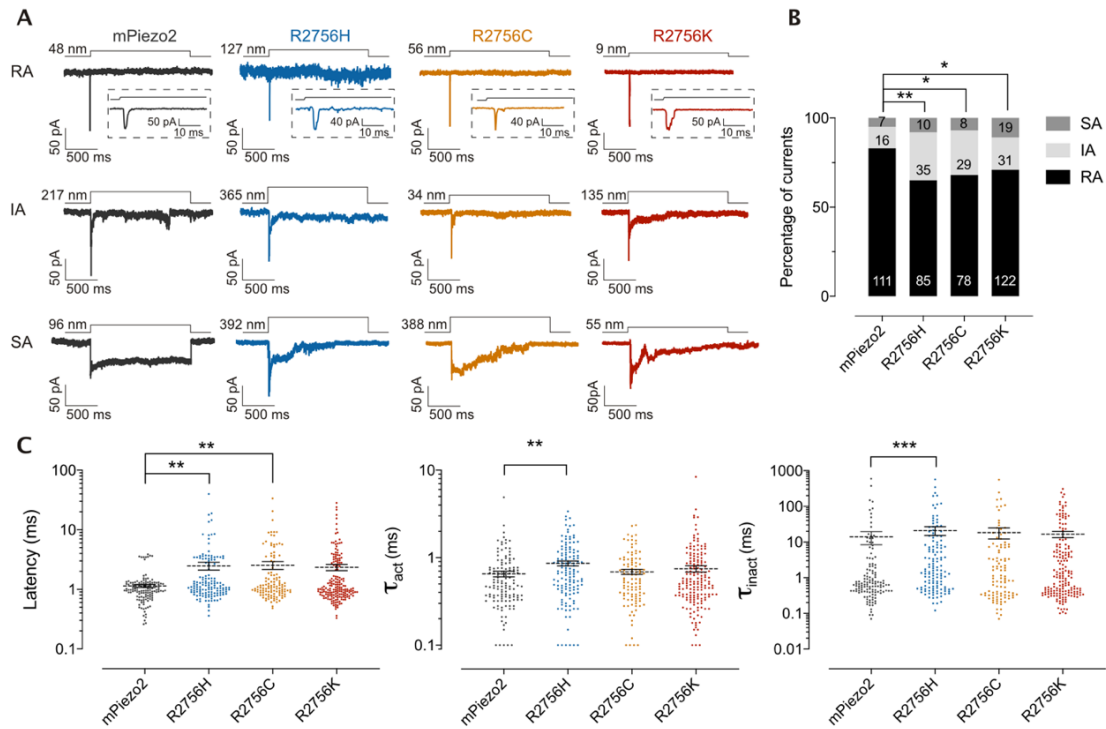


Figure 5.6. Pathogenic mutations that cause GS, DA5 and MWS change the biophysical properties of mPiezo2 channels

A. Representative traces of the three different types of deflection-gated currents from $N2a^{Piezo1-/-}$ cells expressing pathogenic mutants of Piezo2. Rapidly adapting (RA), intermediate adapting (IA) and slowly adapting (SA) currents were observed. The inserts are amplifications of the RA trace showed. The deflection stimuli applied are indicated for each trace. **B.** The percentage of IA and SA currents increased in the pathogenic mutants. The numbers in the histograms represent the number of the currents observed (χ^2 test, * $P < 0.05$, ** $P < 0.005$). **C.** The latency, time constant of activation (τ_{act}) and time constant of inactivation (τ_{inact}) of the deflection-gated currents were affected in some pathogenic mutants. (Kruskal-Wallis test, ** $P < 0.01$, *** $P < 0.0005$).

Table 5.1. Biophysical properties of $N2a^{Piezo1-/-}$ cells overexpressing mPiezo2 mutants

Number of cells and currents analysed from cells overexpressing pathogenic mutations of Piezo2. All data come from, at least, three different transfections. Mechanical latency, τ_{act} and τ_{inact} are shown for all cells including the values or RA, IA and SA groups. All data sets were not normally distributed. (Kruskal-Wallis test, * $P = 0.04$, ** $P < 0.01$, *** $P < 0.001$). Values are shown as mean \pm s.e.m.

	mPiezo2	R2756H	R2756C	R2756K
Cells (no. of currents)	14 (134)	11 (130)	10 (115)	11 (172)
Latency (ms)	1.14 \pm 0.62	2.47 \pm 0.37**	2.54 \pm 0.37**	2.34 \pm 0.27
RA	1.2 \pm 0.83	2.44 \pm 0.55	2.07 \pm 0.35	2.32 \pm 0.35
IA	1.35 \pm 0.28	2.47 \pm 0.54	3.34 \pm 0.65	2.61 \pm 0.76
SA	1.29 \pm 0.41	3.2 \pm 0.65	7.76 \pm 3.9	2.67 \pm 0.81
τ_{act} (ms)	0.65 \pm 0.04	0.86 \pm 0.05**	0.68 \pm 0.04	0.74 \pm 0.06
RA	0.60 \pm 0.05	0.72 \pm 0.05	0.58 \pm 0.03	0.62 \pm 0.04
IA	1.06 \pm 0.17	1.22 \pm 0.13	0.97 \pm 0.19	1.11 \pm 0.27
SA	1.14 \pm 0.23	0.81 \pm 0.18	0.9 \pm 0.25	0.96 \pm 0.16
τ_{inact} (ms)	14.02 \pm 5.64	21.08 \pm 5.86***	18.49 \pm 6.35	16.51 \pm 3.27
RA	0.83 \pm 0.08	1.76 \pm 0.1*	1.04 \pm 0.12	0.99 \pm 0.1
IA	17.62 \pm 3.28	16.74 \pm 2.01	15.25 \pm 1.75	17.99 \pm 3.07
SA	212.2 \pm 75.35	198.2 \pm 50.76	170.7 \pm 56.35	114.4 \pm 17.02

5.3. Voltage sensitivity of mutations related to GS, DA5 and MWS

Recently, it was shown that PIEZO channels are voltage modulated and that mutations related to xerocytosis in PIEZO1 change the channel availability of the mechanosensitive ion channel (Moroni et al., 2018). Therefore, we hypothesize that pathogenic mutations of PIEZO2 also affect the voltage sensitivity of the channel. To address this hypothesis, a stretch-sensitive chimeric channel (mP1/mP2) was generated, combining the N-terminal domain of Piezo1 and the pore forming part of Piezo2 (Moroni et al., 2018). It has been shown that the biophysical properties of mP1/mP2 chimeric channel overexpressed in heterologous systems remain those observed by overexpressing mPiezo2 (Moroni et al., 2018; Zheng, Nikolaev, et al., 2019). The homologous mutations corresponding to R2756 in Piezo2 were inserted in the chimeric channel.

By overexpressing mP1/mP2 mutants and performing HSPC in excised patches from $N2a^{Piezo1-/-}$ cells, robust stretch-activated currents were observed (**Figure 5.7**). As was previously shown (Moroni et al., 2018; Zheng, Nikolaev, et al., 2019), overexpression of mP1/mP2 chimeric channels lead to RA currents (**Figure 5.7 A**), similar to those observed from membrane-indentation Piezo2 currents (Moroni et al., 2018; Taberner et al., 2019; Zheng, Nikolaev, et al., 2019). Interestingly, the inactivation kinetics (τ_{inact}) of R2756H and R2756K were two- and six-times slower than the wildtype chimeric channels (mP1/mP2: 23.42 ± 2.42 ms, R2756H: 68.22 ± 9.45 ms, R2756K: 121 ± 27.93 ms; mean \pm s.e.m.) (**Figure 5.7 A, E**). When analyzing the ratio of the peak and the steady state of the currents (I_{peak} / I_{ss}) (**Figure 5.8**) it was found that R2756 mutants have a I_{peak}/I_{ss} ratio up to 14 times larger than the wildtype chimeric channel (mP1/mP2: 2.15 ± 1.26 ms, R2756H: 17.62 ± 4.41 ms, R2756C: 26.43 ± 5.5 ms, R2756K: 28.9 ± 6.34 ms; mean \pm s.e.m.). This data suggests that mutations in the R2756 of the mP1/mP2 channel lead to an increase of the ion influx, resulting in a slower inactivation of the current. Moreover, as it was seen with the pillar arrays, the time constant of activation (τ_{act}) was ~ 2 -folded slower in the mutants than in the wildtype chimeric channels (mP1/mP2: 4.3 ± 0.46 ms, R2756H: 7.35 ± 0.76 ms, R2756C: 8.25 ± 0.81 ms, R2756K: 7.77 ± 0.76 ms; mean \pm s.e.m.) (**Figure 5.7 D**). Thus, mutations in R2756 of mP1/mP2 chimeric channels corresponding to pathogenic mutations in Piezo2 resulted in change in the stretch sensitivity of the chimeric channel.

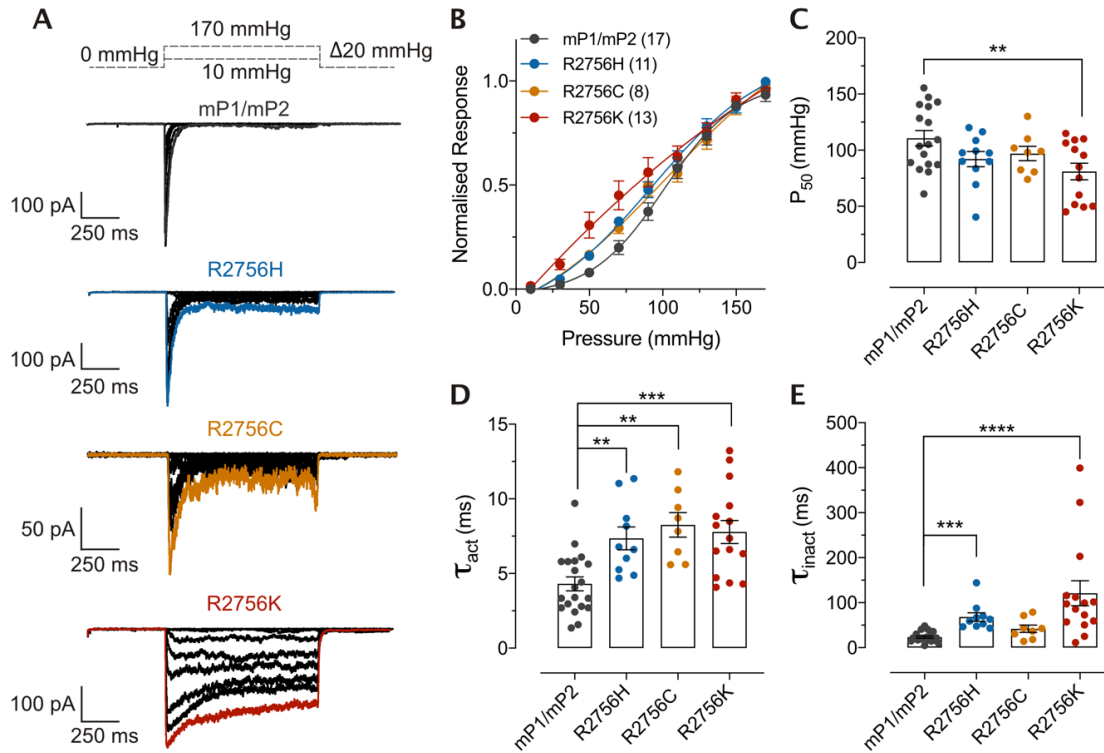


Figure 5.7. Mutations that cause GS, DA5 and MWS alter the biophysical properties of the mP1/mP2 chimeric channel

A. Representative recordings of stretch-sensitive currents of O/O patches from N2a^{Piezo1^{-/-}} cell expressing the chimeric channel mP1/mP2 and pathogenic mutations in PIEZO2. Patched were clamped at -60mV. The dashed lines above show the pressure protocol applied. **B, C.** Stretch-response curve and mechanical sensitivity of the chimeric channels. P₅₀ values were obtained by fitting a Boltzmann equation. The peak currents were normalised according to the maximum amplitude current recorded (one-way ANOVA, Dunnett's test, **P=0.007). Time constant of activation **D**, and inactivation **E** change in pathogenic mutants of the chimeric channels. The values correspond to the currents recorded at 130 mmHg pulse (one-way ANOVA, Dunnett's test, **P<0.005; ***P<0.0005). In all cases, values were plotted as mean ± s.e.m. In **C, D, E**, each dot represents the value of single cell measurements.

With pillar deflection experiments it was observed that mutations in the R2756 of mPiezo2 channels lead to more sensitive ion channels to substrate-deflection stimuli. We hypothesize that mutations in the R2756 of mP1/mP2 chimeric channels increase the stretch-sensitivity of the protein. Therefore, the pressure-response curve from the chimeric channels was measured with a step-pressure protocol (**Figure 5.7 A**) to calculate the half-maximal activation of the currents (P₅₀) by performing a Boltzmann fit. Similarly to what was observed on membrane-deflection experiments, higher sensitivity to stretch stimuli of the R2756K mutant was observed compared to the wildtype chimeric channel (80.98 ± 7.44 and 110.6 ± 6.79 mmHg for R2756K and mP1/mP2 channels, respectively, mean, s.e.m.; **P<0.005) (**Figure 5.7 B,C**). Even though an increase of the stretch sensitivity of R2756H and R2756C mutants was also seen, it was not statistically different than the wildtype chimeric channel (92.05 ± 6.75 and 96.99 ± 6.4 mmHg for R2756H and R2756C, respectively; mean, s.e.m.; P>0.5). Thus, with HSPC, as a complementary

assay, it is shown that mutations in the R2756 of Piezo2 increase the sensitivity of the channel to mechanical stimuli.

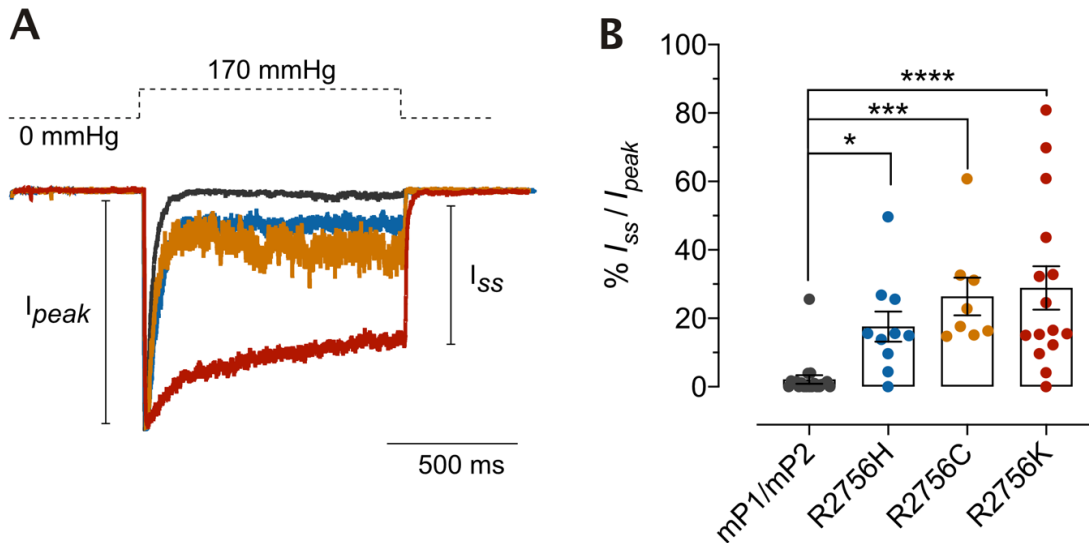


Figure 5.8. Pathogenic mutations in the chimeric channel affect the inactivation state

A. Normalised recordings of stretch-sensitive currents of O/O patches from $N2a^{Piezo1^{-/-}}$ cell expressing the chimeric channel mP1/mP2 and pathogenic mutations in PIEZO2. Patched were clamped at -60mV. The dashed lines above show the pressure protocol applied. **B.** Ratio of peak (I_{peak}) to steady-state (I_{ss}) current graph. The pathogenic mutations in the chimeric channel led to a slower inactivation, resulting in an increase of the flow of ions during the opening. The data were plotted as mean \pm s.e.m. (Kruskal-Wallis test; * $P=0.017$, ** $P=0.0003$, **** $P<0.0001$), each dot represents the value of single cell measurements.

To test whether mutations in R2756 of Piezo2 alter the voltage modulation of the mP1/mP2 chimeric channel, a tail current protocol (*see methods*) was performed. Recently, we found that the apparent open probability of Piezo channels was only ~10% at membrane potential of 0 mV and that mutations in the R2482 of mPiezo1 altered the voltage modulation of the channel by increasing the apparent open probability up to 70% at the same membrane potential (Moroni et al., 2018).

When the tail currents from mP1/mP2 mutants were analysed, the channel availability or apparent open probability of the mutants was increased compared to the wild type chimeric channel (**Figure 5.9**). As it was previously demonstrated (Moroni et al., 2018), the mP1/mP2 wild type channel only showed 10% of channel availability at 0 mV. When R2756 was mutated to Histidine (H), Cysteine (C) or Lysine (K) the apparent open probability increased to 40, 35 and 50% at membrane potential of 0 mV, respectively (see tail currents in **Figure 5.9 A** inserts and **B**). When R2482 was mutated to lysine or histidine in mPiezo1, the voltage modulation (V_{50}) was shifted ~60 mV to negative voltages (Moroni et al., 2018). In contrast to what was observed in pathogenic mutations of Piezo1, mutations in the mP1/mP2 chimeric channel did not change the V_{50} (mP1/mP2 wildtype: $V_{50}= 90.25 \pm 5.36$ mV; R2756H: $V_{50}= 91.32 \pm 5.79$ mV;

R2756C: $V_{50} = 86.25 \pm 5.4$ mV; R2756K: $V_{50} = 77.36 \pm 7.16$ mV) (**Figure 5.9 C**). This data indicates that mutations in the residue R2756 of Piezo2 increase the apparent probability of the channel but do not affect the voltage modulation of the channel.

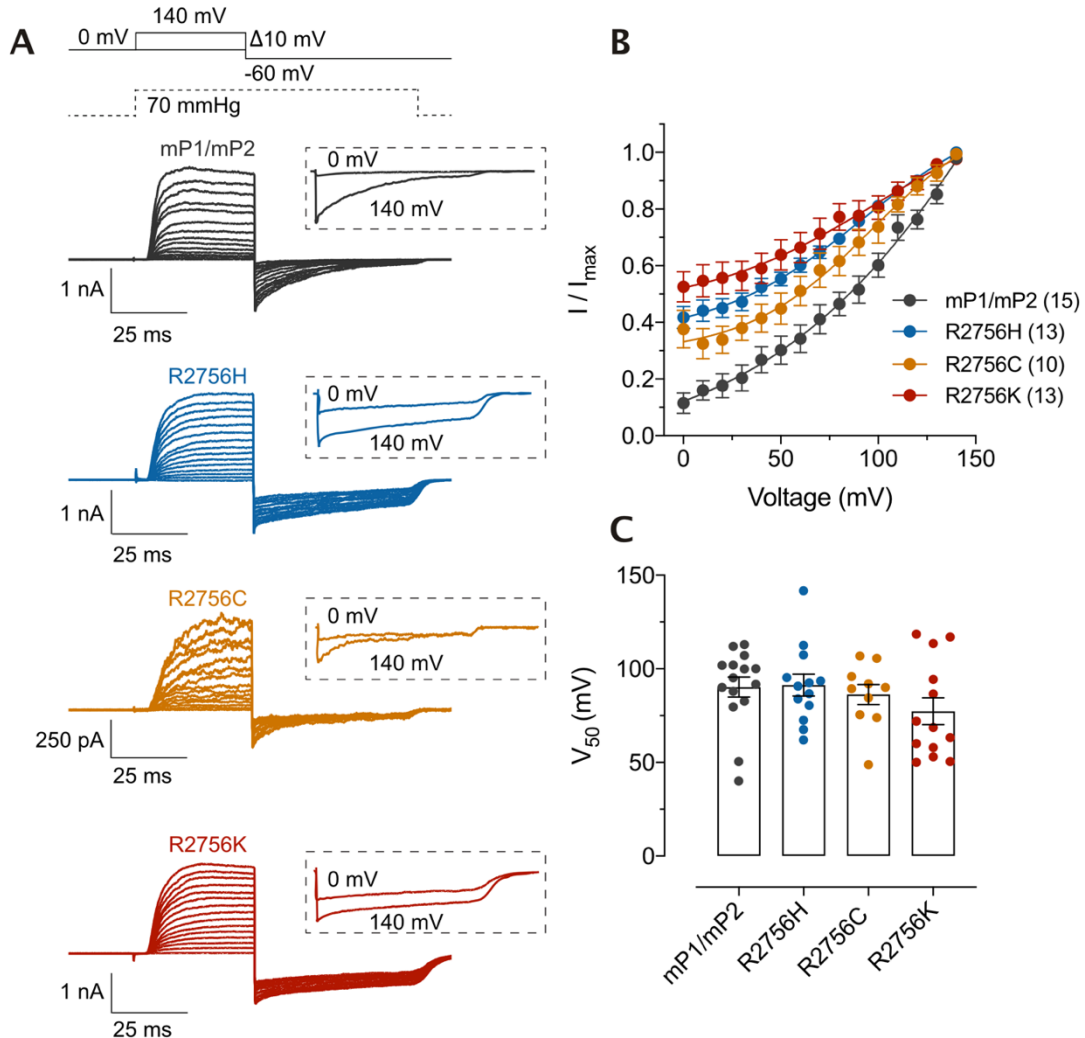


Figure 5.9. Mutations that cause GS, DA5 and MWS modify the voltage modulation of mP1/mP2 chimeric channel
A. Representative traces of the tail current protocol performed in $N2a^{Piezo1-/-}$ cells expressing the chimeric channels to study the apparent open probability of the channel. O/O patches were clamped to voltage steps ranging from 0 to 140 mV (pre-stimuli), followed by a repolarization step to -60 mV in the presence of pressure stimuli of 70 mmHg. In the insert, tail currents evoked after pre-stimuli of 0 and 140 mV are shown. Note that tail currents at 0 mV in the mutants are larger than in the wt (mP1/mP2) channel. **B.** The apparent open probability increased in the mutants. Tail currents were normalized to their maximum and fitted to a Boltzmann relationship. **C.** V_{50} values did not change in the mutants. Values were obtained from the analysis made in B. Each dot represents the value from individual patches (mean \pm s.e.m.; Kruskal-Wallis test; n.s., $P > 0.5$).

When measuring the ratio of the peak and steady-state (50 ms after peak) of the instantaneous tail currents (I_{ss}/I_{peak}) at -60 mV (see schematic in **Figure 5.10 A**), it was found that mutant channels have up to 5-fold larger steady-state current magnitude compared to wildtype channels. Notably, 6/15 of membrane patches of wildtype channels fully inactivated within 50 ms. (**Figure 5.10 A**). Moreover, when fitting the kinetics of the currents after removing the pressure pulse, it

was found that the remaining current from R2756H and R2756K variants deactivated 3 and 5-fold slower than the wildtype chimeric channel (only wildtype patches that did not inactivate completely were considered for this analysis; **Figure 5.10 C**). These data suggest that substitutions of Arg2756 by His and Lys increase the time required to go from inactivated to deactivated states which would result in channels that continue to pass current in the absence of a mechanical stimulus.

Differences in the tail currents from R2756 mutants could be explained because mutations in this residue could affect the outward or inward conductivity of the channel. Therefore, a rectification index protocol ($R_i = I_{\text{ins-60mV}} / I_{60\text{mV}}$) was performed. The R_i protocol consisted in applying a positive voltage step of 60 mV followed by a step of -60 mV to measure the steady-state activation during the positive potential and the instantaneous inward current when clamping the patches at negative potential, respectively (**Figure 5.10 A**). In all cases, the rectification index was close to one, suggesting that the pore conducts outward and inward macroscopic currents equally (mP1/mP2 wildtype: $R_i = 1.04 \pm 0.09$; R2756H: $R_i = 1.1 \pm 0.04$; R2756C: $R_i = 1.06 \pm 0.07$; R2756K: $R_i = 1.23 \pm 0.05$) (**Figure 5.10 B**). Thus, pathogenic mutations in the residue R2756 of Piezo2 do not affect the pore properties of the channel.

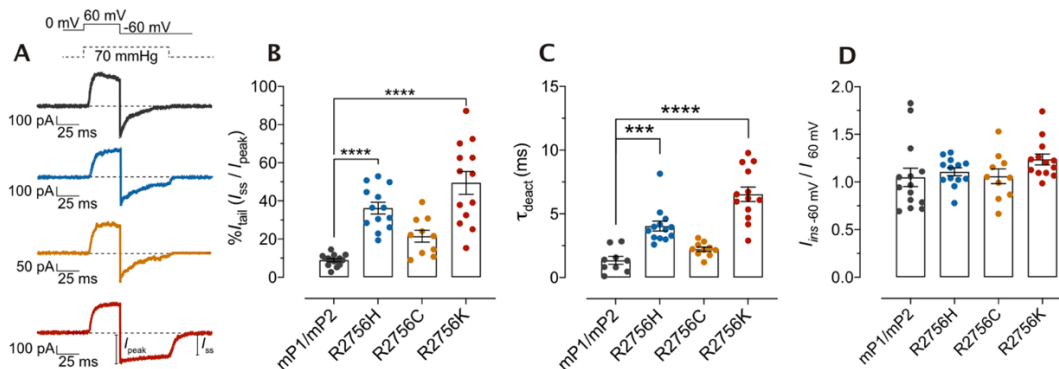


Figure 5.10. The mP1/mP2 variants deactivate slower and conducts equally in both directions

A. Representative traces of the rectification index protocol performed in $N2a^{Piezo1-/-}$ cells expressing the chimeric channels. O/O patches were clamped to a voltage step of +60 mV followed by a step of -60 mV in the presence of pressure stimuli of 70 mmHg. Peak (I_{peak}) and steady-state (I_{ss}) currents are indicated. **B.** Ratio of I_{peak} to I_{ss} from the instantaneous tail currents (I_{tail}) at -60 mV (mean \pm s.e.m.; Dunnett test; **** $P < 0.0001$). **C.** Kinetics of the inactivation-deactivation state (τ_{deact}) from mP1/mP2 variants (mean \pm s.e.m.; Kruskal-Wallis test; ** $P = 0.0015$, **** $P < 0.0001$). **D.** Rectification index ($I_{\text{ins-60mV}} / I_{60\text{mV}}$) plot (mean \pm s.e.m.; Kruskal-Wallis test; n.s., $P > 0.1$). Each dot represents the value from individual patches

We conclude that, *in vitro*, mutations in the residue R2756 of mPiezo2 are gain of function mutations. The pathogenic mutations change the biophysical properties of the channel, increase the pillar deflection- and membrane stretch-sensitivity and dramatically increase the apparent open probability of the channel.

5.4. Physiological characterization of Piezo2^{R2756H} and Piezo2^{R2756K} mice

As shown above, mutations in the R2756 in Piezo2 change the biophysical properties and increase the channel availability and the sensitivity to mechanical stimulation of the channel. To show that these results have relevance *in vivo*, CRISPR-Cas9 technology was used (*see methods*) to generate two *knock-in* (KI) mice that carry the mutations R2756H and R2756K in Piezo2 (Piezo2^{R2756H} and Piezo2^{R2756K}, respectively) (**Figure 5.11 A, B**). Piezo2 mutants were born with normal Mendelian frequencies (**Figure 5.11 C**). Mendelian frequencies were calculated from 10 and 12 litters of Piezo2^{R2756H} and Piezo2^{R2756K}, respectively. The average size of litters was 8 and 6.58 for Piezo2^{R2756H} and Piezo2^{R2756K} mice, respectively.

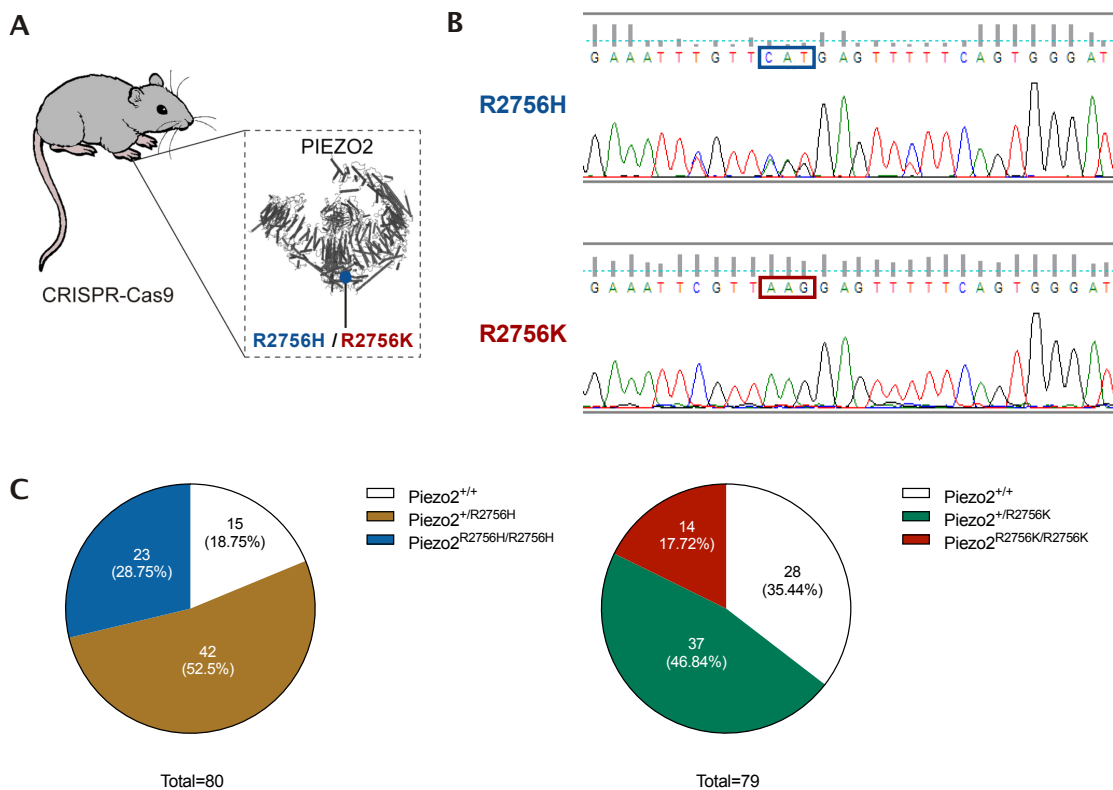


Figure 5.11. Generation of Piezo2 knock-in mice.

A. Cartoon representing the global insertion of mutations R2756H and R2756K of mPiezo2. **B.** Sequencing results from founder mice carrying the mutations R2756H (above) and R2756K (below) in Piezo2. The nucleotides mutated are highlighted inside the squares. Note that in Piezo2 wild type animals Arg is encoded by CGT codon (*not shown*). **C.** Pie charts for the genotype of Piezo2^{R2756H} (*left*) and Piezo2^{R2756K} (*right*) with 80 and 79 cases, respectively. Frequencies fitted to Mendelian rates ($P=0.4$ and $P=0.07$ for Piezo2^{R2756H} and Piezo2^{R2756K}, respectively; χ^2 test).

In humans, pathogenic mutations related to GS, DA5 and MWS are autosomal dominant disorders in which only the mutation of one allele is sufficient to cause pathogenic effects. Therefore, in the present study, heterozygous and homozygous conditions from Piezo2^{R2756H}

(Piezo2^{+/R2756H} and Piezo2^{R2756H/R2756H}, respectively) and Piezo2^{R2756K} (Piezo2^{+/R2756K} and Piezo2^{R2756K/R2756K}, respectively) mice were included.

Patients with GS, DA5 and MWS show short stature and progressive scoliosis, suggesting that PIEZO2 is important to sense and orchestrate biological processes during development (Alisch et al., 2016; Haliloglu et al., 2017; Mcmillin et al., 2014). We hypothesize that in mice, the introduction of mutations in R2756 in mPiezo2 would have a similar effect as in humans. Therefore, Piezo2^{R2756H} and Piezo2^{R2756K} mice were monitored during post-natal development (4 and 8 weeks old) to investigate whether mutations in R2756 affect the size of the animals. To compare the animal size, mice were weighed at 4 and 8 weeks old. Interestingly, only Piezo2^{R2756H/R2756H} mice showed decreased weight at week four compared to wildtype animals (Piezo2^{+/+}: 12.2 ± 0.6 g, Piezo2^{+/R2756H}: 11.8 ± 0.4 g, Piezo2^{R2756H/R2756H}: 8.6 ± 0.7 g, Piezo2^{+/R2756K}: 11.9 ± 0.4 g, Piezo2^{R2756K/R2756K}: 11.1 ± 1.1 g). However, at week eight, Piezo2^{R2756H/R2756H} animals showed similar weight to Piezo2^{+/+} (Piezo2^{+/+}: 20.4 ± 0.6 g, Piezo2^{+/R2756H}: 18.6 ± 0.4 g, Piezo2^{R2756H/R2756H}: 17.2 ± 1.1 g, Piezo2^{+/R2756K}: 19.3 ± 0.6 g, Piezo2^{R2756K/R2756K}: 18.2 ± 1.0 g) (Figure 15.2). Moreover, two out of five Piezo2^{R2756K/R2756K} animals examined, developed spinal cord curvature similar to what is observed in humans that develop scoliosis (Figure 15.3). The rest of the genotypes analysed did not show scoliosis. Thus, R2756 mutations in Piezo2 do not affect the Mendelian ratio but led to short stature and spinal cord curvature in a minority of mice, suggesting that function of PIEZO2 is conserved in mice and humans.

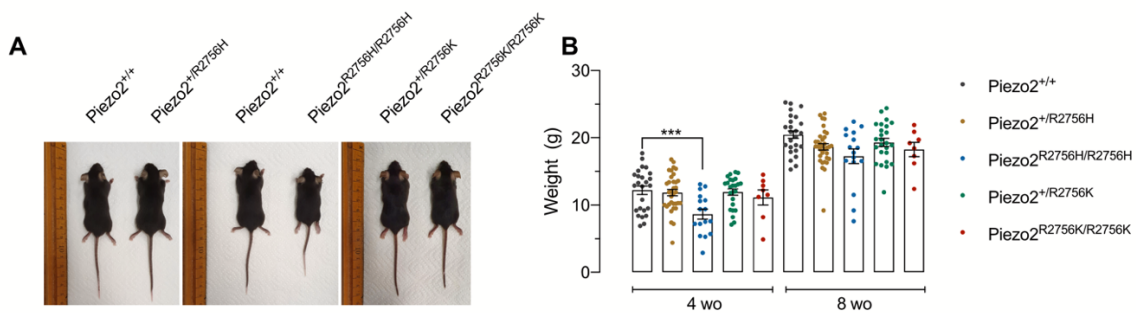


Figure 5.12. Piezo2^{R2756H/R2756H} animals have reduced size compared to wildtype mice

A. Photos of knock-in mice at 5 weeks old (wo). Note that Piezo2^{R2756H/R2756H} mice are smaller than the rest of genotypes. **B.** Bar plot showing that Piezo2^{R2756H/R2756H} mice are smaller at week four after birth but recover normal size by week 8. Each dot represents an animal (n=25, 34, 16, 25 and 8 for Piezo2^{+/+}, Piezo2^{+/R2756H}, Piezo2^{R2756H/R2756H}, Piezo2^{+/R2756K} and Piezo2^{R2756K/R2756K}, respectively; mean ± s.e.m.; One-Way ANOVA test; ***P=0.0008).



Figure 5.13. Piezo2^{R2756K/R2756K} animals develop spinal cord curvature
 Pictures of Piezo2^{+/+} (left), Piezo2^{R2756H} (center) and Piezo2^{R2756K} (right) mice at 10-12 weeks old. Note that in some Piezo2^{R2756K} mice curvature of spinal cord was observed.

5.5. Characterization of MA currents in DRG neurons from Piezo2^{R2756H} and Piezo2^{R2756K} mice

PIEZO2 is highly expressed in DRG neurons and has been proposed to be the major mechanotransducer in sensing light touch and pain sensations in mammals (B. Coste et al., 2010; Maksimovic et al., 2014; Murthy, Loud, et al., 2018; Poole et al., 2014; Szczot et al., 2018). In humans, LoF mutations of *PIEZO2* result the disruption of in vibratory and touch sensations (Chesler et al., 2016; Mahmud et al., 2017; Yamaguchi et al., 2019) as well as reduction of nocifensive responses to pain stimuli (Behunova et al., 2019). Additionally, patients with mutations in the I802 of *PIEZO2* were suspected to have altered pain sensation (B. Coste et al., 2013), suggesting that GoF mutations could increase the sensitivity of the channel to mechanical stimuli. Strikingly, even though missense mutations in the R2686 of *PIEZO2* that cause pathogenic diseases in humans have been proposed as GoF mutations (Alisch et al., 2016; Mcmillin et al., 2014), they have not been characterized in the sensory system in humans and mice. We hypothesized that by substituting the homologous R2686 of hPIEZO2 in mPiezo2 (R2486), the biophysical properties and the sensitivity of MA currents from sensory neurons would result in GoF mutations, changing their inactivation and increasing their sensitivity to mechanical stimuli as we observed *in-vitro*. Therefore, mechanoreceptors and nociceptors from Piezo2^{R2756H} and Piezo2^{R2756K} mice were isolated and cultured on elastomeric pillar arrays to study the properties of endogenous MA currents.

Sensory neurons were classified into mechanoreceptors and nociceptors according to their size and action potential (AP) shape as was previously reported (Koerber et al., 1988; Lechner et al., 2009; Poole et al., 2014; Rose et al., 1986) (**Figure 5.14**). Mechanoreceptors have narrow APs while nociceptors can be identified by their broad and humped APs. By performing current-clamp recordings from wildtype and mutant sensory neurons, APs without and with humps in the repolarization phase corresponding to mechanoreceptors and nociceptors, respectively, were recorded. When analyzing the resting membrane potential (E_m) between mechanoreceptors and nociceptors from wildtype and *knock-in* mice, no differences were found (**Table 5.2, 5.3**). Thus, in mice, mutations in R2756 of Piezo2 do not change E_m in sensory neurons.

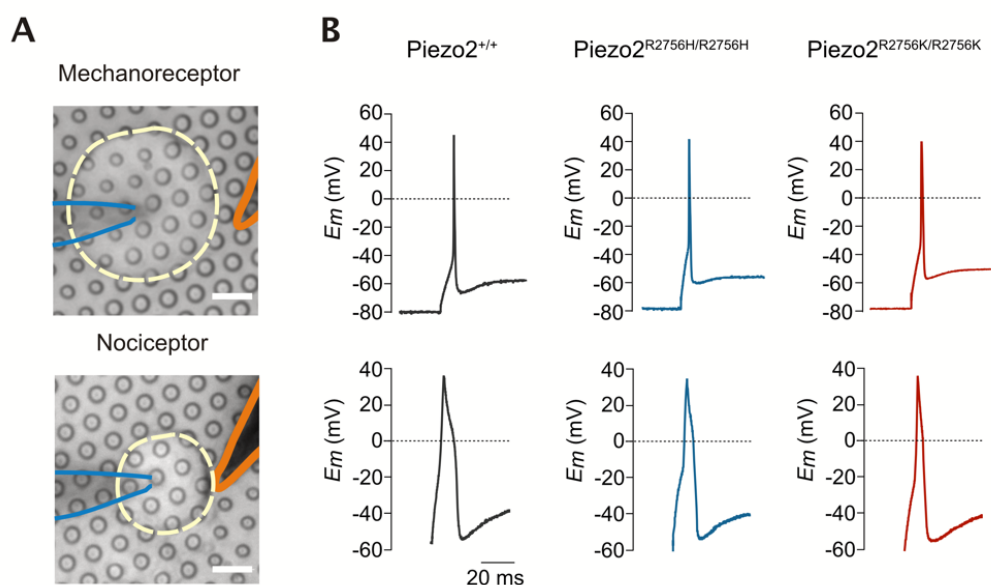


Figure 5.14. Types of sensory neurons

A. DRG neurons were cultured on pillar arrays and classified into mechanoreceptors (above, large cells) and nociceptors (below, small cells) according to their size and the shape of their APs. In blue and orange, the electrodes corresponding the recording electrode and mechanical stimulator are shown, respectively. Bar scale indicates 10 μm . **B.** Representative APs in sensory neurons from Piezo2^{+/+}, Piezo2^{R2756H/R2756H} and Piezo2^{R2756K/R2756K} mice.

5.5.1. Characterization of MA currents in mechanoreceptors from Piezo2^{R2756H} and Piezo2^{R2756K} mice

To characterize MA currents in mechanoreceptors from *knock-in* mice, sensory neurons with narrow AP were stimulated with the pillar arrays technique. In the range of 1-1000 nm stimuli, 13 out of 17 (76.4%) mechanoreceptors from wildtype mice responded to mechanical pulses. A similar percentage was observed in mechanoreceptors from *knock-in* mice (75%, 83%, 70% and 75% for Piezo2^{+/R2756H}, Piezo2^{R2756H/R2756H}, Piezo2^{+/R2756K} and Piezo2^{R2756K/R2756K}, respectively; **Figure 5.15 A**). Additionally, when analysing the deflection-current amplitude relationship no differences were detected between the different genotypes (**Figure 5.15 B**). However, consistent

to the *in-vitro* experiments in the heterologous system, mechanoreceptors from Piezo2^{R2756K/R2756K} reached a current amplitude saturation. By using a Boltzmann sigmoidal fit, the half-maximal activation of mechanoreceptors from Piezo2^{R2756K/R2756K} was ~110 nm (Figure 5.15 B). Additionally, when calculating the deflection threshold of MA currents in mechanoreceptors, neurons from all mutants required lower deflections to evoke mechanosensitive currents. Mechanoreceptors from *knock-in* mice were up to five-fold more sensitive compared to wildtype neurons (Piezo2^{+/+}: 145.5 ± 30.6 nm, Piezo2^{+/R2756H}: 29.1 ± 6.0 nm, Piezo2^{R2756H/R2756H}: 26.2 ± 5.0 nm, Piezo2^{+/R2756K}: 40.25 ± 8.9 nm, Piezo2^{R2756K/R2756K}: 44.8 ± 13.2 nm) (Figure 5.15 E). Moreover, when comparing the percentage of MA current types from mechanoreceptors, a reduction of ~10% of RA currents was observed in Piezo2^{R2756H/R2756H} and Piezo2^{+/R2756K}, as it was observed in the heterologous system (Figure 5.15 C, D). Thus, mutations in one of the alleles of *piezo2* is sufficient to increase the mechanical sensitivity to deflection-stimuli and change the inactivation kinetics of mechanoreceptors from mice *in-vitro*.

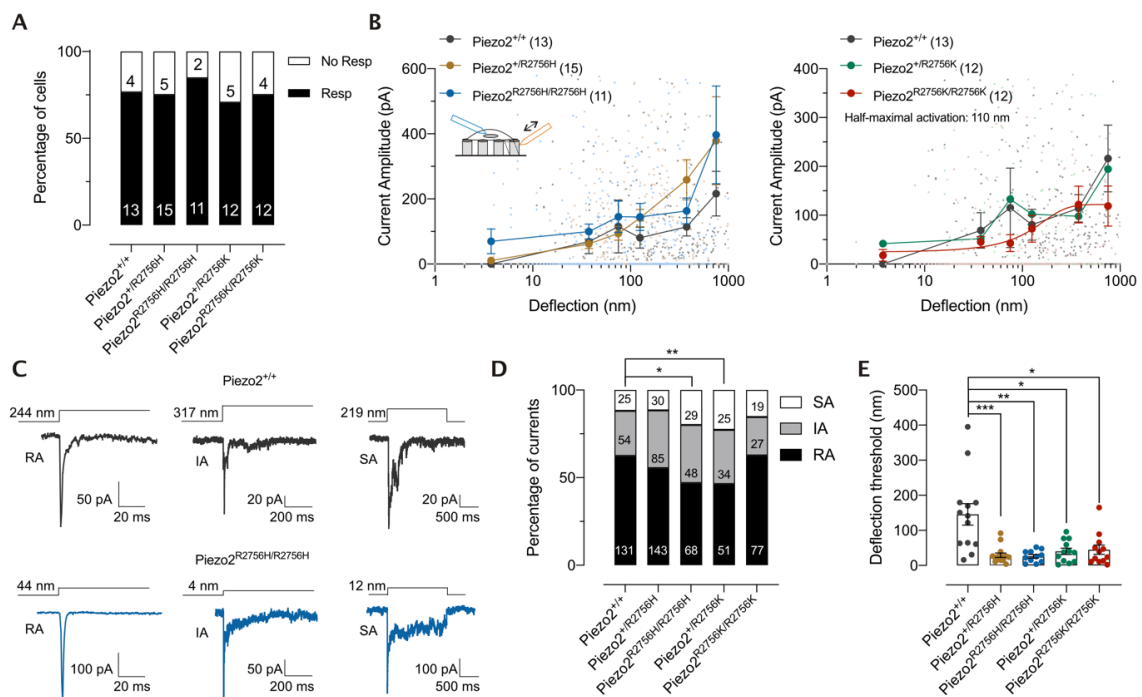


Figure 5.15. Insertion of R2756 mutations in Piezo2 changes IA and SA current ratios and increase sensitivity of mechanoreceptors

A. Stacked histogram showing the percentage of responsive (Resp) and non-responsive (No Resp) mechanoreceptors to pillar deflection. Numbers indicate the number of cells. **B.** Stimulus-response plot of the deflection sensitive currents in mechanoreceptors from Piezo2^{+/+} and *knock-in* mice. Each small circle represents the value of individual peak currents. Big circles show the mean ± s.e.m of binned currents. Note that current saturation was observed in Piezo2^{R2756K/R2756K} DRGs. **C.** Representative traces of the three different types of deflection-gated currents in mechanoreceptors from Piezo2^{+/+} and Piezo2^{R2756H/R2756H} mice. RA, IA and SA currents were observed. **D.** The percentage of IA and SA currents increased in mechanoreceptors from *knock-in* mice. The numbers in the histograms represent the number of the currents observed (χ^2 test, *P=0.01, **P=0.009). **E.** Deflection threshold was increased in mechanoreceptors from *knock-in* mice. Dots represent the deflection threshold in individual cells. Data is shown as mean ± s.e.m (Kruskal-Wallis test; *P<0.1, **P=0.001, ***P=0.0008)

When analysing the Maximum Peak Current (Max. Peak Current) recorded from individual cells, no differences were found between mutants and wildtype DRG mechanoreceptors (**Figure 5.16 A**). However, when comparing the deflection stimulus- Max. Peak Current relationship from each cell, mechanoreceptors from *knock-in* mice reached the Max. Peak Currents at lower pillar deflections (**Figure 5.16 B, C**). This data supports the evidence that mutations in one allele of *piezo2* that encodes R2756 is sufficient to increase deflection-sensitivity in large DRG neurons.

Finally, consistent with what was observed in the heterologous system, evoked MA currents in mechanoreceptors from *knock-in* mice displayed different biophysical properties compared to wildtype sensory neurons (**Figure 15.17 and Table 5.2**). When pooling all deflection-sensitive currents, a delay in the latency of mechanosensitive currents in neurons from *Piezo2*^{R2756K} was observed (**Figure 15.17 A**). Additionally, the τ_{act} was slower in all mutants and inactivation kinetics were slower in *Piezo2*^{R2756H/R2756H} and in *Piezo2*^{+ /R2756K} (**Figure 5.17 B, C**). Moreover, when analysing the kinetics values according to type of currents classification, the biophysical properties of RA and IA currents from mutant neurons were clearly different compared to wildtype currents (**Table 5.2**). These data support previous studies indicating that RA currents are Piezo2-dependent in sensory neurons (B. Coste et al., 2010; Ranade, Woo, et al., 2014). Thus, *Piezo2*^{R2756H} and *Piezo2*^{R2756K} mechanoreceptors display more sensitive MA currents with different biophysical properties than wild type sensory neurons.

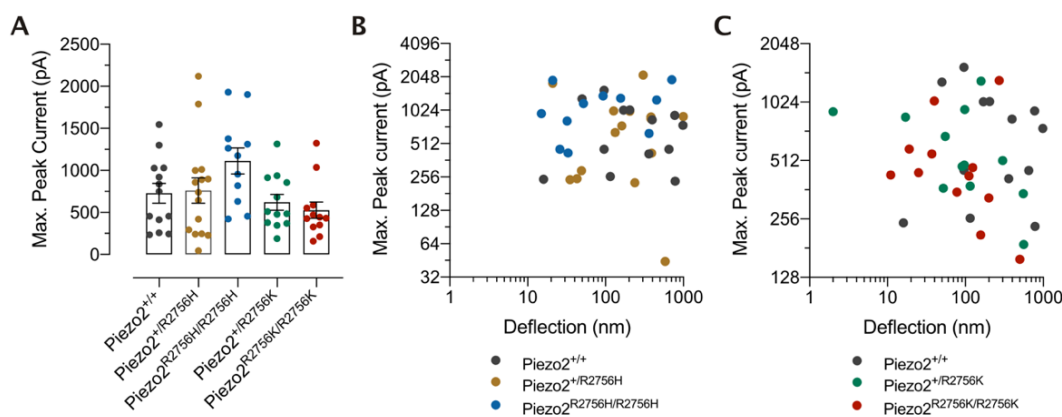


Figure 5.16. Maximum peak currents of mechanoreceptors were reached at smaller deflections *knock-in* mice. A. Maximum peak current values obtained in mechanoreceptors. Data is shown as mean \pm s.e.m. B, C. Stimulus Response-Maximum peak current relationships of mechanoreceptors from *Piezo2*^{+/+} and *Piezo2*^{R2756} mutants. Note that in neurons from knock in mice the maximum peak currents were obtained at smaller pillar deflections compared to wild type DRGs.

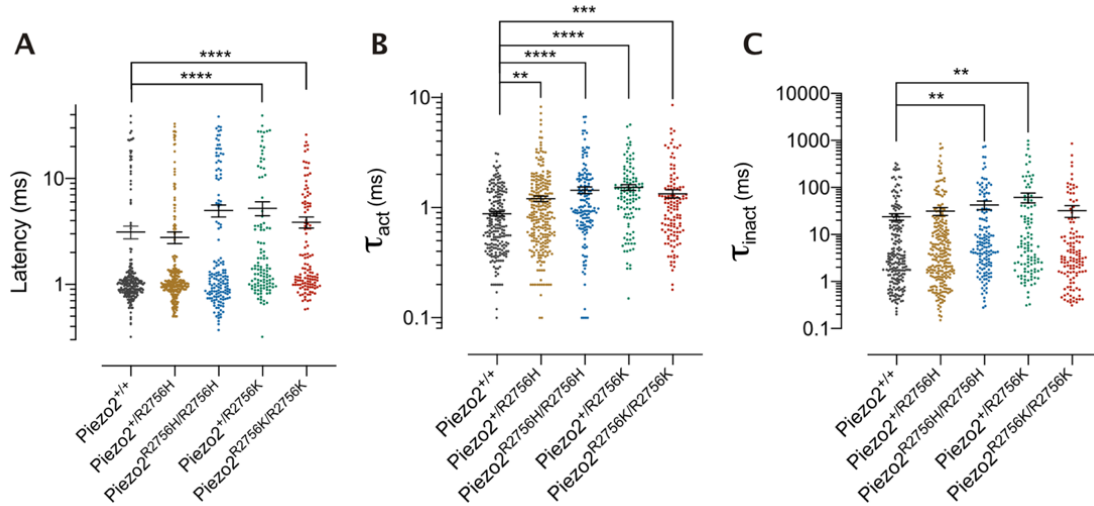


Figure 5.17. Mutations in R2756 of Piezo2 channels change biophysical properties of mechanoreceptors in mice
A. Latency of MA currents was increased in mechanoreceptors from knock on mice. The τ_{act} (**B**) and τ_{inact} (**C**) of MA currents from mechanoreceptors were slower in Piezo2 mutants. Each dot represents the biophysical properties of each current in all cells tested. Bars indicate mean \pm s.e.m. (Kruskal-Wallis test, ** $P<0.01$, *** $P<0.001$, **** $P<0.0001$).

Table 5.2. Biophysical properties of deflection gated currents in mechanoreceptors from Piezo2^{R2756H/K} mice

Sex and number of animals (m, male, f, female) used in the study. Cells and currents analysed in mechanoreceptors for each genotype are shown. Cell size and half peak (HP) of APs were used to classified DRG neurons into mechanoreceptors. Mechanical latency, τ_{act} and τ_{inact} are shown for all genotypes including the values or RA, IA and SA groups. All data sets were not normally distributed. (Kruskal-Wallis test, * $P<0.1$, ** $P<0.01$, *** $P<0.001$, **** $P<0.0001$). Values are shown as mean \pm s.e.m.

	Piezo2 ^{+/+}	Piezo2 ^{+/R2756H}	Piezo2 ^{R2756H/R2756H}	Piezo2 ^{+/R2756K}	Piezo2 ^{R2756K/R2756K}
Animals (m,f)	6 (5,1)	7 (6,1)	6 (4,2)	4 (3,1)	5 (3,2)
Cells (no. of currents)	13 (210)	15 (258)	11 (145)	12 (110)	12 (123)
Cell size (μm)	37.96 \pm 0.98	41.33 \pm 0.69	37.3 \pm 1.05	39.44 \pm 1.96	36.87 \pm 0.68
HP (ms)	0.66 \pm 0.05	0.65 \pm 0.12	0.6 \pm 0.11	0.7 \pm 0.08	0.61 \pm 0.08
Em_{rep} (mV)	-66.72 \pm 1.04	-66.78 \pm 1.64	-65.16 \pm 2.33	-64.89 \pm 1.08	-63.13 \pm 1.31
Latency (ms)	3.19 \pm 0.42	2.77 \pm 0.34	4.98 \pm 0.64	5.23 \pm 0.78****	3.86 \pm 0.45****
RA	3.98 \pm 0.9	1.73 \pm 0.3	4.79 \pm 0.87	4.73 \pm 1.07**	3.21 \pm 0.53*
IA	3.10 \pm 0.87	4.49 \pm 0.86	4.64 \pm 1.18	5.05 \pm 1.39	5.57 \pm 1.25**
SA	2.22 \pm 0.81	2.01 \pm 0.47	5.92 \pm 1.81	5.52 \pm 1.62	4.18 \pm 0.91
τ_{act} (ms)	0.87 \pm 0.04	1.2 \pm 0.06**	1.43 \pm 0.09****	1.52 \pm 0.09****	1.33 \pm 0.11***
RA	0.71 \pm 0.04	0.84 \pm 0.05	1.27 \pm 0.13****	1.25 \pm 0.11****	0.97 \pm 0.07**
IA	1.07 \pm 0.09	1.72 \pm 0.15**	1.57 \pm 0.19	1.65 \pm 0.15**	1.96 \pm 0.35*
SA	1.26 \pm 0.12	1.46 \pm 0.21	1.62 \pm 0.23	1.85 \pm 0.26	1.96 \pm 0.32
τ_{inact} (ms)	23.86 \pm 3.83	31.43 \pm 6.05	42.37 \pm 8.96**	61.89 \pm 14.67**	32.2 \pm 8.98
RA	1.79 \pm 0.1	1.82 \pm 0.11	2.43 \pm 0.16**	1.95 \pm 0.14	1.94 \pm 0.14
IA	18.8 \pm 1.57	16.16 \pm 1.32	14.02 \pm 1.36*	17.35 \pm 2.16	13.48 \pm 1.75
SA	149.5 \pm 16.8	215.9 \pm 37.45	184.4 \pm 34.45	246.4 \pm 50.27	181.4 \pm 45.45

5.5.2. Characterization of MA currents in nociceptors from Piezo2^{R2756H} and Piezo2^{R2756K} mice

Sensory neurons with broad and humped AP were classified as nociceptors. When stimulating nociceptors with the pillar arrays technique in the range of 1-1000 nm stimuli, 15 out of 22 cells (68.1%) from wildtype mice responded to the mechanical stimulus (**Figure 5.18**). Similar percentages of responsive cells were observed in nociceptors from *knock-in* mice (Piezo2^{+/R2756H}: 66.6%, Piezo2^{R2756H/R2756H}: 76.4%, Piezo2^{+/R2756K}: 75%, Piezo2^{R2756K/R2756K}: 87.5%; **Figure 5.18 A**). Even though, there was an increase of ~10 and ~20% in responsive cells from Piezo2^{R2756K/R2756K} and Piezo2^{R2756K/R2756K}, respectively, this was not statistically different (P=0.72 and P=0.25 for Piezo2^{R2756K/R2756K} and Piezo2^{R2756K/R2756K} nociceptors, respectively; Fisher's exact test). However, when comparing the deflection-current amplitude relationships, nociceptors from Piezo2^{R2756H/R2756H} exhibited larger currents than those observed in wildtype to the deflection ranges 1-50, 50-100 and 100-250 nm (**Figure 5.18 B**). Moreover, nociceptors from Piezo2^{+/R2756K} animals showed larger currents at the deflection range of 500-1000 nm while neurons from Piezo2^{R2756K/R2756K} mice displayed larger currents to deflection ranges of 10-50, 250-500 and 500-1000 nm (**Figure 5.18 B**). Consistently, when calculating the deflection threshold, nociceptors from Piezo2 *knock-in* animals were up to three-fold more sensitive than wild type cells (Piezo2^{+/+}: 424.2 ± 71.7 nm, Piezo2^{+/R2756H}: 206.9 ± 44.93 nm, Piezo2^{R2756H/R2756H}: 149.5 ± 35.9 nm, Piezo2^{+/R2756K}: 339.9 ± 59.4 nm, Piezo2^{R2756K/R2756K}: 202.3 ± 45.1 nm; **Figure 5.18 E**). These findings suggest that MA channels in nociceptors from *knock-in* mice are more sensitive compared to wildtype cells, possibly due to the increase channel availability related to mutations in R2756.

RA, IA and SA currents were recorded from wild type and *knock-in* nociceptors. Surprisingly, only a difference in the proportion of RA currents was observed in heterozygous conditions for both Piezo2 mutants (**Figure 5.18 C**). Thus, similarly to what was observed in mechanoreceptors, mutations in one of the alleles of Piezo2 is sufficient to change the inactivation kinetics of nociceptors from mice *in-vitro*.

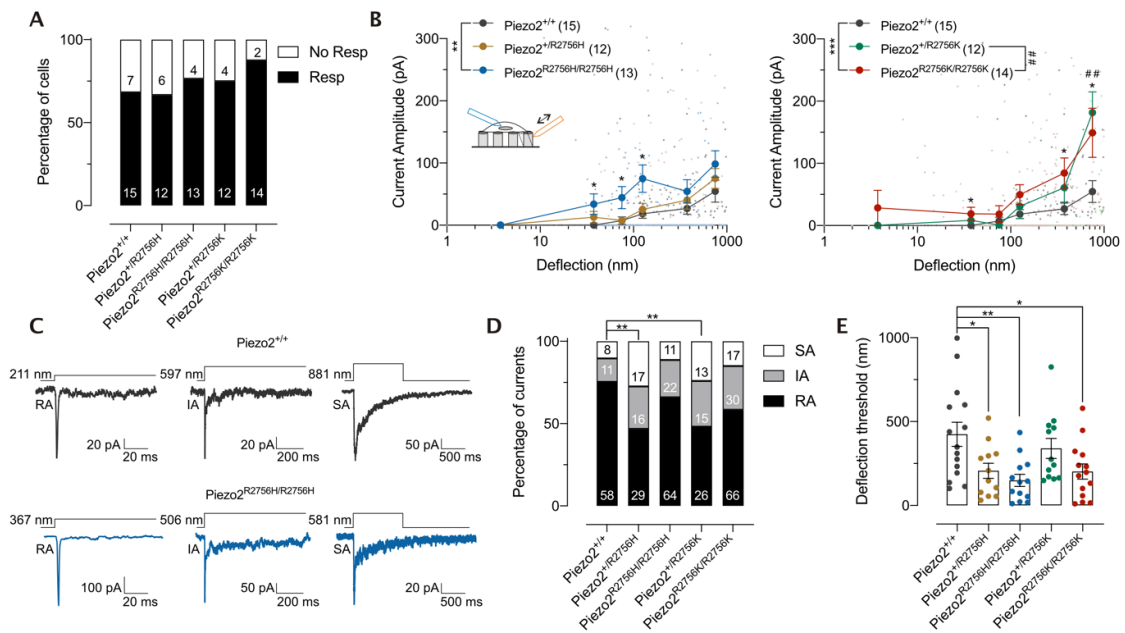


Figure 5.18. Mutations in the R2756 of Piezo2 increase sensitivity of MA currents in nociceptors.

A. Stacked histogram showing the percentage of responsive (Resp) and non-responsive (No Resp) nociceptors to pillar deflection. Numbers indicate the number of cells. **B.** Stimulus-response plot of the deflection sensitive currents in nociceptors from *Piezo2*^{+/+} and *knock-in* mice. Each small circle represents the value of individual peak currents. Big circles show the mean \pm s.e.m of binned currents. (Two-Way ANOVA tests were made to compare genotypes overall: ** $P < 0.01$, ## $P < 0.01$, *** $P < 0.001$. Mann-Whitney tests were made to compare binned data: * $P < 0.1$, ## $P < 0.01$). **C.** Representative traces of the three different types of deflection-gated currents in nociceptors from *Piezo2*^{+/+} and *Piezo2*^{R2756H/R2756H} mice. RA, IA and SA currents were observed. **D.** The percentage of IA and SA currents increased in heterozygous *knock-in* mice. Numbers in the histograms represent the number of the currents observed (χ^2 test, ** $P < 0.01$). **E.** Deflection threshold was increased in nociceptors from knock in mice. Dots represent the deflection threshold in individual cells. Data is shown as mean \pm s.e.m (Dunnett test; * $P < 0.1$, ** $P < 0.01$).

Max Peak current was similar in all mutants, except in *Piezo2*^{+/R2756K}, and in contrast to what was observed in mechanoreceptors, there was not a clear cluster of groups when analyzing the deflection stimulus-Max. Peak current relationships from the different genotypes (Figure 5.19). However, consistent with the higher sensitivity observed, when plotting the deflection threshold-amplitude current relationships from individual cells, nociceptors from *Piezo2* mutants displayed larger currents at lower deflection thresholds compared to wildtype animals (Figure 5.20 A, B). Moreover, when analyzing the percentage of response to pillar deflections, nociceptors from *Piezo2*^{R2756H/R2756H} and *Piezo2*^{R2756K/R2756K} were ~2 fold more responsive than wild type cells (*Piezo2*^{+/+}: $17.2 \pm 3.0\%$, *Piezo2*^{+/R2756H}: $26.3 \pm 2.8\%$, *Piezo2*^{R2756H/R2756H}: $32.9 \pm 4.6\%$, *Piezo2*^{+/R2756K}: $19.7 \pm 1.7\%$, *Piezo2*^{R2756K/R2756K}: $41.7 \pm 4.5\%$; Figure 5.20 C). These findings support the hypothesis that mutations in Arg2756 of Piezo2 increase channel availability.

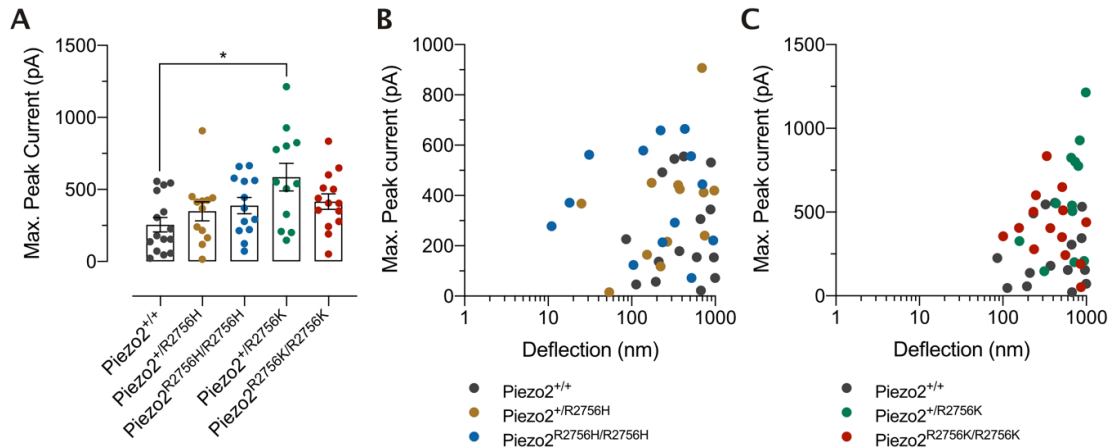


Figure 5.19. Maximum peak currents of nociceptors

A. Maximum peak current values obtained in nociceptors. Data is shown as mean \pm s.e.m. (Kruskal-Wallis test, * $P=0.01$) B, C. Deflection-Maximum peak current relationships of nociceptors from Piezo2^{+/+} and Piezo2^{R2756} mutants. Note that most of neurons from knock in mice reached maximum peak currents larger than wild type DRGs.

When comparing the biophysical properties from all MA currents in nociceptors, it was found that deflection sensitive currents from Piezo2^{R2756K} cells had longer latencies and slower τ_{act} compared to wildtype neurons (Figure 5.21 A, B). Interestingly, in nociceptors from Piezo2^{+/R2756H}, Piezo2^{+/R2756K} and Piezo2^{R2756K/R2756K} mice, MA currents displayed slower inactivation kinetics compared to wildtype, but this feature was not observed in nociceptors from Piezo2^{R2756H/R2756H} mice (Figure 5.21 C).

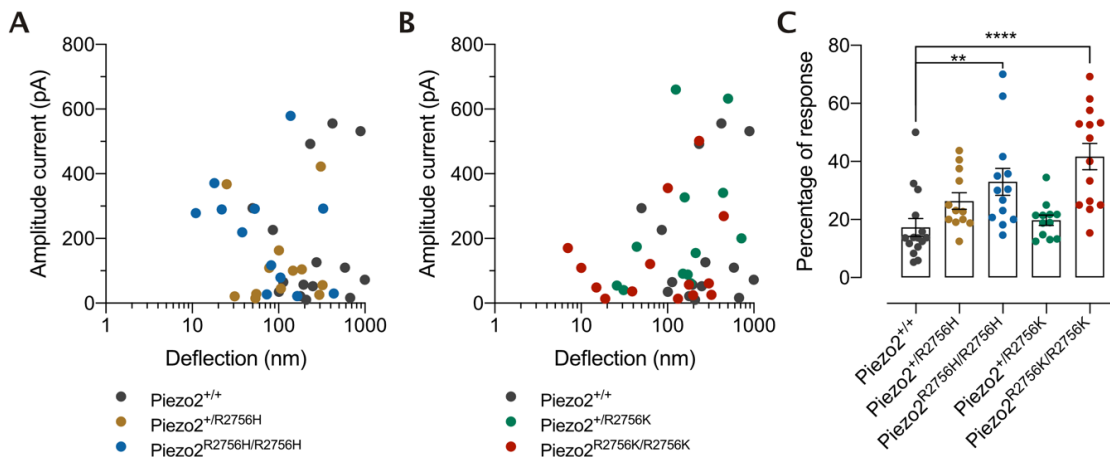


Figure 5.20. Nociceptors from knock-in mice were more sensitive and responsive to deflection stimuli

A, B. Deflection threshold-amplitude current relationship of nociceptors from Piezo2^{+/+} and Piezo2^{R2756} mutants. Each dot represents the current obtained at the minimum deflection-stimuli in which individual cells responded to mechanical stimuli (deflection threshold). Note that in nociceptors from knock in mice, deflection-sensitive currents were obtained at lower deflection. C. Percentage of response to deflection stimuli for responsive nociceptors from Piezo2^{+/+} and Piezo2^{R2756} mutants. The total amount of stimuli was considered as 100%. Each dot represents the percentage of individual cells. Data was plotted as mean \pm s.e.m. (Kruskal-Wallis test; ** $P=0.005$, **** $P<0.0001$).

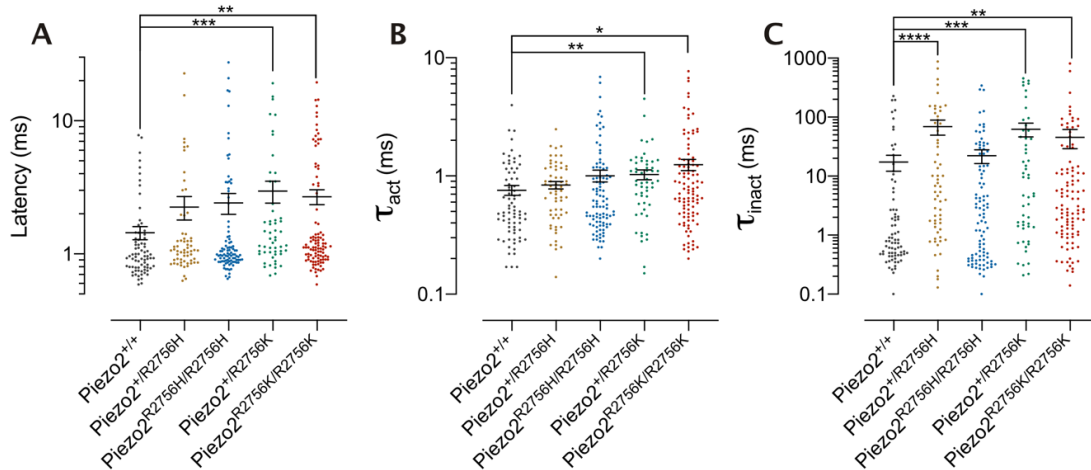


Figure 5.21. Mutations in R2756 of Piezo2 channels change biophysical properties of nociceptors in mice
 A. Latency of MA currents was increased in nociceptors from Piezo2^{R2756K} mice. The activation (B) and inactivation (C) of MA currents from mechanoreceptors was slower in Piezo2^{R2756} mice. Each dot represents the biophysical properties of each current in all cells tested. Bars indicate mean \pm s.e.m. (Kruskal-Wallis test, * $P < 0.1$, ** $P < 0.01$, *** $P < 0.001$, **** $P < 0.0001$).

When dissecting the biophysical properties according to the types of currents, in nociceptors, only the latencies of RA currents from Piezo2^{+/R2756H}, Piezo2^{+/R2756K} and Piezo2^{R2756K/R2756K} neurons were affected compared to wildtype currents (Table 5.3). Thus, mutations in Arg22756 of Piezo2 increase mechanical-sensitivity of MA currents in nociceptors by decreasing the deflection-threshold to mechanical stimuli and by increasing the responsiveness of cells to pillar deflection.

5.5.3. Mechanical nociception in Piezo2 *KI* mice increases *in-vivo*

To test whether the sensitization effect observed in isolated nociceptors from knock-in mice is conserved *in-vivo*, mechanical nociceptive responses were studied in mice by assessing paw withdrawal responses using von Frey filaments. Similar to previous studies (Dhandapani et al., 2018), the 50% paw withdrawal threshold (50% PWT) of wildtype animals was 0.39 ± 0.04 g. However, both Piezo2^{R2756H/R2756H} and Piezo2^{R2756K/R2756K} mice developed mechanical hypersensitivity (50% PWT = 0.21 ± 0.02 and 0.22 ± 0.06 g, respectively) (Figure 5.22).

Pathogenic mutations of *PIEZO2* in humans lead to progressive disorders. To test whether knock-in mice experience progressive hypersensitivity to nociceptive responses, von Frey responses were measured during three consecutive weeks. Interestingly, *knock-in* mice showed a slight increase in the hypersensitivity at week two compared to the responses measured at week one. However, no difference was observed between week two and week three. Consistent to the nociceptive responses observed in Figure 5.22 B, Piezo2^{R2756H/R2756H} and Piezo2^{R2756K/R2756K} mice were more sensitive to filament stimuli, compared to wildtype animals. Thus, mutations in the R2756 of Piezo2 increase the animal's sensitivity to mechanical stimulation *in-vivo*.

Table 5.3. Biophysical properties of deflection gated currents in nociceptors from Piezo2^{R2756H/K} mice

Sex and number of animals (m, male, f, female) used in the study. Cells and currents analysed in nociceptors for each genotype are shown. Cell size and half peak (HP) of APs were used to classified DRG neurons into nociceptors. Mechanical latency, τ_{act} and τ_{inact} are shown for all genotypes including the values for RA, IA and SA groups. All data sets were not normally distributed. (Kruskal-Wallis test, *P<0.1, **P<0.01, ***P<0.001, ****<0.0001). Values are shown as mean \pm s.e.m.

	Piezo2 ^{+/+}	Piezo2 ^{+/R2756H}	Piezo2 ^{R2756H/R2756H}	Piezo2 ^{+/R2756K}	Piezo2 ^{R2756K/R2756K}
Animals (m,f)	5 (4,1)	4 (3,1)	4 (2,2)	3 (2,1)	4 (3,1)
Cells (no. of currents)	15 (77)	12 (62)	13 (97)	12 (54)	14 (113)
Cell size (μm)	26.67 \pm 1.13	23.61 \pm 0.66	26.04 \pm 1.32	24.84 \pm 0.72	24.45 \pm 0.86
HP (ms)	2.21 \pm 0.27	2.54 \pm 0.36	2.59 \pm 0.31	1.75 \pm 0.17	2.18 \pm 0.25
Em_{rep} (mV)	-54.6 \pm 2.6	-52.5 \pm 2.7	-52.9 \pm 3.1	-54.7 \pm 2.4	-49.7 \pm 3.2
Latency (ms)	1.44 \pm 0.16	2.24 \pm 0.45	2.41 \pm 0.43	2.96 \pm 0.55***	2.68 \pm 0.34**
RA	1.25 \pm 0.15	1.85 \pm 0.53*	2.31 \pm 0.59	2.29 \pm 0.49**	2.28 \pm 0.44**
IA	1.81 \pm 0.53	2.2 \pm 0.56	2.78 \pm 0.76	4.41 \pm 1.14	2.73 \pm 0.53
SA	2.29 \pm 0.77	2.95 \pm 1.28	2.25 \pm 0.66	3.7 \pm 1.63	3.96 \pm 0.92
τ_{act} (ms)	0.75 \pm 0.07	0.83 \pm 0.05	1.00 \pm 0.11	1.02 \pm 0.09**	1.24 \pm 0.13*
RA	0.6 \pm 0.05	0.67 \pm 0.8	0.63 \pm 0.05	0.77 \pm 0.09	0.73 \pm 0.08
IA	0.89 \pm 0.17	0.85 \pm 0.1	1.97 \pm 0.4	1.39 \pm 0.25	1.37 \pm 0.19
SA	1.86 \pm 0.34	1.08 \pm 0.08	1.18 \pm 0.26	1.1 \pm 0.19	2.61 \pm 0.55
τ_{inact} (ms)	17.32 \pm 5.02	69.29 \pm 19.78****	22.15 \pm 5.78	62.41 \pm 16.36***	45.57 \pm 16.44**
RA	0.9 \pm 0.1	1.58 \pm 0.23	1.32 \pm 0.17	1.6 \pm 0.26	1.47 \pm 0.14
IA	16.92 \pm 3.29	15.59 \pm 2.84	22.71 \pm 2.52	21.91 \pm 3.56	16.56 \pm 3.26
SA	136.9 \pm 22.05	235.3 \pm 55.26	142.2 \pm 33.37	230.8 \pm 41.94	257.4 \pm 85.34

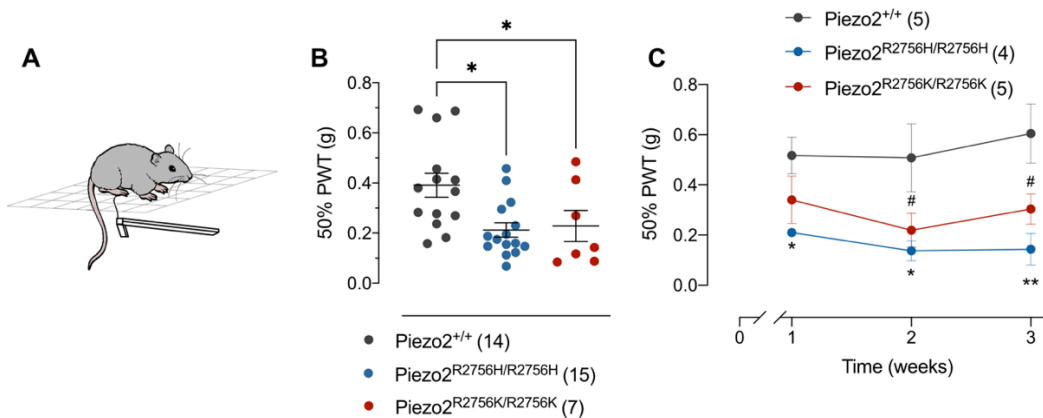


Figure 5.22. Piezo2 knock-in mice develop reduced 50% PWT

A. Von Frey experiments consisted of presenting filaments of differing forces perpendicularly to hind paws of mice. When mice withdrew or licked their paw, the stimulation was considered as a positive response. **B.** 50% PWT values of Piezo2 wildtype and *knock in* mice. Each dot represents average values from different measures taken on different days in each animal. Bars indicate mean \pm s.e.m. (Kruskal-Wallis test, *P<0.1). **C.** Progressive von Frey responses measured in three consecutive weeks. Week 0 indicates week of habituation. Bars indicate mean \pm s.e.m. (Two-way ANOVA, Bonferroni test, */#P<0.1, **<P0.01).

5.6. Native MA currents in DRG neurons from Piezo2^{-/-} mice

Previous studies reporting the biophysical and pharmacological properties of MA currents in sensory neurons show some serious discrepancies with the idea that Piezo2 is the major transducer of the endogenous MA conductance. The native RA current found in isolated DRG neurons was first studied in detail by Hu and Lewin (Hu & Lewin, 2006). They found that RA mechanically gated currents reverse at very positive potentials (~80 mV) indicating a high degree of Na⁺ selectivity. Additionally, RA mechanically gated currents were abolished when Na⁺ ions were substituted by the non-permeant cation *N*-methyl-D-glucamine (NMDG⁺). Furthermore, the native RA current was not blocked by the non-selective cation channel blocker RR. These findings are neither consistent with the described properties of Piezo channels in the N2a cell line, nor those properties of Piezo2 channels in sensory neurons (Bertrand Coste et al., 2010; Poole et al., 2014). Furthermore, *ex-vivo* skin-nerve experiments in Piezo2^{CKO} mice showed that, even though the low threshold mechanoreceptor fibers (A β -fibers) were more insensitive to mechanical stimuli, mechanosensitivity in most neurons was preserved. Additionally, the threshold for mechanical response to nociceptive fibers (A δ -nociceptors and C-fiber nociceptors) was higher, however the number of responsive fibers was not affected (Murthy, Loud, et al., 2018; Ranade, Woo, et al., 2014). Thus, these data suggest that there are other MA channels expressed in sensory neurons.

We hypothesized that by deleting *piezo2* in sensory neurons, MA currents Piezo2-independent would be recorded in DRG neurons. Piezo2^{-/-} mice die within 24 h after birth (Nonomura et al., 2017), therefore DRG neurons from embryos (E18.5) were isolated and cultured on pillar arrays (Figure 5.23). Embryonic DRG neurons exhibit mechanically activated currents at E13.5 when stimulating with the indentation technique (Lechner et al., 2009).

To characterize deflection-gated currents in sensory neurons at embryonic stages (E18.5), embryonic DRG neurons from the Piezo2^{+/+} and Piezo2^{+/-} mice were dissected and plated on the top of the elastomeric pillar arrays coated with laminin. After 24h of plating, the MA currents were recorded as it was previously described (Patkunarajah et al., 2020; Poole et al., 2014; Servin-Vences et al., 2017). Here, for the first time, deflection-gated currents from embryonic DRG neurons were recorded in Piezo2^{+/+} and Piezo2^{+/-} mice. In adults, the percentage of responsive DRG neurons to mechanical stimuli with the pillar arrays method is ~75% (Figure 5.15-18). In contrast, only 56% (13 of 23 cells) and 64% (11 of 17 cells) of the embryonic cells from Piezo2^{+/+} and Piezo2^{+/-}, respectively, responded to the mechanical deflection within the range of 1-1000 nm (Figure 5.23 B, C).

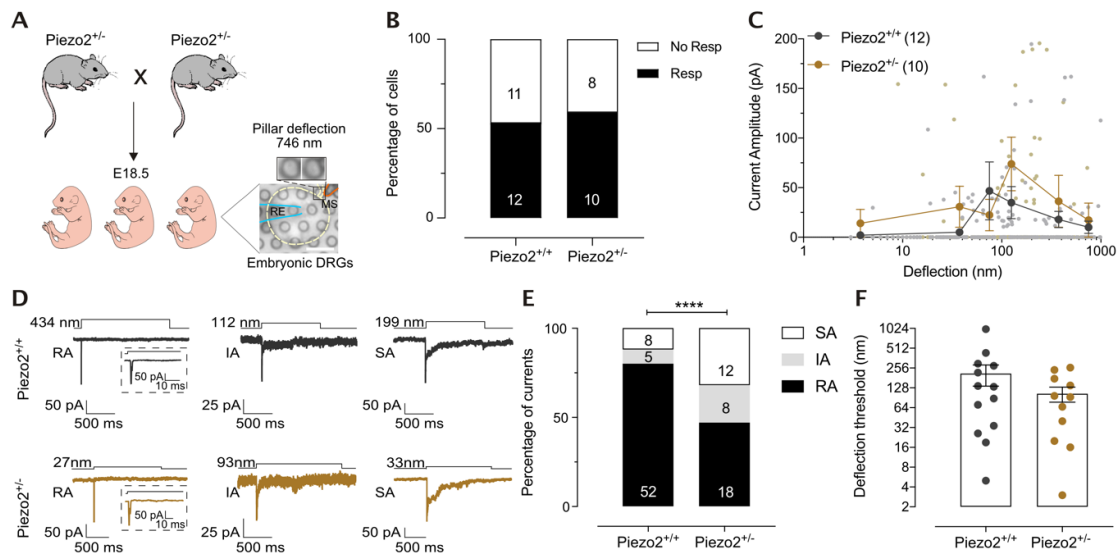


Figure 5.23. Types of mechanically gated currents from embryonic DRG neurons

A. Cartoon representing the acquisition of Piezo2 embryonic DRG neurons. *Right*, bright field image of an embryonic DRG neuron cultured on laminin-coated pillar arrays. In the insert, the position of a single pilus is shown before and during the deflection. **B.** Stacked histogram showing the percentage of responsive (Resp) and non-responsive (No Resp) embryonic DRG neurons to pillar deflection. Numbers indicate the number of cells. **C.** Stimulus-response plot of the deflection sensitive currents from Piezo2^{+/+} (gray) and Piezo2^{+/-} mice (gold) isolated DRGs. Each small circle represents the value of individual peak currents. The big circles are plotted as mean \pm s.e.m. **D.** Representative traces of the three different types of MA currents in embryonic DRG neurons from Piezo2^{+/+} (gray) and Piezo2^{+/-} mice (gold). RA, IA and SA currents were observed. The inserts, amplifications of the RA traces are shown. The deflection stimuli applied are indicated for each trace. **E.** The percentage of SA currents increased in DRG neurons from Piezo2^{+/-} mice. The numbers in the histograms represent the number of the currents observed (χ^2 test; $P < 0.0001$). **F.** Thresholds were defined as the smallest deflection stimuli necessary that resulted in MA currents. Each dot represents the threshold of individual cells (mean \pm s.e.m.).

The three types of mechanically gated currents were observed in embryonic DRG neurons (**Figure 5.23 D**). Most of the currents recorded were RA, followed by SA and IA currents in both genotypes (80, 33 and 12% of 65 MA currents recorded from 12 neurons in Piezo2^{+/+} were RA, IA and SA, respectively. 47, 21 and 32% of 38 MA currents from 10 neurons in Piezo2^{+/-} were RA, IA and SA, respectively) (**Figure 5.23 E**). Interestingly, in DRG neurons from Piezo2^{+/-}, the proportion of SA currents was higher than in the Piezo2^{+/+} cells (**Figure 5.23 E**). The smallest stimulus necessary to gate MA currents (deflection threshold) in Piezo2^{+/+} and Piezo2^{+/-} DRG neurons was similar (145 ± 39 , 12 cells; and 104.5 ± 26.9 , 11 cells; respectively; mean + s.e.m.; t -test, $p=0.4$) (**Figure 5.23 F**).

Interestingly, when examining the biophysical properties of the MA currents from embryonic DRGs, Piezo^{+/-} sensory neurons showed currents with slower τ_{act} and τ_{inac} compared to Piezo2^{+/+}, while latencies were similar in both genotypes (**Figure 5.24, Table 5.4**).

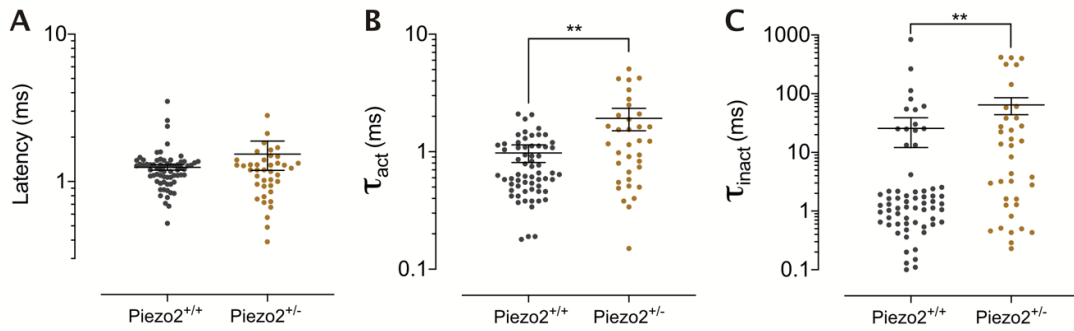


Figure 5.24. Biophysical properties of MA currents from embryonic DRG neurons.

A. Latency, time constant of activation (τ_{act} , **B**) and time constant of inactivation (τ_{inact} , **C**) of deflection gated currents from embryonic sensory neurons. Dots indicate the values from individual currents. Data are plotted as mean \pm s.e.m. (Mann-Whitney test, ** $P < 0.01$).

These data suggest that the lack of one allele of the *piezo2* gene leads to a change in the proportion of the types of mechanically gated currents with the pillar arrays technique, affects the kinetics, but not to a change in sensitivity to mechanical stimuli.

Table 5.4. Electrophysiological properties of MA currents recorded from embryonic DRG neurons.

The MA currents were classified according to their τ_{inact} value (RA currents, $\tau_{inact} < 5$ ms; IA currents, $\tau_{inact} = 5$ -50ms; SA currents, $\tau_{inact} > 50$ ms). The ** indicates $P < 0.01$ (Mann-Whitney test).

	Piezo2 ^{+/+}	Piezo2 ^{+/-}
Cells (no. of currents)	12 (65)	10 (38)
Animals	10	8
Latency (ms)	1.24 \pm 0.05	1.53 \pm 0.34
RA	1.2 \pm 0.05	2.01 \pm 0.65
IA	1.53 \pm 0.2	0.98 \pm 0.09**
SA	1.33 \pm 0.18	1.07 \pm 0.09
τ_{act} (ms)	0.97 \pm 0.16	1.92 \pm 0.41**
RA	0.74 \pm 0.06	1.69 \pm 0.81
IA	3.15 \pm 1.91	2.65 \pm 0.68
SA	1.11 \pm 0.11	1.9 \pm 0.36
τ_{inact} (ms)	25.55 \pm 13.4	69.29 \pm 20.83**
RA	1.3 \pm 0.2	2.01 \pm 0.4
IA	22.58 \pm 2.3	20.2 \pm 2.1
SA	187 \pm 97.1	219 \pm 52.5

Previously, it was described that with the indentation method, DRG neurons from Piezo2^{CKO} mice showed a decrease of the proportion of RA mechanically gated currents, suggesting that Piezo2 codes for the major cationic mechanosensitive conductance in DRG neurons (Ranade, Woo, et al., 2014; S. Woo, Ranade, et al., 2014). However, because those experiments were

performed with a conditional *knockout* mouse line, it is unknown whether the recorded currents in those cells were because of the presence of another MA channel or because a remaining expression of *piezo2*. Consistent with the previous observations of DRG neurons from the *Piezo2*^{CKO}, when recording deflection-gated currents in embryonic DRGs only 2 out of 8 cells (25 %) responded to mechanical stimuli (**Figure 5.25**). Thus, disruption of *piezo2* in mice leads to a major loss of deflection-gated currents in embryonic DRGs.

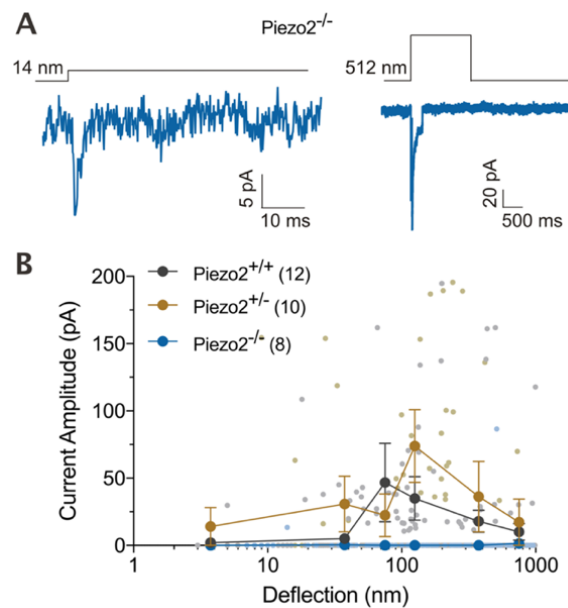


Figure 5.25. MA currents from embryonic *Piezo2*^{-/-} DRG neurons.

A. Traces of MA currents recorded from embryonic DRG neurons (E18.5) in *Piezo2*^{-/-} mice with pillar arrays method. Each trace was recorded from different cells from different *Piezo2*^{-/-} embryos. **B.** Stimulus-response plot of the deflection sensitive currents from isolated DRGs of *Piezo2*^{+/+} (gray), *Piezo2*^{+/-} (golden) and *Piezo2*^{-/-} (blue) mice. Each small circle represents the value of individual peak currents. Recordings from each cell were binned according to the size of the stimuli and the current amplitudes were averaged within each bin, then across the cells. Big circles are plotted as mean \pm s.e.m. Note that the *Piezo2*^{-/-} neurons lack of most of the deflection sensitive currents.

5.7. Native MA currents in DRG neurons from *Piezo2*^{CKO} mice

The proportion of responsive cells to pillar deflection in embryonic DRG neurons was lower compared to sensory neurons from adults (**Fig. 5.15, 5.23**). These findings suggest either the embryonic DRG neurons at E18.5 have not all the machinery needed for the mechanotransduction evoked by pillar deflection or that gating of MA currents is different at embryonic stages. Therefore, pillar deflection experiments were carried out in *Piezo2*^{CKO} sensory neurons from pups (6 days old, P6) to investigate whether *Piezo2*-independent-deflection-gated currents are present at this stage of development (**Figure 5.26 A**).

Lumbar DRG neurons were isolated and cultured on elastomeric pillar arrays. As expected, lumbar DRG neurons from Piezo2^{CKO} animals expressed td-Tomato, indicating Cre expression and therefore the excision of *piezo2* gene (**Figure 5.26 A**). When recording deflection threshold from Piezo2^{Ctrl} animals, ~75% of cells responded to mechanical stimuli. However, only of ~25% Piezo2^{CKO} dorsal DRG neurons were responsive to deflection stimuli (**Figure 5.26 B**). When plotting the deflection-current amplitude relationship, it was found that responsive cells from Piezo2^{CKO} had similar deflection responses to that of Piezo2^{Ctrl} sensory neurons (**Figure 5.26 C**). Moreover, in both genotypes the three types of currents (RA, IA and SA) were found, but a decrease in the proportion of RA currents in Piezo2^{CKO} was observed compared to control conditions (**Figure 5.26 D, E**). The deflection thresholds of responsive cells, either from Piezo2^{Ctrl} and Piezo2^{CKO} were similar (207.8 ± 77.1 and 143.8 ± 79.2 nm, respectively) (**Figure 5.26 D, E**).

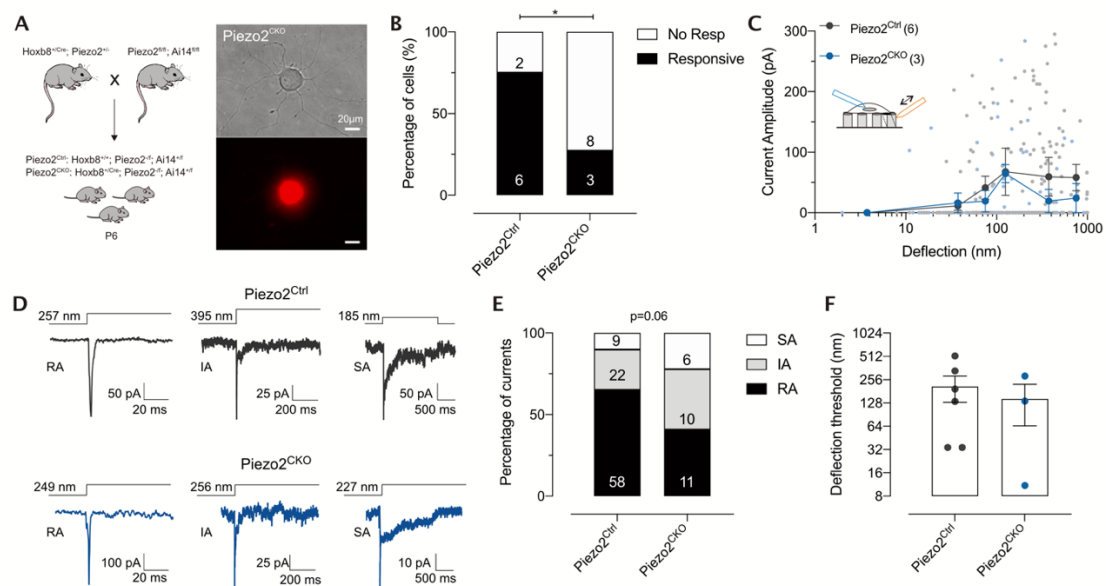


Figure 5.26. Types of deflection gated currents from Piezo2^{CKO} mice

A. *Left*, a Cartoon representing the acquisition of Piezo2^{Ctrl} and Piezo2^{CKO} animals. *Right*, acutely prepared dorsal DRG neuron from Piezo2^{CKO} expressing tdTomato. **B.** Stacked histogram showing the percentage of responsive (Resp) and non-responsive (No Resp) dorsal DRG neurons to pillar deflection. Numbers indicate the number of cells ($P=0.03$, χ^2 test). **C.** Stimulus-response plot of the deflection sensitive currents in dorsal DRGs from Piezo2^{Ctrl} (gray) and Piezo2^{CKO} mice (blue). Each small circle represents the value of individual peak currents. The big circles are plotted as mean \pm s.e.m. **D.** Representative traces of the three different types of MA currents in dorsal DRG neurons from Piezo2^{Ctrl} (gray) and Piezo2^{CKO} mice (blue). RA, IA and SA currents were observed. The deflection stimuli applied are indicated for each trace. **E.** The percentage of RA is slightly reduced in DRG neurons from Piezo2^{CKO} mice. The numbers in the histograms represent the number of the currents observed (χ^2 test; $P=0.06$). **F.** Deflection threshold from individual cells of each mutant. Each dot represents the threshold of individual cells (mean \pm s.e.m.).

When analysing the biophysical properties of deflection sensitive currents, no statistical difference was found when comparing latency, τ_{act} and τ_{inact} from Piezo2^{Ctrl} and Piezo2^{CKO} sensory

neurons (**Figure 5.27**). However, MA currents from Piezo2^{CKO} showed slightly slower τ_{inact} compared to control cells ($P=0.56$, t -test).

Thus, conditional deletion of *piezo2* in pups results in loss of most of deflection sensitive currents, consistent with what was observed in embryonic DRG from Piezo2^{-/-}. However, the remaining MA currents with slower inactivation suggest the presence of different mechanosensitive ion channels.

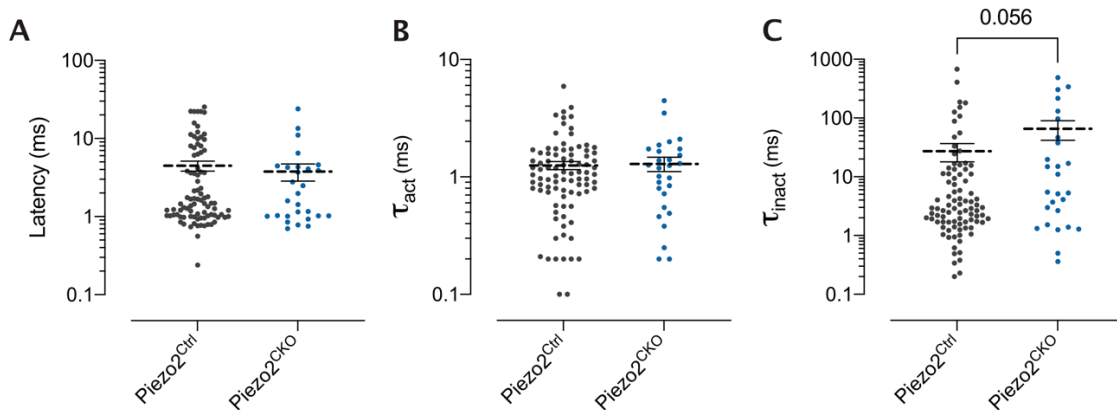


Figure 5.27. Biophysical properties of deflection sensitive currents in DRG neurons from Piezo2^{CKO}
A Latency, time constant of activation (τ_{act} , **B**) and time constant of inactivation (τ_{inact} , **C**) of deflection gated currents from embryonic sensory neurons. Dots indicate the values from individual currents. Data are plotted as mean \pm s.e.m. (Mann-Whitney test, ** $P<0.01$).

5.8. Modulation of PIEZO channels by the STOML3 protein

PIEZO channels are regulated by the integral membrane protein STOML3 (Poole et al., 2014; Qi et al., 2015). Previous studies showing STOML3 regulation on PIEZO channels were performed using indentation and pillar arrays assays, raising the question whether Stoml3 increases PIEZO channels sensitivity to mechanical stimuli by direct interaction or via components from the extracellular matrix and/or cytoplasmic components. Using HSPC recordings in outside-out configuration we show that STOML3 sensitizes PIEZO channels to membrane stretch.

mPiezo1, hPIEZO1 and the chimeric mP1/mP2 channels were overexpressed in N2a^{Piezo1^{-/-}} cells in the presence or absence of mouse Stoml3 (mStoml3) and human STOML3 (hSTOML3). At membrane level, mPiezo1 and mP1/P2 channels were sensitized by mStoml3 to pressure pulses (**Figure 5.28**, **Table 5.5**). Strikingly, hSTOML3 did not increase stretch-sensitivity of hPIEZO1 (**Figure 5.28 B, C**; **Table 5.5**), suggesting that, in membrane patches, STOML3 regulation on PIEZO channels is specific to murine proteins. However, when co-expressing mP1/mP2 with hSTOML3 a shift to the right in the pressure-response was observed, but mStoml3 failed to

sensitize hPIEZO1 channels. Thus, mStoml3 and hSTOML3 sensitize mP1/mP2 and mPiezo1, but do not increase the sensitivity of hPIEZO1 to membrane stretch (Figure 5.28 B, C; Table 5.5).

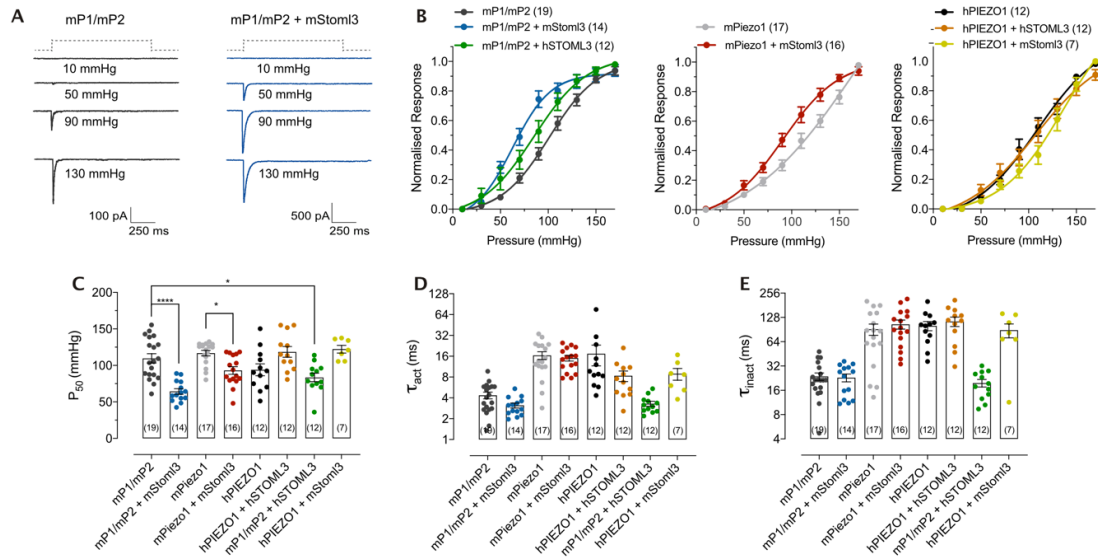


Figure 5.28. Sensitization of PIEZO channels by STOML3.

A. Representative recordings from mP1/mP2 expressed and co-expressed with mStoml3 in N2a^{Piezo1}^{-/-} in the outside-out configuration. Patches were clamped at -60 mV and different pressure pulses (dashed lines) were applied. **B, C.** Pressure-response relationships and P₅₀ values of PIEZO channels expressed in the presence or absence of STOML3. P₅₀ values were obtained by fitting a Boltzmann equation. The peak currents were normalised according to the maximum amplitude current recorded (one-way ANOVA, *P<0.1, ****P=0.0001). **D, E.** τ_{act} and τ_{inact} kinetics of PIEZO channels expressed or co-expressed with STOML3 proteins. The biophysical properties were not change. Data are plotted as mean \pm s.e.m.

When comparing τ_{act} and τ_{inact} kinetics between PIEZO channels expressed with or without STOML3, no differences were found (Figure 5.28 D, E; Table 5.5). These data indicate that STOML3 does not change biophysical properties of PIEZO channels at membrane level.

Table 5.5. Biophysical properties of PIEZO channels co-expressed with STOML3

Number of cells is indicated. All data come from, at least, three different transfections. P₅₀, τ_{act} and τ_{inact} are shown. Values are shown as mean \pm s.e.m.

	mP1/mP2	mP1/mP2 + mStoml3	mPiezo1	mPiezo1 + mStoml3	hPIEZO1	hPIEZO1 + hSTOML3	mP1/mP2 + hSTOML3	hPIEZO1 + mStoml3
Cells	19	14	17	16	12	12	12	7
P₅₀ (mmHg)	109.6 \pm 6.4	64.3 \pm 3.8	116.8 \pm 3.7	93.1 \pm 5.1	93.9 \pm 8.1	118.5 \pm 7.3	83.5 \pm 5.8	122.3 \pm 5.2
τ_{act} (ms)	4.3 \pm 0.4	3.1 \pm 0.2	16.4 \pm 2.1	15.0 \pm 1.4	17.3 \pm 5.7	8.3 \pm 1.4	3.2 \pm 0.2	8.9 \pm 1.7
τ_{inact} (ms)	23.7 \pm 2.5	22.9 \pm 2.5	91.3 \pm 14.5	105.1 \pm 13.5	100.6 \pm 13.0	113.9 \pm 15.1	19.6 \pm 2.1	88.8 \pm 17.3

PIEZO channels are voltage modulated ion channels. It was shown that at physiological resting membrane potential, PIEZO channels availability is ~10% (Moroni et al., 2018). To date, there is no direct evidence that shows whether accessory proteins can regulate the voltage modulation of PIEZO channels. Here, PIEZO1 and the chimeric channel mP1/mP2 were co-transfected with STOML3 proteins in N2a^{Piezo1^{-/-}} cells to test if the presence of the integral membrane protein changes their voltage modulation (**Figure 5.29**). When performing the tail current protocol with HSPC, it was found that at 0 mV the channel availability of the chimeric channel mP1/mP2 increased in the presence of mStoml3. As it was previously described, at 0 mV ~10% of the mP1/mP2 channels were available (**Figure 5.29 A, B**). However, in the presence of mStoml3, the apparent open probability of the channel increased up to ~30% at 0 mV (**Figure 5.29 A, B**). The increase in the channel availability was also observed at more depolarized voltage pulses (**Figure 5.29 B**). Surprisingly, the effect on the voltage modulation was not observed when co-transfecting mPiezo1 + mStoml3, mP1/mP2 + hSTOML3, hPIEZO1 + hSTOML3 nor when co-expressing hPIEZO1 + mStom3. Thus, the increase in the channel availability observed in mP1/mP2 is specific to the presence of mStoml3.

When analysing whether the co-expression of STOML3 shifts the V_{50} of PIEZO channels, it was found that STOML3 does not affect the voltage modulation of the channels (**Figure 5.29 C**). These data indicate that STOML3 proteins can sensitize PIEZO channels to membrane stretch and that mStoml3 increases the apparent open probability of mP1/mP2 channels.

5.9. Role of PIEZO1 in Cardiomyocytes

Since their discovery in embryonic chick skeletal myocytes, MA currents have been proposed to control the excitability and contractility of cardiomyocytes at the cellular level (Guharay & Sachs, 1984). However, their molecular identity and function in heart had not been characterized. PIEZO1 has crucial role in vascular biology (J. Li, Hou, Tumova, Muraki, Bruns, Ludlow, Sedo, Hyman, McKeown, et al., 2014; Ranade, Qiu, et al., 2014), together with erythrocyte volume homeostasis (Albuisson et al., 2013; Andolfo et al., 2013; Bae et al., 2013; Cahalan et al., 2015; Zarychanski et al., 2012) and regulation of the baroreceptor reflex (Zeng et al., 2018). Moreover, recent studies showed that *PIEZO1* is expressed in human cardiomyocytes (Wong et al., 2018) and is upregulated in heart failure upon myocardial infarction in isolated neonatal rat ventricular cardiomyocytes (Liang et al., 2017), highlighting the potential clinical relevance of PIEZO1 in cardiac cells. Here, in collaboration with Maria Bikou, from AG Hübner (MDC, Berlin), we found that human induced pluripotent stem cell-derived cardiomyocytes (hiPSC-CMs) lacking

PIEZO1 (hiPSC-CMs^{PIEZO1KO}) lost their endogenously stretch-activated currents, suggesting that *PIEZO1* is an important mechanotransducer in cardiomyocytes.

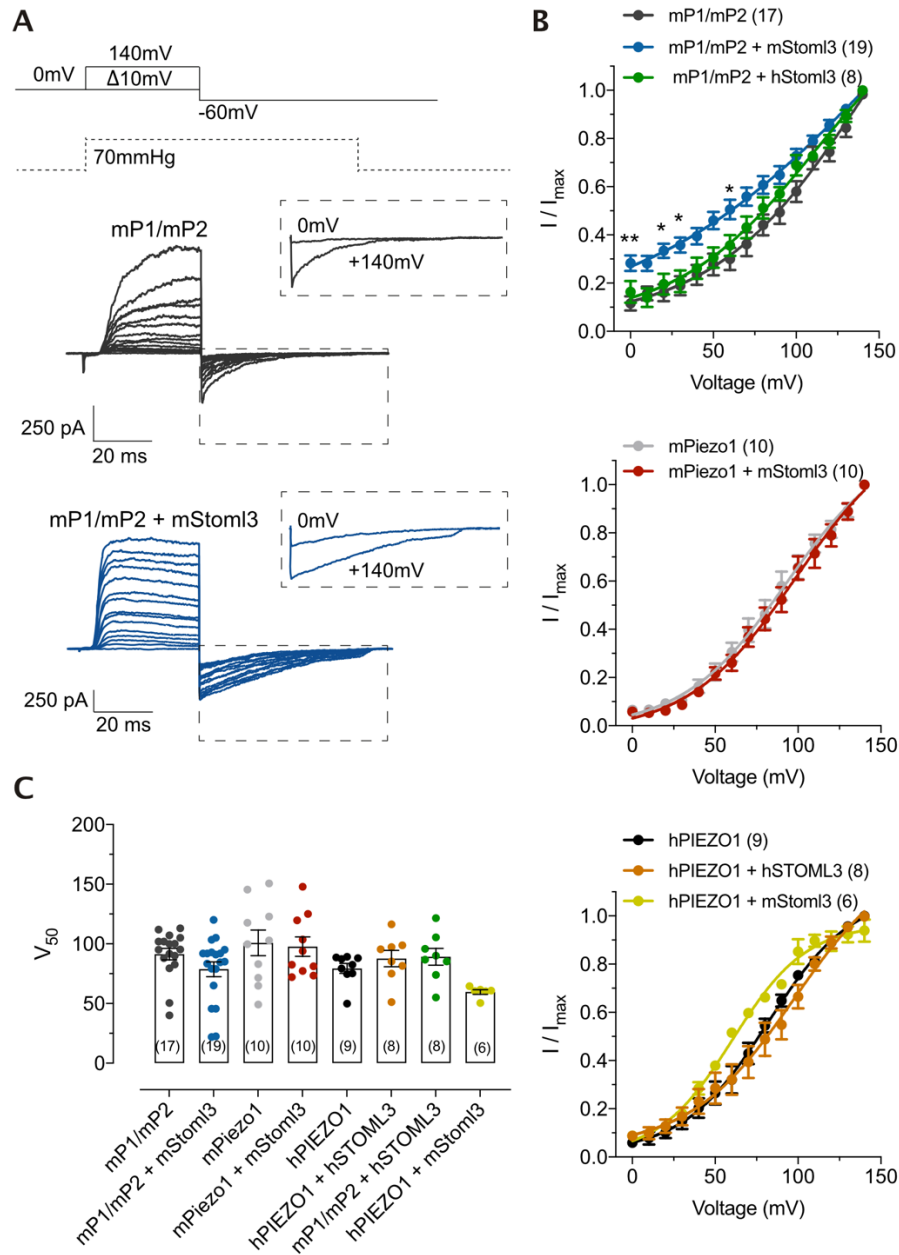


Figure 5.29. The mStoml3 protein increases the channel availability of the mP1/mP2 channel

A. Representative traces of the tail current protocol performed in $N2a^{Piezo1-/-}$ cells expressing the chimeric channel mP1/mP2 in the presence or absence of mStoml3 to study the apparent open probability of the channel. O/O patches were clamped to voltage steps ranging from 0 to 140 mV (pre-stimuli), followed by a repolarization step to -60 mV in the presence of pressure stimuli of 70 mmHg. In the insert, tail currents evoked after pre-stimuli of 0 and 140 mV are shown. Note that tail currents at 0 mV are larger when co-expressing mP1/mP2 + mStoml3 than when mStoml3 is absent. **B.** Tail currents were normalized to their maximum and fitted to a Boltzmann relationship. Note that the channel availability of mP1/mP2 increases in the presence of mStoml3 (mean \pm s.e.m.; Two-Way ANOVA, Bonferroni test; * $P < 0.1$, ** $P < 0.01$). **C.** V_{50} of PIEZO channels did not change in the presence of STOML3 proteins. Values were obtained from the analysis made in B. Each dot represents the value from individual patches (mean \pm s.e.m.; Kruskal-Wallis test; n.s., $P > 0.5$).

Positive pressure pulses evoked opening of stretch-sensitive channels in 16 out of 18 membrane patches of hiPSC-CMs^{wt} with a P₅₀ of 76.9 ± 6.3 mmHg (**Figure 5.30 A, B**). However, all hiPSC-CMs^{PIEZO1KO} recorded lacked completely stretch-sensitive currents (**Figure 5.30 A, B**). τ_{act} kinetics of endogenously stretch-activated currents in hiPSC-CMs^{wt} were statistically similar to those observed when overexpressing hPIEZO1 in N2a^{Piezo1^{-/-}} (28.1 ± 6.5 and 12.8 ± 2.9 ms for hiPSC-CMs^{wt} and hPIEZO1, respectively; *t*-test, P=0.1) (**Figure 5.30 C**). However, stretch-sensitive currents recorded from hiPSC-CMs^{wt} were non-inactivating compared to currents evoked from N2a^{Piezo1^{-/-}} cells overexpressing hPIEZO1, which currents inactivate within milliseconds (**Figure 5.30 A**). These data suggest that the MA currents observed in hiPSC-CMs^{wt} are PIEZO1-dependent.

Chemical activation of PIEZO1 channels is possible with the PIEZO1-specific modulator Yoda1 (Syeda et al., 2015). Thus, calcium imaging experiments were carried out to investigate whether Yoda1 evokes calcium influx in hiPSC-CMs. Strikingly, only hiPSC-CMs^{wt} but none of the PIEZO1^{KO} cells responded to Yoda1 (**Figure 5.30 D**). When hiPSC-CMs were perfused with RR (10 μ M), the Yoda1-induced-calcium-influx was decreased, suggesting the blocking of PIEZO1 channels (**Figure 5.30 D**). We also noted a decrease in the calcium signal in the hiPSC-CMs^{PIEZO1KO}, which could be related to the blocking of other MA channels expressed in hiPSC-CMs (**Figure 5.30 D**).

Recently, we showed that PIEZO channels are voltage modulated (Moroni et al., 2018). Using HPSC, the tail current protocol was used to investigate whether the stretch-activated currents in hiPSC-CMs^{wt} were voltage modulated. MA channels on hiPSC-CMs^{wt} were voltage sensitive and showed an apparent open probability of ~50% at 0 mV. This percentage is higher compared to the ~10% of availability of hPIEZO1 heterologously expressed in Na2^{Piezo1^{-/-}} cells (**Figure 5.31**). Additionally, similar to what was observed in the pressure-step protocol, tail currents from hiPSC-CMs^{wt} patches did not show inactivation (**Figure 5.31 A**). Thus, despite the differences in the inactivation kinetics and voltage sensitivity between hPIEZO1-dependent currents in hiPSC-CMs and hPIEZO1 channels heterologously expressed in Na2^{Piezo1^{-/-}} cells, these data clearly show that hiPSC-CMs express PIEZO1 channels and is necessary to mediate stretch-activated currents.

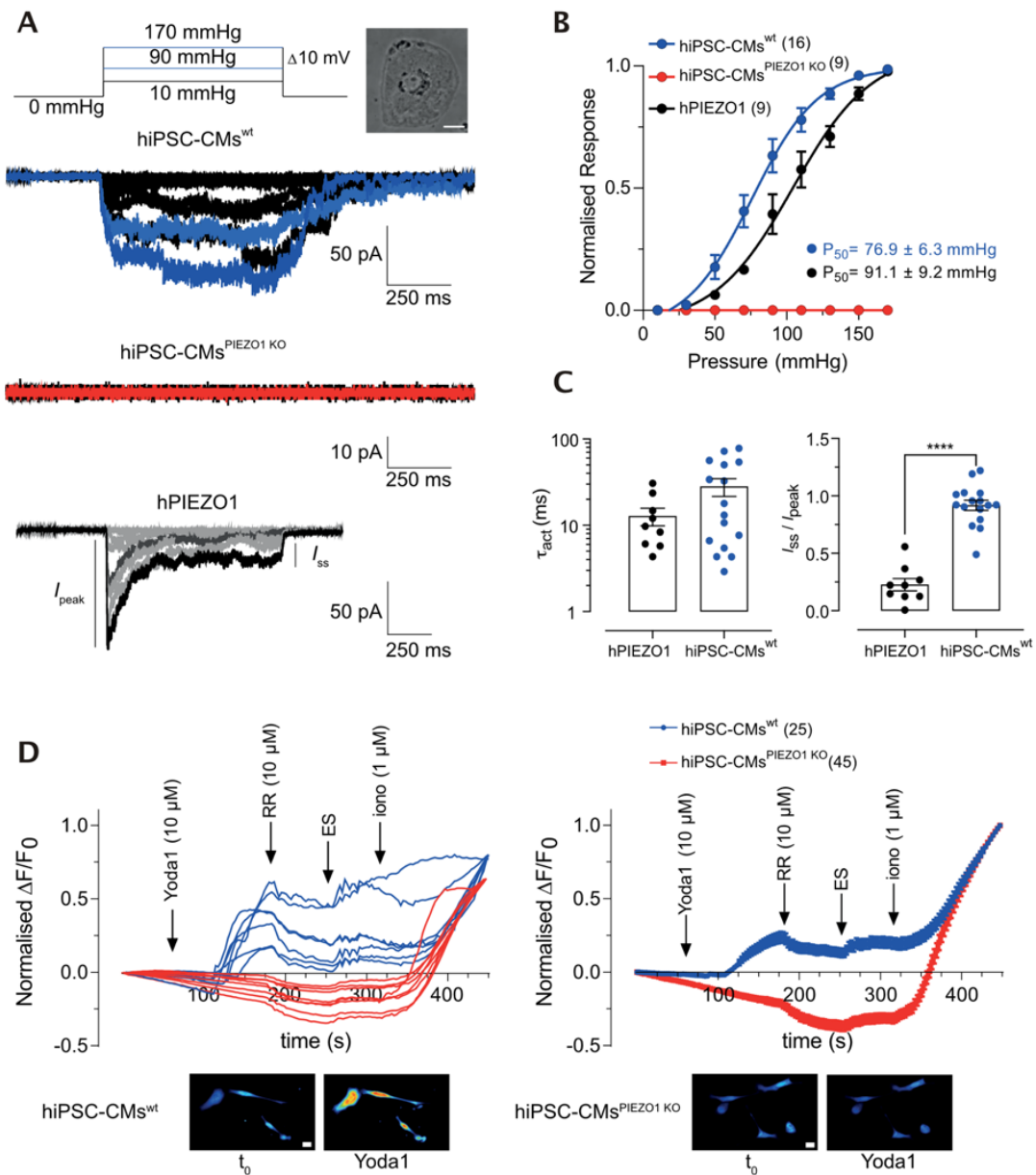


Figure 5.30. Stretch-sensitive currents in hiPSC-CMs are PIEZO1-dependent

A. Representative traces of HSPC recordings from O/O patches from hiPSC-CMs^{wt} (upper panel), hiPSC-CMs^{PIEZO1KO} (middle panel) and N2a^{Piezo1-/-} cells overexpressing PIEZO1 (hPIEZO1, lower panel). A pictures of a hiPSC-CMs^{wt} is shown above. Scale bar 10 μm . B. Stimulus-response of stretch-sensitive currents from patches of hiPSC-CMs^{wt} (blue), hiPSC-CMs^{PIEZO1KO} (red) and N2a^{Piezo1-/-} cells overexpressing hPIEZO1 (black), normalised to the maximal amplitude measured in each cell. Data was plotted as mean \pm s.e.m. C. τ_{act} and peak ratio (I_{peak} to steady-state (I_{ss}) current graphs (parameters shown in A). The peak ratio was calculated at 130 mmHg. Note that the inactivation kinetics from hiPSC-CMs is slower than kinetics of hPIEZO1 resulting in a bigger peak ratio (Student's t-test, **** $p < 0.0001$). D. Right, examples of individual calcium influx responses from hiPSC-CMs^{wt} (blue) and hiPSC-CMs^{PIEZO1KO} (red). Left, plot representing the average of the total cells recorded as mean \pm s.e.m. The arrows indicate the time perfusion of the different solutions. Below, representative images of calcium imaging experiments from hiPSC-CMs^{wt} and hiPSC-CMs^{PIEZO1KO} loaded with Cal520 before (t_0) and after perfusion with Yoda1 (10 μM).

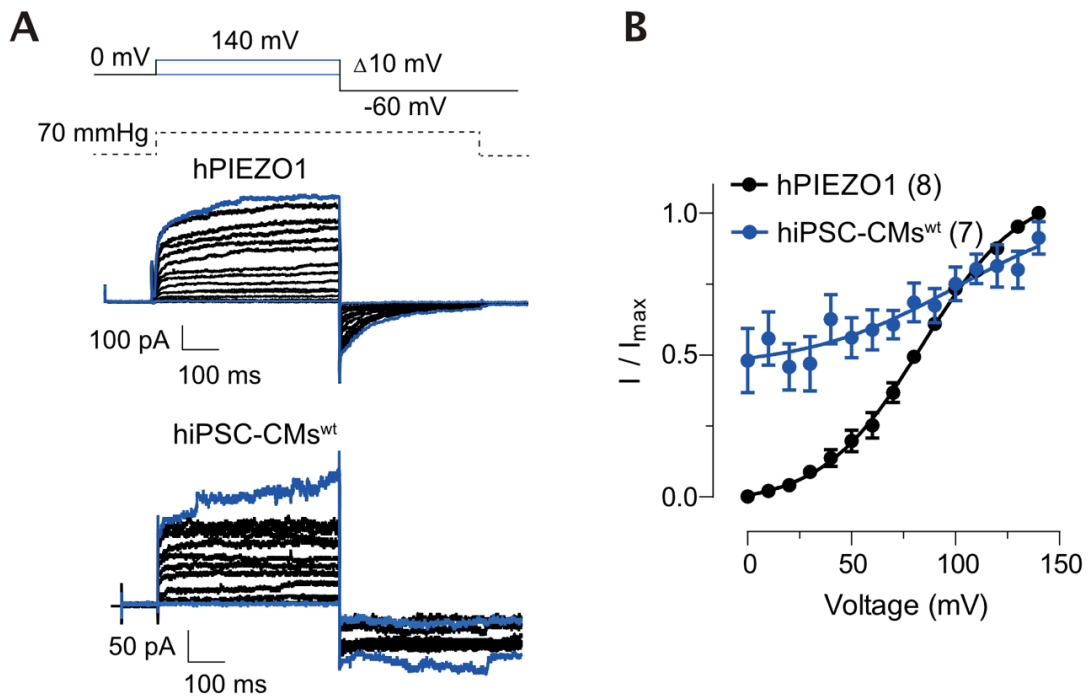


Figure 5.31. Voltage modulation of PIEZO1-dependent currents in hiPSC-CMs

A. Current responses to pressure stimulus of 70 mmHg during the tail current protocol from patches of $N2a^{Piezo1-/-}$ cells overexpressing hPIEZO1 and hiPSC-CMs^{wt}. The tail current protocol consisted in the clamping of depolarizing voltage steps running from 0 to 140 mV, followed by a repolarizing step of -60 mV. **B.** Tail currents from individual cells were normalised to their maximum and fitted to a Boltzmann relationship. Data is shown as mean \pm s.e.m.

6. Discussion

6.1. Mutations in the R2765 in PIEZO2 are GoF mutations

In mammals, PIEZO2 plays a role in a variety of physiological processes, including light touch and pain sensations, proprioception, respiration and urination. Recent clinical exome sequencing analysis have identified numerous missense mutations in PIEZO2 related to different types of arthrogryposis. DA5, GS and MWS are types of autosomal dominant multisystem arthrogryposis that result in developmental malformations and joint contractures, among other characteristics. Mutations in PIEZO2 could result in malfunction of the mechanosensitive channel leading to altered mechanotransduction in proprioceptive organs that are essential for skeletal integrity (Assaraf et al., 2020). Other authors consider that mutations in PIEZO2 can dysregulate neuromuscular signalling that controls the development of muscle tone during embryogenesis (B. Coste et al., 2013). Surprisingly, even though a variety of missense mutations are linked to the afore mention human disorders, only two PIEZO2 variants related to DA5 have been characterized. I802F and E2727del PIEZO2 mutants showed accelerated recovery from inactivation and E2727del variant exhibited slower inactivation kinetics. These properties classify I802F and E2727del as GoF mutations (B. Coste et al., 2013).

Most of the missense mutations identified in PIEZO2 are located in the C-terminal region of the channel (including the OH, Cap, IH and CTD; **Table 2.5**). Interestingly, mutations in Arg2686 of PIEZO2 were found in different patients who belong to non-related families. Moreover, R2686 PIEZO2 variants are related to DA, GS and MWS and when performing an amino acid alignment between human and mouse PIEZO2 sequences, it was found that this Arg is conserved in these two species (R2686 in hPIEZO2, R2486 in mPiezo2), suggesting a crucial role in mechanotransduction.

Here, the variants R2756H and R2756C of mPiezo2 (homologous mutants to R2686H and R2686C of hPIEZO2 related to DA5, GS and MWS patients) were characterised. Additionally, the R2756K mutant was included in the study due to previous studies showed that substitution of the homologous arginine in PIEZO1 by a lysine residue showed a strong effect in the biophysical properties the channel (Bae et al., 2013; Moroni et al., 2018). With two patch-clamp complementary assays, it was shown that R2556 variants are GoF mutations.

By overexpressing the mutants in a heterologous system, it was found that with the pillar array technique, the latency to activate the R2486 PIEZO2 variants with mechanical stimuli was approximately two-fold slower than the wild type channel. This result is consistent with what was

observed in pathogenic mutations of PIEZO1 related to HX, where mutations R2456H and R2456K showed longer latencies for activation (Bae et al., 2013). It has been proposed that longer latencies to activate PIEZO1 result from rupture of channel nanodomains in the membrane (Bae et al., 2013). Further investigation studying the spatial distribution with super resolution microscopy of pathogenic variants of PIEZO channels would be needed to elucidate whether these mutants disrupt channel microdomains.

It was shown that τ_{act} and τ_{inact} kinetics were slower in the R2756H mutant compared to mPiezo2 wild type channels when measuring deflection-gating with pillar arrays. Furthermore, when performing HSPC experiments using the chimeric channel mP1/mP2, it was found that the τ_{act} was slower in all the mutants and τ_{inact} kinetics were slower only in R2756H and R2756K variants. Interestingly, consistent with what was observed in pathogenic mutations of PIEZO1 (Bae et al. 2013), it was found that the sensitivity of R2756K mutant channels was dramatically increased to mechanical stimuli. R2746C and R2756H variants showed a slight increase in their sensitivity to mechanical stimuli, but this was not statistically different. It was suggested that substitutions of this amino acid could result in decreased stress within the resting channel protein or in changes in local stress sensed by channel microdomains (Bae et al., 2013), however, to date there is no direct evidence for this idea. When over-expressing the channels in N2a^{Piezo1-/-} cells, the current density was similar in Piezo2 mutants compared to wild type channels. That indicates that the channel trafficking to the membrane is similar in all the variants tested but would not indicate if the channel distribution in membrane nanodomains is equally comparable.

Previously, we found that under physiological resting membrane potentials, mammalian PIEZO channels are ~10% available for mechanical gating and that xerocytosis mutants shift the voltage modulation 60 mV leftward and increase considerably channel availability (Moroni et al., 2018). Here, it was shown that mutations in PIEZO2 related to DA5, GS and MWS increase dramatically the open probability of the chimeric channel mP1/mP2 up to ~50%. Additionally, it was found that the pathogenic mutations increase up to 5-fold the time required to go from the inactivated to deactivated states. The studied Arg is located at the bottom of the pore forming IH of PIEZO2. As we discussed previously (Moroni et al., 2018), in other ion channels Arg residues surrounding pore regions have been shown to be crucial for anchoring helices to the lipid bilayer and to stabilize the closed state of the channel. In fact, based on structural analysis, it has been proposed that residue R2482 of Piezo1 (homologue residue to the Arg2756 here studied, **Figure 5.3**) interacts electrostatically with the residue E2133 located in the anchor domain (Saotome et al., 2018). Substitution of the Arg2756 by His, Cys or Lys would change the interactions with the surrounding residues and therefore affect protein properties, including the opening-inactivating-

closing states. Further structural analysis from Cryo-EM structures of PIEZO2 variants would help us to elucidate the effect of amino acid residue substitutions in this region of the channel.

The net ion flux through PIEZO2 channels depends on the time that they remain open. R2656 mutants showed an increased open probability, lower deflection thresholds to mechanical activation, slower inactivation kinetics and longer time transitions from inactivated to deactivated states, which would increase the cation flux through the channels (**Figure 6.1**). However, a pronounced latency and a slower τ_{act} observed in the mutants could be counteracting the ion flux, which could prevent a more severe effect on the biological processes where PIEZO2 is involved.

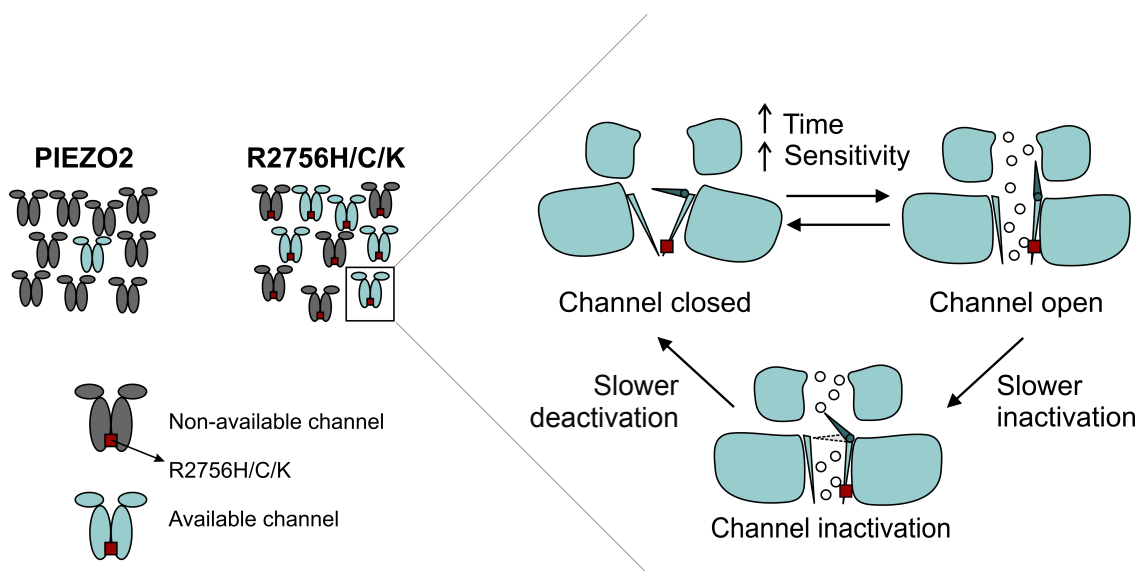


Figure 6.1. Mutations in Arg2756 of Piezo2 are gain of function mutations

Cartoon representing biophysical properties of PIEZO2 channels based on results from the mouse protein. Under physiological resting membrane potentials, only ~10% of the channels are available for mechanical gating. Pathogenic mutations in R2756 (represented as red square) causing DA5, GS or MWS increase channel availability up to 50%. When stimulating mechanically, R2756 mutants show lower deflection threshold to mechanical stimuli, pronounced latency to activation, slower τ_{act} and τ_{inact} kinetics and longer time required to go from inactivated to deactivated states.

6.2. *KI* Piezo2 mice resembles clinical features of DA5, GS and MWS patients

GoF *piezo1* mouse lines have been generated to investigate the role of the channel in pathogenic diseases (S. Ma et al., 2018). By generating global GoF *piezo2* mice lines related to DA5, GS and MWS disorders it was found that engineered *KI* mice recapitulate some clinical features of patients, such as short stature and scoliosis in *Piezo2*^{R2756H} and *Piezo2*^{R2756K} mice, respectively. Short statures and scoliosis were observed in a subpopulation of examined animals reflecting the heterogeneity of penetrance that has been reported in humans (**Table 2.6**). The arthrogryposis

types discussed in this research are congenital disorders in humans. Congenital contractures have been associated with mechanotransduction mediated by proprioceptors during embryo and adult development (Assaraf et al., 2020; Y. Ma et al., 2019). Further studies tracking the expression of *piezo2* in *KI* mice at different developmental stages would help to determine the role of the channel to the clinical characteristics observed in mice and humans carrying R2756 and R2686 mutations in PIEZO2, respectively. Additionally, it will be of interest to generate *KI* mice expressing tissue-specific *piezo2* GoF mutations to explore the role of this channel in different biological systems.

Differences in the severity of the phenotype observed in the *KI* mice models studied could be explained by several factors. With bioinformatics modelling, it was found that depending on the properties of amino acids in the same residue could lead to different conformational changes in the 3D structure of the protein (by forming loops or hydrogen bond) and therefore differences in the severity of the phenotype (S. Li et al., 2018). Cryo-EM structures of PIEZO2 variants would be necessary to investigate the changes that could occur at the atomic level.

6.3. Piezo2 *KI* DRG neurons are more sensitive to mechanical stimuli

In humans, LoF mutations in PIEZO2 resulted in partial loss of touch and pain sensations. Interestingly, in patients with GoF mutations, the clinical characterizations of light- and noxious-touch sensations were not well characterized. In addition to the *in-vitro* analysis of the Piezo2 variants in the heterologous system, here it was shown that the biophysical properties of MA currents from mechanoreceptors and nociceptors were altered in isolated sensory neurons from Piezo2^{R2756H} and Piezo2^{R2756K} mice and that the deflection-gated currents were more sensitive to mechanical stimulation. Remarkably, the presence of one mutant allele was sufficient to change the properties and sensitivity of MA currents.

When comparing the biophysical properties of MA currents from mechanoreceptors, there was a prolongation of the latency for activation in Piezo2^{R2756K} neurons. Overall, in all mutants the τ_{act} was slower and τ_{inact} was affected in Piezo2^{R2756H/R2756H}, Piezo2^{+/R2756K} and Piezo2^{R2756K/R2756K} mice. It has been described that Piezo2 is a major contributor to RA currents in DRG neurons (Bertrand Coste et al., 2010; Ranade, Woo, et al., 2014). When analysing the biophysical properties of RA currents in the *KI* mutants, it was observed that most of the parameters measured were altered (Table 5.2), supporting the idea that Piezo2 is crucial for RA currents in sensory neurons. Particularly, consistent with the *in-vitro* analysis, only RA currents from Piezo2^{R2756H/R2756H} neurons showed slower inactivation kinetics. In some cases, IA currents showed altered kinetics too. The latest observation could be product of two possible (not exclusive) explanations: 1) it is

conceivable that Piezo2 mediates IA currents to pillar deflection (as it was found in the characterization of mPiezo2 channel in N2a^{Piezo1^{-/-}} cells, where 12% where IA currents), and/or 2) if substitutions of Arg by His or Lys lead to slower inactivation kinetics, it may be that RA currents showed, overall, slower inactivation and therefore were included in the analysis as IA currents.

In nociceptors the major differences in the biophysical properties of MA currents were observed in sensory neurons from Piezo2^{R2756K} mice. It was found that the three parameters (latency, τ_{act} and τ_{inact}) were slower in the homozygous and heterozygous conditions compared to wildtype currents. In contrast to what was observed in mechanoreceptors, in nociceptors only the latency to activation of RA currents from Piezo2^{+/R2756H}, Piezo2^{+/R2756K} and Piezo2^{R2756K/R2756K} neurons was prolonged. The rest of the properties remained unaffected. Differences between nociceptors and mechanoreceptors could be explained by the presence of other MA ion channels in nociceptors (Beaulieu-Laroche et al., 2020) which could mask the effect observed in mechanoreceptors.

Even though differences in the kinetics of MA currents from sensory neurons were observed in Piezo2 *KI* mice compared to currents from wildtype neurons, it is crucial to point out that changes in the kinetics were not observed in all the mechanosensitive currents recorded. It is possible that such heterogeneity was because MA channels are at different mechanical coupling states when stimulated. Another possibility is that the presence of other molecularly distinct mechanosensitive channels mask the changes in the kinetics of Piezo2 variants. Such a hypothesis comes from recent studies that showed the expression of other MA ion channels in sensory neurons (Beaulieu-Laroche et al., 2020). Additionally, our results from Piezo2^{CKO} sensory neurons indicate that ~25% of DRGs express Piezo2-independent MA currents which exhibit biophysical properties similar to wildtype neurons. Thus, in our analysis there is a subpopulation of recordings from other deflection gated ion channels and/or neurons that exhibit MA currents that were Piezo2-independent. Further experiments where MA channels other than Piezo2 expressed in sensory neurons are deleted or down-regulated would be needed to show whether kinetics of MA currents from sensory neurons in Piezo2 *KI* mice show a stronger effect.

Sensory neurons from Piezo2 mutants showed lower deflection thresholds to deflection stimuli. Remarkably, as a consequence of higher sensitivity to mechanical stimuli, MA currents from mechanoreceptors of Piezo2^{R2756K/R2756K} reached a current amplitude saturation. Additionally, nociceptors from Piezo2^{R2756K/R2756K} and Piezo2^{R2756H/R2756H} showed larger MA currents to smaller deflection stimuli compared to wildtype. The *in-vitro* analysis of Piezo2 variants in N2a^{Piezo1^{-/-}} cells showed that mutations in Arg2756 by His or Lys increase the apparent open probability. A

combination of higher sensitivity and the increased channel availability could explain the current saturation and larger currents to smaller deflections observed in sensory neurons. We hypothesized that these changes may potentiate firing of APs in sensory neurons. Using two complementary techniques, skin nerve and current clamp assays (*data not shown*), we found that nociceptors from Piezo2 *KI* mice exhibit increased firing frequencies when mechanically stimulated. Moreover, nociceptors showed AP firing in the absence of mechanical stimulus (spontaneous activity). Thus, pathogenic mutations increase Piezo2 sensitivity to mechanical stimuli and increase the channel availability which causes more pronounced firing of AP in nociceptors.

6.4. GoF mutations in Piezo2 increase sensitivity to stimulus-evoked pain-like behaviour

More pronounced AP firing in sensory neurons could be translated into more pronounced nocifensive responses to mechanical stimuli *in-vivo*. Here, it was shown that Piezo2^{R2756H/R2756K} and Piezo2^{R2756K/R2756K} mice responded to lighter von-Frey filaments, indicating mechanical hyperalgesia. Previously, it was demonstrated that Piezo2^{CKO} mice had impaired mechanonocifensive responses (Murthy, Loud, et al., 2018). The data shown here confirm that Piezo2 at least in part mediates mechanical hypersensitivity.

In addition to the increase in the channel availability, mutations in the R2756 of Piezo2 showed altered kinetics and increased apparent open probability that would result in higher ion flux through the channel. In this regard, in nociceptors, a higher ion flux may result in increased firing of APs or spontaneous activity that would result in mechanical hypersensitivity (**Figure 6.2**). Further studies involving biochemical characterization of sensory neurons from Piezo2 *KI* mice will elucidate whether altered ion flux through Piezo2 channels in the mutants result in altered downstream cell signaling processes, such as protein phosphorylation, gene expression, etc. Thus, new roles of PIEZO2 in cellular biology may be discovered.

Here, it was shown for the first time the physiological relevance of the voltage regulation of mPiezo2 channels in the somatosensory system and how the voltage block (in wildtype conditions ~10% of channels are available for opening) regulates nocifensive responses. Mechanoreceptors and nociceptors have $E_{m,rep}$ of ~-65 mV and ~-55 mV, respectively. However, during AP firing, sensory neurons can reach $E_{m,rep}$ of >40 mV. Based on our *in vitro* experiments, in physiological conditions the channel availability of mPiezo2 at +40 mV would increase up to 25% (**Figure 5.9 B**). However, here it was found that when inserting point mutations in the R2756 of mPiezo2, the channel availability at +40 mV would be double (>50%) compared with the

percentage observed in wildtype conditions. An increase in the channel availability would result in higher ion influx which could trigger AP firing. Thus, based on our data, we hypothesize that the voltage block of Piezo2 in the somatosensory system controls the AP firing in sensory neurons which regulates and prevents mechanical hyperalgesia.

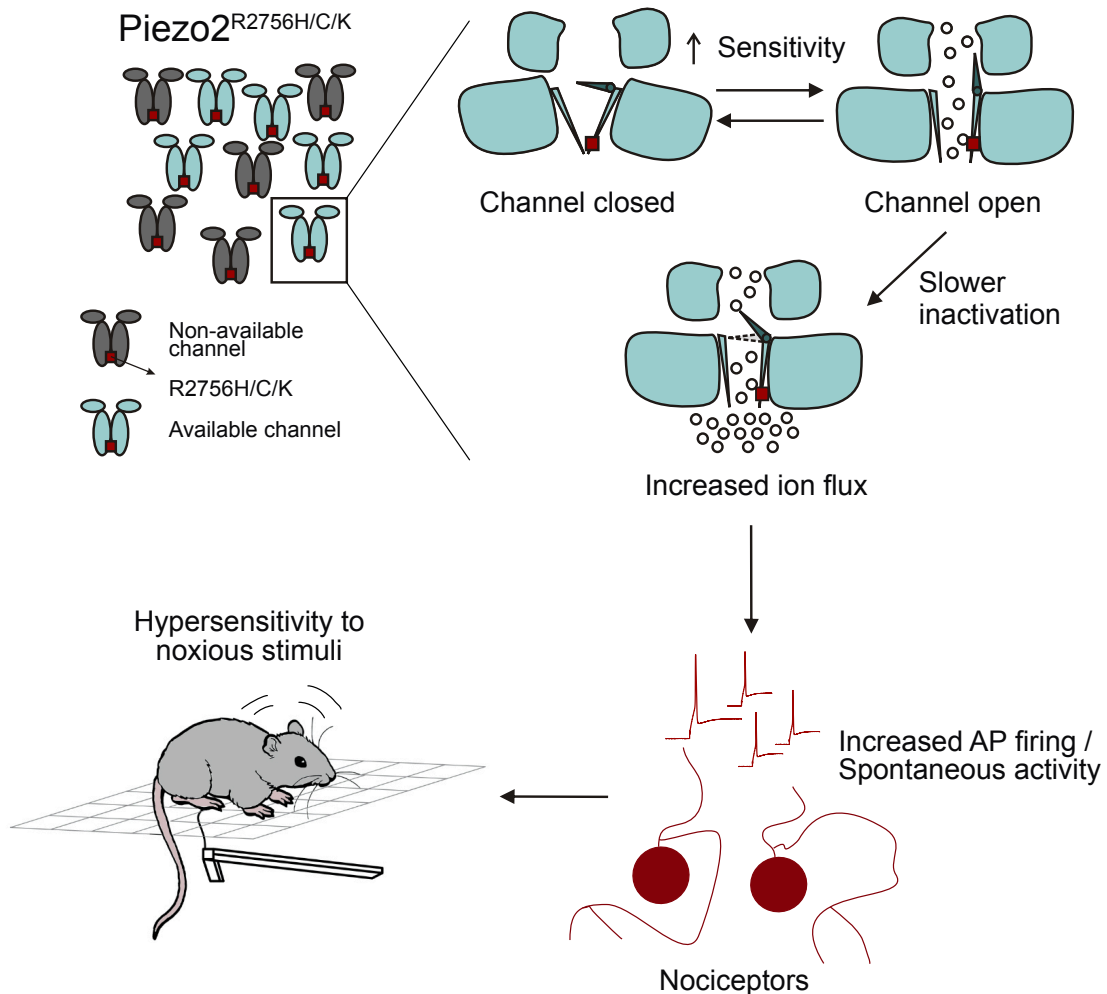


Figure 6.2. GoF mutations in Piezo2 increases sensitivity to noxious responses

Proposed model of noxious responses observed in *Piezo2*^{R2756H/C/K} mice. GoF mutations in *piezo2* increase apparent open probability and sensitivity to mechanical stimuli of the channel resulting in higher ion influx (i.e., Ca²⁺). In nociceptors, this influx causes firing of APs which triggers pain behaviour in mice.

6.5. Mechanotransduction in *Piezo2*^{-/-} and *Piezo2*^{CKO} mice

The recent discovery of new MA ion channels raises the question whether other ion channels play a role in the somatosensory system. By abolishing *piezo2* expression in sensory neurons, remaining mechanosensitive currents could be recorded from *Piezo2*^{-/-} and *Piezo2*^{CKO}

mice. Here, it was found that *Piezo2*^{-/-} embryonic sensory neurons lack most deflection sensitive currents and that *Piezo2*^{CKO} neurons showed a reduction in the proportion of RA currents by ~25% compared to control neurons (65% in *Piezo2*^{Ctrl} versus 40% in *Piezo2*^{CKO}). Discrepancies between these two phenotypes could be explained by considering the fact that the experiments were performed at two different developmental stages (E18.5 vs P6), and therefore, it is possible that all the molecular machinery necessary for mechanotransduction in embryonic stages is different than in adults. For instance, it is known that *mStoml3* is required for sensing mechanical stimuli *in vivo* (Wetzel et al., 2007), moreover, this protein shifts the mechanosensitive currents from DRG neurons to smaller deflections (Poole et al., 2014). In the lab, comparing the gene expression between E11.5 and P0 developmental stages, it was found that the expression of *stoml3* was slightly downregulated at P0 (Herget Regina, unpublished data). Thus, one hypothesis is that the low percentage of responsive cells to pillar deflection observed in *Piezo2*^{-/-} cells is due to the downregulation of *stoml3* at the last stage of development before birth. A second explanation could be that in *Piezo2*^{CKO} sensory neurons, the deletion of *piezo2* is not completely performed (Murthy, Loud, et al., 2018). However, in our experimental conditions the expression of tdTomato indicated the excision of *piezo2*. In previous studies, the conditional deletion of *piezo2* resulted in specific loss of RA currents when stimulating sensory neurons with the poking technique (<10% of the currents were RA in *Piezo2*^{CKO} cells compared to 40-80% from wildtype neurons) (Murthy, Loud, et al., 2018; Ranade, Woo, et al., 2014). Here it was shown that with the pillar array method, even though the proportion of responsive cells from *Piezo2*^{CKO} mice was reduced compared to wildtype neurons, 40% percent of MA currents showed RA properties. Differences could be explained by considering that with the pillar array technique, ion channels that are not mechanically gated by membrane indentation can be activated by mechanical deflection (Servin-Vences et al., 2017). The presence of MA currents *Piezo2*-independent in sensory neurons support the idea that there must be other molecularly distinct mechanosensitive channels in DRG neurons.

The remaining currents in *Piezo2*^{CKO} sensory neurons are mostly IA and SA currents. Recently, two non-selective ion channels were discovered, TACAN and Elkin channels (Beaulieu-Laroche et al., 2020; Patkunarajah et al., 2020). The TACAN channel is expressed in nociceptors and genetically downregulation of this channel leads to loss of SA currents in small diameter sensory neurons and impairs detection of nociceptive mechanical stimuli *in-vivo* (Beaulieu-Laroche et al., 2020). Thus, TACAN channels are involved in sensing mechanical pain. Elkin channels were found in a melanoma cell line and characterization of this protein with complementary electrophysiological recordings showed that evoked currents of cell lines expressing this channel

led to MA currents with inactivation kinetics of ~30 ms (IA currents) (Patkunarajah et al., 2020). Current research in our lab indicates that Elkin is expressed in sensory neurons and on-going work investigates its role in mechanotransduction in the sensory system. Further studies involving the downregulation or genetic deletion of *piezo2*, *TACAN* and *Elkin* genes in DRGs will elucidate whether additional ion channels contribute to MA currents in sensory neurons.

6.6. PIEZO channels are sensitized by STOML3 in membrane patches

STOML3 potentiates the sensitivity of PIEZO channels to deflection stimuli (Poole et al., 2014). STOML3 is an integral membrane protein that inserts like a hairpin into the plasma membrane and forms a banana-shaped dimer (Brand et al., 2012; Lapatsina et al., 2012). It has been proposed that STOML3 could form a scaffold that regulates sensitivity of PIEZO channels (Poole et al., 2015). Here, it was shown that STOML3 increases sensitivity of PIEZO channels to stretch stimuli when recording MA currents from membrane patches. These results support the model that suggests that sensitization of PIEZO channels by STOML3 is at membrane level (Qi et al., 2015, p. 3), but do not exclude other models proposed by Poole et al. and other authors, where ECM, transmembrane proteins and/or cytoskeletal proteins form a scaffolding protein complexes and, thus, regulate PIEZO2 sensitization (Poole et al., 2015; Schwaller et al., 2021). By performing stretch-sensitive recordings using HSPC, evoked ion currents through PIEZO proteins have similar inactivation kinetics (RA currents), however when using the pillar arrays method, inactivation kinetics of PIEZO channels are heterogenous and RA, IA and SA currents are observed, suggesting 1) the existence of accessory proteins in the ECM and cytoskeleton that regulate PIEZO channels gating, or 2) there are different channel states in mechanical coupling.

It was found that mStoml3 increases the channel availability of the chimeric channel mP1/mP2. It was shown that in the absence of mStoml3, the mP1/mP2 channel had ~10% of apparent open probability. However, in the presence of mStoml3 30% of the channels were available. The release of the voltage block by STOML3 was not observed in mPiezo1 nor in hPIEZO1, suggesting that the effect of mStoml3 by increasing the apparent open probability is specific to the pore of mPiezo2 channels. PIEZO2 channels are poorly gated by membrane stretch (L. Wang et al., 2019), therefore the effect of STOML3 on heterologously expressed PIEZO2 channels makes it hard to study the voltage modulation of the channels. The experiments that showed that PIEZO2 channels are sensitive to membrane stretch were made at non-physiological resting membrane potential (<-100 mV), raising the question whether at physiological $E_{m,rep}$, PIEZO2 channels are stretch-sensitive. However, it is possible that by co-expressing STOML3 with PIEZO2 channels the sensitivity of the channels to membrane stretch increases by releasing

the voltage block. Further experiments can be performed to study whether STOML3 increases stretch-sensitivity and channel availability of PIEZO2 channels at physiological membrane potentials.

6.7. PIEZO1 is essential for mechanotransduction in hiPSC-CMs

Previous studies have demonstrated the expression of PIEZO1 in red blood cells, endothelial cells and cardiac fibroblasts (Liang et al., 2017; Wong et al., 2018). Therefore, it has been proposed that PIEZO1 plays a role in mechanotransduction of cardiac contraction. However, there was no direct electrophysiological evidence supporting the latter. Here, by performing calcium imaging experiments, it was shown that deletion of PIEZO1 in human induced pluripotent stem cell-derived cardiomyocytes (hiPSC-CMs) resulted in total loss of calcium influx when exposed to Yoda1. Furthermore, HSPC recordings indicated that the stretch-sensitive currents observed in hiPSC-CMs were PIEZO1-dependent, suggesting a critical role of PIEZO1 in mechanotransduction of cardiomyocytes.

We showed that the inactivation kinetics and voltage modulation of PIEZO1-dependent MA currents in hiPSC-CMs^{wt} were different to the properties of PIEZO1 heterologously expressed in N2a^{Piezo1^{-/-}} (Figure 5.29-30). The discrepancy in the inactivation kinetics has been described before when recording Piezo1 directly from vein endothelial cells, arterial myocytes and chondrocytes, where channels exhibited very slow inactivation kinetics (J. Li, Hou, Tumova, Muraki, Bruns, Ludlow, Sedo, Hyman, McKeown, et al., 2014; Retailleau et al., 2015; Servin-Vences et al., 2017). Recent studies showed that kinetics of PIEZO channels can be modulated by the lipid composition of the membrane (Ridone et al., 2020; Romero et al., 2019). Thus, it is possible that the observed differences in the inactivation kinetics is due to different lipid composition between N2a^{Piezo1^{-/-}} and hiPSC-CMs^{wt}. The apparent open probability of PIEZO1-dependent MA currents in hiPSC-CMs^{wt} was 5-fold higher than the channel availability of PIEZO1 heterologously expressed in N2a^{Piezo1^{-/-}}. Despite this difference, the stretch-sensitive current from hiPSC-CMs^{wt} was voltage dependent as previously observed in PIEZO channels (Moroni et al., 2018). It is conveyable that membrane lipid composition or proteins endogenously expressed in hiPSC-CMs modulate and increase the open probability of Piezo channels. Similar experiments can be performed in the future to evaluate whether human or murine isolated cardiomyocytes express stretch-sensitive PIEZO1-dependent currents.

7. Conclusions

These investigations showed that mutations in the R2756 of Piezo2 channels are gain-of-function mutations. By overexpressing heterologously the Piezo2 variants in N2a^{Piezo1^{-/-}} cells, it was shown that mutant channels exhibited longer latencies, slower τ_{act} and τ_{inact} kinetics as well as slower time-transitions from inactivated to deactivated states compared to wildtype channels. Additionally, by performing two complementary techniques to stimulate mechanosensitive ion channels, it was found that Piezo2 mutants showed higher sensitivity to mechanical stimuli than under control conditions. Furthermore, it was shown that pathogenic mutations dramatically increase the apparent open probability of the channels. All these features increase the ion flow through the channel and therefore can be classified as gain-of-function mutations.

By generating two *knock-in* mice carrying Piezo2^{R2756H} and Piezo2^{R2756K} mutations, it was shown that a subpopulation of mutant mice developed short stature and scoliosis – features that have been observed in human patients with mutations in *PIEZO2* as well. This supports the idea that the role of PIEZO2 channels is highly conserved in mammals. Moreover, when characterizing the MA currents from isolated sensory neurons from *knock-in* mice, it was found that the MA currents showed similar properties to those observed in the *in-vitro* experiments: currents showed longer latencies and slower τ_{act} and τ_{inact} kinetics than currents from wildtype neurons. Additionally, it was shown that in the native environment, the MA currents from sensory neurons were more sensitive to substrate deflection compared to wildtype cells. Furthermore, it was shown that animals carrying *piezo2* mutations exhibited mechanical hyperalgesia. The *ex-vivo* and *in-vivo* experiments confirm that pathogenic mutations related to DA5, GS and MWS are gain-of-function mutations.

In this work, it was found that sensory neurons lacking *piezo2* showed MA currents. This confirms the idea that other mechanosensitive ion channels have a role in the somatosensory system. Experiments using genetic tools to delete or *knock-down* potential candidates (i.e., Elkin channels) (Patkunarajah et al., 2020) may be performed to further determine the contribution of different MA channels in sensory neurons.

It was shown that the STOML3 protein increases the mechanical sensitivity of PIEZO channels at the membrane level. Additionally, the effect of mStoml3 on increasing the apparent open probability of the chimeric channel mP1/mP2 was discussed. Further experiments *ex-vivo* and *in-vivo* may be needed to understand the physiological role of STOML3 in the voltage regulation of PIEZO2 channels.

In these investigations, by performing patch-clamp and calcium imaging recordings, it was found that the PIEZO1 channel is a major contributor to the stretch sensitive currents in human induced pluripotent stem cell-derived cardiomyocytes (hiPSC-CMs). Further experiments from human cardiac cells may be needed to demonstrate the role of PIEZO1 under more physiological conditions.

PIEZO1 and PIEZO2 channels are evolutionary conserved proteins that are involved in different biological processes. The generation of *knock-out* and *knock-in* mice models is very important for understanding the role of PIEZO proteins in biology. In this thesis, the effect of pathogenic mutations of Piezo2 in the somatosensory system was shown. However, PIEZO2 channels are involved in other biological processes (e.g., respiration, urination, etc.) as well. Using the Piezo2 *knock-in* and *knock-out* mice would help to deeply understand the role of PIEZO2 in these processes and identify further unknown functions.

8. Appendix

8.1. List of figures

Figure 2.1. Structure of PIEZO channels	6
Figure 2.2. Mechanotransduction techniques.....	9
Figure 2.3. Pore module of Piezo1	13
Figure 2.4. Sequence comparison between IH of PIEZO channels.....	14
Figure 2.5. Mechanotransduction in mammalian skin.....	15
Figure 2.6. Expression of PIEZO2 in mechanoreceptors	16
Figure 2.7. Expression of PIEZO2 in nociceptors	19
Figure 4.1. XO-response patterns	39
Figure 5.1. Pillar deflection	44
Figure 5.2. Characterization of the MA currents in N2a ^{Piezo1^{-/-}} cell with pillar arrays technique	45
Figure 5.3. Amino acid residue alignment of the C-terminal domain of PIEZO channels.....	46
Figure 5.4. Expression of mPiezo2 channels in N2a ^{Piezo1^{-/-}} cells lead to deflection-gated currents	47
Figure 5.5. Mutations in R2756 of mPiezo2 increase the deflection sensitivity of the channel	48
Figure 5.6. Pathogenic mutations that cause GS, DA5 and MWS change the biophysical properties of mPiezo2 channels.....	49
Figure 5.7. Mutations that cause GS, DA5 and MWS alter the biophysical properties of the mP1/mP2 chimeric channel.....	51
Figure 5.8. Pathogenic mutations in the chimeric channel affect the inactivation state.....	52
Figure 5.9. Mutations that cause GS, DA5 and MWS modify the voltage modulation of mP1/mP2 chimeric channel.....	53
Figure 5.10. The mP1/mP2 variants deactivate slower and conducts equally in both directions.....	54
Figure 5.11. Generation of Piezo2 <i>knock-in</i> mice.....	55
Figure 5.12. Piezo2 ^{R2756H/R2756H} animals have reduced size compared to wildtype mice.....	56
Figure 5.13. Piezo2 ^{R2756K/R2756K} animals develop spinal cord curvature.....	57
Figure 5.14. Types of sensory neurons	58
Figure 5.15. Insertion of R2756 mutations in Piezo2 changes IA and SA current ratios and increase sensitivity of mechanoreceptors.....	59
Figure 5.16. Maximum peak currents of mechanoreceptors were reached at smaller deflections <i>knock-in</i> mice.....	60
Figure 5.17. Mutations in R2756 of Piezo2 channels change biophysical properties of mechanoreceptors in mice	61
Figure 5.18. Mutations in the R2756 of Piezo2 increase sensitivity of MA currents in nociceptors.....	63
Figure 5.19. Maximum peak currents of nociceptors	64
Figure 5.20. Nociceptors from knock-in mice were more sensitive and responsive to deflection stimuli. 64	

Figure 5.21. Mutations in R2756 of Piezo2 channels change biophysical properties of nociceptors in mice	65
Figure 5.22. Piezo2 <i>knock-in</i> mice develop reduced 50% PWT	66
Figure 5.23. Types of mechanically gated currents from embryonic DRG neurons	68
Figure 5.24. Biophysical properties of MA currents from embryonic DRG neurons	69
Figure 5.25. MA currents from embryonic Piezo2 ^{-/-} DRG neurons.	70
Figure 5.26. Types of deflection gated currents from Piezo2 ^{CKO} mice	71
Figure 5.27. Biophysical properties of deflection sensitive currents in DRG neurons from Piezo2 ^{CKO}	72
Figure 5.28. Sensitization of PIEZO channels by STOML3.....	73
Figure 5.29. The mStoml3 protein increases the channel availability of the mP1/mP2 channel	75
Figure 5.30. Stretch-sensitive currents in hiPSC-CMs are PIEZO1-dependent	77
Figure 5.31. Voltage modulation of PIEZO1-dependent currents in hiPSC-CMs.....	78
Figure 6.1. Mutations in Arg2756 of Piezo2 are gain of function mutations	83
Figure 6.2. GoF mutations in Piezo2 increases sensitivity to noxious responses	87

8.2. List of tables

Table 2.1. Biophysical properties of PIEZO1 channels.....	10
Table 2.2. Biophysical properties of PIEZO1 mutants related to human diseases	11
Table 2.3. Biophysical properties of PIEZO2 channels.....	11
Table 2.4. Biophysical properties of PIEZO2 mutants related to human diseases	12
Table 2.5 Clinical features associated with LoF mutations in PIEZO2	25
.....	25
Table 2.6 Clinical characteristics associated with PIEZO2 mutations	26
Table 4.1. PCR primers used for site-directed mutagenesis.....	33
Table 4.2. gRNA and ssDNA donor sequences used to insert point mutations in Piezo2	35
Table 4.3. PCR primers used for genotyping transgenic mice.....	37
Table 5.1. Biophysical properties of N2a ^{Piezo1^{-/-}} cells overexpressing mPiezo2 mutants	49
Table 5.2. Biophysical properties of deflection gated currents in mechanoreceptors from Piezo2 ^{R2756H/K} mice	61
.....	61
Table 5.3. Biophysical properties of deflection gated currents in nociceptors from Piezo2 ^{R2756H/K} mice....	66
Table 5.4. Electrophysiological properties of MA currents recorded from embryonic DRG neurons.....	69
Table 5.5. Biophysical properties of PIEZO channels co-expressed with STOML3.....	73

8.3. Abbreviations

3D	three-dimensional	hiPSCs	human induced pluripotent stem cells
AP	action potential	His	histidine
Arg	arginine	HP	half peak
ATP	adenosine triphosphate	HSPC	high-speed pressure clamp
CMs	cardiomyocytes	HX	hereditary Xerocytosis
Cry-EM	cryo-electron microscopy	IA	intermediate adapting
CTD	C-terminal domain	IH	inner helix
Cys	cysteine	KI	knock-in
DA5	distal arthrogyrosis type 5	LoF	loss-of-function
DNA	deoxyribonucleic acid	Lys	lysine
DRG	dorsal root ganglia	MA	mechanically activated
EC	enterochromaffin cells	Min	minutes
ECM	extracellular matrix	mmHg	millimeter of mercury
Em _{rep}	resting membrane potential	MS	mechanical stimulator
GFP	green fluorescent protein	ms	millisecond
GoF	gain-of-function	MS	muscle spindle
gRNAs	guide RNA	mV	millivolts
GS	Gordon syndrome	MWS	Marden-Walker syndrome
GTO	Golgi tendon organ	N2a	neuro 2a cells
HEK-293 cells 293	human embryonic kidney cells 293	nd	not determined
hiPSC-CMs	human induced pluripotent stem cell-derived cardiomyocytes	Nm	nanometer

O/O outside-out patch clamp
configuration

OH outer helix

P₅₀ half-activation pressure

pA picoampere

PDMS polydimethylsiloxane

PLL poly-L-lysine

PCR polymerase chain reaction

PWT paw withdrawal threshold

RA rapidly adapting

RE recording electrode

s.d. standard deviation

s.e.m. standard error of the mean

SA slowly adapting

ssDNA single-stranded DNA

TM transmembrane domain

wt wildtype

τ_{act} time constant of activation

τ_{inact} time constant of inactivation

9. References

- Abdo, H., Calvo-Enrique, L., Lopez, J. M., Song, J., Zhang, M. D., Usoskin, D., Manira, A. El, Adameyko, I., Hjerling-Leffler, J., & Ernfors, P. (2019). Specialized cutaneous schwann cells initiate pain sensation. *Science*, *365*(6454), 695–699. <https://doi.org/10.1126/science.aax6452>
- Abraira, V. E., & Ginty, D. D. (2013). The sensory neurons of touch. *Neuron*, *79*(4), 618–639. <https://doi.org/10.1016/j.neuron.2013.07.051>
- Albuisson, J., Murthy, S. E., Bandell, M., Coste, B., Louis-dit-Picard, H., Mathur, J., Fénéant-Thibault, M., Tertian, G., de Jaureguiberry, J.-P., Syfuss, P.-Y., Cahalan, S. M., Garcon, L., Toutain, F., Rohrich, P. S., Delaunay, J., Picard, V., Jeunemaitre, X., & Patapoutian, A. (2013). Dehydrated hereditary stomatocytosis linked to gain-of-function mutations in mechanically activated PIEZO1 ion channels. *Nature Communications*, *May*. <https://doi.org/10.1038/ncomms2899>
- Alcaino, C., Knutson, K. R., Treichel, A. J., Yildiz, G., Strega, P. R., Linden, D. R., Li, J. H., Leiter, A. B., Szurszewski, J. H., Farrugia, G., & Beyder, A. (2018). A population of gut epithelial enterochromaffin cells is mechanosensitive and requires Piezo2 to convert force into serotonin release. *Proceedings of the National Academy of Sciences of the United States of America*, *115*(32), E7632–E7641. <https://doi.org/10.1073/pnas.1804938115>
- Alisch, F., Weichert, A., Kalache, K., Paradiso, V., Longardt, A. C., Dame, C., Hoffmann, K., & Horn, D. (2016). Familial Gordon syndrome associated with a PIEZO2 mutation. *American Journal of Medical Genetics, Part A*, *173*(1), 254–259. <https://doi.org/10.1002/ajmg.a.37997>
- Andolfo, I., Alper, S. L., Franceschi, L. De, Auriemma, C., Russo, R., Falco, L. De, Vallefuoco, F., Esposito, M. R., Vandorpe, D. H., Shmukler, B. E., Narayan, R., Montanaro, D., Armiento, M. D., Vetro, A., Limongelli, I., Zuffardi, O., Glader, B. E., Schrier, S. L., Brugnara, C., ... Iolascon, A. (2013). Regular Article Multiple clinical forms of dehydrated hereditary stomatocytosis arise from mutations in PIEZO1. *Blood*, *121*(19), 3925–3936. <https://doi.org/10.1182/blood-2013-02-482489>.The
- Arber, S., Ladle, D. R., Lin, J. H., Frank, E., & Jessell, T. M. (2000). ETS gene Er81 controls the formation of functional connections between group Ia sensory afferents and motor neurons. *Cell*, *101*(5), 485–498. [https://doi.org/10.1016/s0092-8674\(00\)80859-4](https://doi.org/10.1016/s0092-8674(00)80859-4)
- Assaraf, E., Blecher, R., Heinemann-Yerushalmi, L., Krief, S., Carmel Vinestock, R., Biton, I. E., Brumfeld, V., Rotkopf, R., Avisar, E., Agar, G., & Zelzer, E. (2020). Piezo2 expressed in proprioceptive neurons is essential for skeletal integrity. *Nature Communications*, *11*(1), 1–15. <https://doi.org/10.1038/s41467-020-16971-6>
- Bae, C., Gnanasambandam, R., Nicolai, C., Sachs, F., & Gottlieb, P. A. (2013). Xerocytosis is caused by mutations that alter the kinetics of the mechanosensitive channel PIEZO1. *Proceedings of the National Academy of Sciences of the United States of America*, *116*2–1168. <https://doi.org/10.1073/pnas.1219777110> /DCSupplemental.www.pnas.org/cgi/doi/10.1073/pnas.1219777110
- Beaulieu-Laroche, L., Christin, M., Donoghue, A., Agosti, F., Yousefpour, N., Petitjean, H., Davidova, A., Stanton, C., Khan, U., Dietz, C., Faure, E., Fatima, T., MacPherson, A., Mouchbahani-Constance, S., Bisson, D. G., Haglund, L., Ouellet, J. A., Stone, L. S., Samson, J., ... Sharif-Naeini, R. (2020). TACAN Is an Ion Channel Involved in Sensing Mechanical Pain. *Cell*, *180*(5), 956–967.e17. <https://doi.org/10.1016/j.cell.2020.01.033>

- Behunova, J., Gerykova Bujalkova, M., Gras, G., Taylor, T., Ihm, U., Kircher, S., Rehder, H., & Laccone, F. (2019). Distal Arthrogryposis with Impaired Proprioception and Touch: Description of an Early Phenotype in a Boy with Compound Heterozygosity of PIEZO2 Mutations and Review of the Literature. *Molecular Syndromology*, 9(6), 287–294. <https://doi.org/10.1159/000494451>
- Bewick, G. S., & Banks, R. W. (2014). Mechanotransduction in the muscle spindle. *Pflügers Archiv European Journal of Physiology*, 467(1), 175–190. <https://doi.org/10.1007/s00424-014-1536-9>
- Bockenhauer, D., Zilberberg, N., & Goldstein, S. A. N. (2001). KCNK2: Reversible conversion of a hippocampal potassium leak into a voltage-dependent channel. *Nature Neuroscience*, 4(5), 486–491. <https://doi.org/10.1038/87434>
- Brand, J., Smith, E. S. J., Schwefel, D., Lapatsina, L., Poole, K., Omerbašić, D., Kozlenkov, A., Behlke, J., Lewin, G. R., & Daumke, O. (2012). A stomatin dimer modulates the activity of acid-sensing ion channels: Structure of the stomatin dimer. *The EMBO Journal*, 31(17), 3635–3646. <https://doi.org/10.1038/emboj.2012.203>
- BurrIDGE, P. W., Matsa, E., Shukla, P., Lin, Z. C., Churko, J. M., Ebert, A. D., Lan, F., Diecke, S., Huber, B., Mordwinkin, N. M., Plews, J. R., Abilez, O. J., Cui, B., Gold, J. D., & Wu, J. C. (2014). Chemically defined generation of human cardiomyocytes. *Nature Methods*, 11(8), 855–860. <https://doi.org/10.1038/nMeth.2999>
- Cahalan, S. M., Lukacs, V., Ranade, S. S., Chien, S., Bandell, M., & Patapoutian, A. (2015). Piezo1 links mechanical forces to red blood cell volume. *ELife*. <https://doi.org/10.7554/eLife.07370>
- Caterina, M. J., Schumacher, M. A., Tominaga, M., Rosen, T. A., Levine, J. D., & Julius, D. (1997). The capsaicin receptor: A heat-activated ion channel in the pain pathway. *Nature*, 389(6653), 816–824. <https://doi.org/10.1038/39807>
- Chaplan, S. R., Bach, F. W., Pogrel, J. W., Chung, J. M., & Yaksh, T. L. (1994). Quantitative assessment of tactile allodynia in the rat paw. *Journal of Neuroscience Methods*, 53(1), 55–63. [https://doi.org/10.1016/0165-0270\(94\)90144-9](https://doi.org/10.1016/0165-0270(94)90144-9)
- Chesler, A. T., Szczot, M., Bharucha-Goebel, D., Čeko, M., Donkervoort, S., Laubacher, C., Hayes, L. H., Alter, K., Zampieri, C., Stanley, C., Innes, A. M., Mah, J. K., Grosman, C. M., Bradley, N., Nguyen, D., Foley, A. R., Le Pichon, C. E., & Bönnemann, C. G. (2016). The role of PIEZO2 in human mechanosensation. *New England Journal of Medicine*, 375(14), 1355–1364. <https://doi.org/10.1056/NEJMoa1602812>
- Christensen, S. L., Hansen, R. B., Storm, M. A., Olesen, J., Hansen, T. F., Ossipov, M., Izarzugaza, J. M. G., Porreca, F., & Kristensen, D. M. (2020). Von Frey testing revisited: Provision of an online algorithm for improved accuracy of 50% thresholds. *European Journal of Pain*, 24(4), 783–790. <https://doi.org/10.1002/ejp.1528>
- Chubinskiy-Nadezhdin, V. I., Vasileva, V. Y., Vassilieva, I. O., Sudarikova, A. V., Morachevskaya, E. A., & Negulyaev, Y. A. (2019). Agonist-induced Piezo1 activation suppresses migration of transformed fibroblasts. *Biochemical and Biophysical Research Communications*, 514(1), 173–179. <https://doi.org/10.1016/j.bbrc.2019.04.139>
- Coste, B., Houge, G., Murray, M. F., Stitzel, N., Bandell, M., Giovanni, M. A., Philippakis, A., Hoischen, A., Riemer, G., Steen, U., Steen, V. M., Mathur, J., Cox, J., Lebo, M., Rehm, H., Weiss, S. T., Wood, J. N., Maas, R. L., Sunyaev, S. R., & Patapoutian, A. (2013). Gain-of-function mutations in the mechanically activated ion channel PIEZO2 cause a subtype of Distal Arthrogryposis. *Proceedings of the National Academy of Sciences*, 110(12), 4667–4672. <https://doi.org/10.1073/pnas.1221400110>

- Coste, B., Mathur, J., Schmidt, M., Earley, T. J., Ranade, S., Petrus, M. J., Dubin, A. E., & Patapoutian, A. (2010). Piezo1 and Piezo2 Are Essential Components of Distinct Mechanically Activated Cation Channels. *Science*, 330(6000), 55–60. <https://doi.org/10.1126/science.1193270>
- Coste, Bertrand, Mathur, J., Schmidt, M., Earley, T. J., Ranade, S., Petrus, M. J., Dubin, A. E., & Patapoutian, A. (2010). Piezo1 and Piezo2 Are Essential Components of Distinct Mechanically Activated Cation Channels. *Science*, 330, 55–60.
- Coste, Bertrand, Xiao, B., Santos, J. S., Syeda, R., Grandl, J., Spencer, K. S., Kim, S. E., Schmidt, M., Mathur, J., Dubin, A. E., Montal, M., & Patapoutian, A. (2012). Piezo proteins are pore-forming subunits of mechanically activated channels. *Nature*, 483, 176–181. <https://doi.org/10.1038/nature10812>
- Davies, J. E., Lopresto, D., Apta, B. H. R., Lin, Z., Ma, W., & Harper, M. T. (2019). Using Yoda-1 to mimic laminar flow in vitro: A tool to simplify drug testing. *Biochemical Pharmacology*, 168, 473–480. <https://doi.org/10.1016/j.bcp.2019.08.013>
- de Groat, W. C. & Yoshimura, N. A. (2009). Afferent nerve regulation of bladder function in health and disease. *Handb. Exp. Pharmacol.*, 194, 91–138. <https://doi.org/10.1007/978>
- Delle Vedove, A., Storbeck, M., Heller, R., Hölker, I., Hebbar, M., Shukla, A., Magnusson, O., Cirak, S., Girisha, K. M., O'Driscoll, M., Loeys, B., & Wirth, B. (2016). Biallelic Loss of Proprioception-Related PIEZO2 Causes Muscular Atrophy with Perinatal Respiratory Distress, Arthrogryposis, and Scoliosis. *American Journal of Human Genetics*, 99(5), 1206–1216. <https://doi.org/10.1016/j.ajhg.2016.09.019>
- Dhandapani, R., Arokiaraj, C. M., Taberner, F. J., Pacifico, P., Raja, S., Nocchi, L., Portulano, C., Franciosa, F., Maffei, M., Hussain, A. F., de Castro Reis, F., Reymond, L., Perlas, E., Garcovich, S., Barth, S., Johnsson, K., Lechner, S. G., & Heppenstall, P. A. (2018). Control of mechanical pain hypersensitivity in mice through ligand-targeted photoablation of TrkB-positive sensory neurons. *Nature Communications*, 9(1), 1640. <https://doi.org/10.1038/s41467-018-04049-3>
- Dixon, W. J. (1980). Efficient Analysis of Experimental Observations. *Annual Review of Pharmacology and Toxicology*, 20(1), 441–462. <https://doi.org/10.1146/annurev.pa.20.040180.002301>
- Dubin, A. E., Schmidt, M., Mathur, J., Petrus, M. J., Xiao, B., Coste, B., & Patapoutian, A. (2012). Inflammatory Signals Enhance Piezo2-Mediated Mechanosensitive Currents. *Cell Reports*, 2(3), 511–517. <https://doi.org/10.1016/j.celrep.2012.07.014>
- Eijkelkamp, N., Linley, J. E., Torres, J. M., Bee, L., Dickenson, A. H., Gringhuis, M., Minett, M. S., Hong, G. S., Lee, E., Oh, U., Ishikawa, Y., Zwartkuis, F. J., Cox, J. J., & Wood, J. N. (2013). A role for Piezo2 in EPAC1-dependent mechanical allodynia. *Nature Communications*, 4. <https://doi.org/10.1038/ncomms2673>
- Florez-Paz, D., Bali, K. K., Kuner, R., & Gomis, A. (2016). A critical role for Piezo2 channels in the mechanotransduction of mouse proprioceptive neurons. *Nature Scientific Reports*. <https://doi.org/10.1038/srep25923>
- García-Mesa, Y., García-Piqueras, J., García, B., Feito, J., Cabo, R., Cobo, J., Vega, J. A., & García-Suárez, O. (2017). Merkel cells and Meissner's corpuscles in human digital skin display Piezo2 immunoreactivity. *Journal of Anatomy*, 231(6), 978–989. <https://doi.org/10.1111/joa.12688>

- Ge, J., Li, W., Zhao, Q., Li, N., Chen, M., Zhi, P., Li, R., Gao, N., Xiao, B., & Yang, M. (2015). Architecture of the mammalian mechanosensitive Piezo1 channel. *Nature*, *527*(7576), 64–69. <https://doi.org/10.1038/nature15247>
- Guharay, F., & Sachs, F. (1984). Stretch-activated single ion channel currents in tissue-cultured embryonic chick skeletal muscle. *J. Physiol.*, *352*, 685–701.
- Guo, Y. R., & MacKinnon, R. (2017). Structure-based membrane dome mechanism for Piezo mechanosensitivity. *ELife*, *6*, 1–19. <https://doi.org/10.7554/elife.33660>
- Haliloglu, G., Becker, K., Temucin, C., Talim, B., Küçüksahin, N., Pergande, M., Motameny, S., Nürnberg, P., Aydingoz, U., Topaloglu, H., & Cirak, S. (2017). Recessive PIEZO2 stop mutation causes distal arthrogryposis with distal muscle weakness, scoliosis and proprioception defects. *Journal of Human Genetics*, *62*(4), 497–501. <https://doi.org/10.1038/jhg.2016.153>
- Hu, J., & Lewin, G. R. (2006). Mechanosensitive currents in the neurites of cultured mouse sensory neurones. *The Journal of Physiology*, *3*, 815–828. <https://doi.org/10.1113/jphysiol.2006.117648>
- Ikeda, R., Cha, M., Ling, J., Jia, Z., Coyle, D., & Gu, J. G. (2014). Merkel cells transduce and encode tactile stimuli to drive $\alpha\beta$ -Afferent impulses. *Cell*, *157*(3), 664–675. <https://doi.org/10.1016/j.cell.2014.02.026>
- Jia, Y., Zhao, Y., Kusakizako, T., Wang, Y., Pan, C., Zhang, Y., Nureki, O., Hattori, M., & Yan, Z. (2020). TMC1 and TMC2 Proteins Are Pore-Forming Subunits of Mechanosensitive Ion Channels. *Neuron*, *105*(2), 310–321.e3. <https://doi.org/10.1016/j.neuron.2019.10.017>
- Johnson, K. O. (2001). The roles and functions of cutaneous mechanoreceptors. *Current Opinion in Neurobiology*, *11*(4), 455–461. [https://doi.org/10.1016/S0959-4388\(00\)00234-8](https://doi.org/10.1016/S0959-4388(00)00234-8)
- Johnson, Kenneth O., Yoshioka, T., & Vega Bermudez, F. (2000). Tactile functions of mechanoreceptive afferents innervating the hand. *Journal of Clinical Neurophysiology*, *17*(6), 539–558. <https://doi.org/10.1097/00004691-200011000-00002>
- Koerber, H. R., Druzinsky, R. E., & Mendell, L. M. (1988). Properties of somata of spinal dorsal root ganglion cells differ according to peripheral receptor innervated. *Journal of Neurophysiology*, *60*(5), 1584–1596. <https://doi.org/10.1152/jn.1988.60.5.1584>
- Lai, A., Chen, Y. C., Cox, C. D., Jaworowski, A., Peter, K., & Baratchi, S. (2020). Analyzing the shear-induced sensitization of mechanosensitive ion channel Piezo-1 in human aortic endothelial cells. *Journal of Cellular Physiology*, *jcp.30056*. <https://doi.org/10.1002/jcp.30056>
- Lapatsina, L., Brand, J., Poole, K., Daumke, O., & Lewin, G. R. (2012). Stomatin-domain proteins. *European Journal of Cell Biology*, *91*(4), 240–245. <https://doi.org/10.1016/j.ejcb.2011.01.018>
- Lechner, S. G., Frenzel, H., Wang, R., & Lewin, G. R. (2009). Developmental waves of mechanosensitivity acquisition in sensory neuron subtypes during embryonic development. *The EMBO Journal*, *28*(10), 1479–1491. <https://doi.org/10.1038/emboj.2009.73>
- Lechner, S. G., & Lewin, G. R. (2013). Hairy Sensation. *Physiology (Bethesda, Md.)*, *28*(52), 142–150. <https://doi.org/10.1152/physiol.00059.2012>
- Lewin, G. R., & Moshourab, R. (2004). Mechanosensation and pain. *Journal of Neurobiology*, *61*(1), 30–44. <https://doi.org/10.1002/neu.20078>

- Li, J., Hou, B., Tumova, S., Muraki, K., Bruns, A., Ludlow, M. J., Sedo, A., Hyman, A. J., Mckeown, L., Young, R. S., Yuldasheva, N. Y., Majeed, Y., Wilson, L. A., Rode, B., Bailey, M. A., Kim, H. R., Fu, Z., Carter, D. A. L., Bilton, J., ... Beech, D. J. (2014). Piezo1 integration of vascular architecture with physiological force. *Nature*, *515*(7526), 279–282. <https://doi.org/10.1038/nature13701>
- Li, S., You, Y., Gao, J., Mao, B., Cao, Y., Zhao, X., & Zhang, X. (2018). Novel mutations in TPM2 and PIEZO2 are responsible for distal arthrogryposis (DA) 2B and mild da in two Chinese families. *BMC Medical Genetics*, *19*(1), 1–11. <https://doi.org/10.1186/s12881-018-0692-8>
- Liang, J., Huang, B., Yuan, G., Chen, Y., Liang, F., Zeng, H., Zheng, S., Cao, L., Geng, D. F., & Zhou, S. X. (2017). Stretch-activated channel Piezo1 is up-regulated in failure heart and cardiomyocyte stimulated by Angii. *American Journal of Translational Research*, *9*(6), 2945–2955.
- Lukacs, V., Mathur, J., Mao, R., Bayrak-Toydemir, P., Procter, M., Cahalan, S. M., Kim, H. J., Bandell, M., Longo, N., Day, R. W., Stevenson, D. A., Patapoutian, A., & Krock, B. L. (2015). Impaired PIEZO1 function in patients with a novel autosomal recessive congenital lymphatic dysplasia. *Nature Communications*, *6*, 1–7. <https://doi.org/10.1038/ncomms9329>
- Ma, S., Cahalan, S., LaMonte, G., Grubaugh, N. D., Zeng, W., Murthy, S. E., Paytas, E., Gamini, R., Lukacs, V., Whitwam, T., Loud, M., Lohia, R., Berry, L., Khan, S. M., Janse, C. J., Bandell, M., Schmedt, C., Wengelnik, K., Su, A. I., ... Patapoutian, A. (2018). Common PIEZO1 Allele in African Populations Causes RBC Dehydration and Attenuates Plasmodium Infection. *Cell*, *173*(2), 443–455.e12. <https://doi.org/10.1016/j.cell.2018.02.047>
- Ma, Y., Zhao, Y., Cai, Z., & Hao, X. (2019). Mutations in PIEZO2 contribute to Gordon syndrome, Marden-Walker syndrome and distal arthrogryposis: A bioinformatics analysis of mechanisms. *Experimental and Therapeutic Medicine*, *17*, 3518–3524. <https://doi.org/10.3892/etm.2019.7381>
- Madisen, L., Zwingman, T. A., Sunkin, S. M., Oh, S. W., Zariwala, H. A., Gu, H., Ng, L. L., Palmiter, R. D., Hawrylycz, M. J., Jones, A. R., Lein, E. S., & Zeng, H. (2010). A robust and high-throughput Cre reporting and characterization system for the whole mouse brain. *Nature Neuroscience*, *13*(1), 133–140. <https://doi.org/10.1038/nn.2467>
- Mahmud, A. A., Nahid, N. A., Nassif, C., Sayeed, M. S. B., Ahmed, M. U., Parveen, M., Khalil, M. I., Islam, M. M., Nahar, Z., Rypens, F., Hamdan, F. F., Rouleau, G. A., Hasnat, A., & Michaud, J. L. (2017). Loss of the proprioception and touch sensation channel PIEZO2 in siblings with a progressive form of contractures. *Clinical Genetics*, *91*(3), 470–475. <https://doi.org/10.1111/cge.12850>
- Maingret, F., Honoré, E., Lazdunski, M., & Patel, A. J. (2002). Molecular Basis of the Voltage-Dependent Gating of TREK-1, a Mechano-Sensitive K⁺ Channel. *Biochemical and Biophysical Research Communications*, *292*(2), 339–346. <https://doi.org/10.1006/bbrc.2002.6674>
- Maksimovic, S., Nakatani, M., Baba, Y., Nelson, A. M., Marshall, K. L., Wellnitz, S. A., Firozi, P., Woo, S. H., Ranade, S., Patapoutian, A., & Lumpkin, E. A. (2014). Epidermal Merkel cells are mechanosensory cells that tune mammalian touch receptors. *Nature*, *509*(7502), 617–621. <https://doi.org/10.1038/nature13250>
- Marshall, K. L., Saade, D., Ghitani, N., Coombs, A. M., Szczot, M., Keller, J., Ogata, T., Daou, I., Stowers, L. T., Bönnemann, C. G., Chesler, A. T., & Patapoutian, A. (2020). PIEZO2 in

- sensory neurons and urothelial cells coordinates urination. *Nature*, *March*.
<https://doi.org/10.1038/s41586-020-2830-7>
- Martinac, B., Buechner, M., Delcour, A. H., Adler, J., & Kung, C. (1987). Pressure-sensitive ion channel in *Escherichia coli*. *Proceedings of the National Academy of Sciences*, *84*(8), 2297–2301. <https://doi.org/10.1073/pnas.84.8.2297>
- Mcmillin, M. J., Beck, A. E., Chong, J. X., Shively, K. M., Buckingham, K. J., Gildersleeve, H. I. S., Aracena, M. I., Aylsworth, A. S., Bitoun, P., Carey, J. C., Clericuzio, C. L., Crow, Y. J., Curry, C. J., Devriendt, K., Everman, D. B., Fryer, A., Gibson, K., Luisa, M., Uzielli, G., ... Bamshad, M. J. (2014). Mutations in PIEZO2 Cause Gordon Syndrome, Marden-Walker Syndrome, and Distal Arthrogyriposis Type 5. *The American Journal of Human Genetics*, *94*(5), 734–744. <https://doi.org/10.1016/j.ajhg.2014.03.015>
- Moroni, M., Servin-ences, M. R., Fleischer, R., Sánchez-Carranza, O., & Lewin, G. R. (2018). Voltage gating of mechanosensitive PIEZO channels. *Nature Communications*, *2018*, 1–15. <https://doi.org/10.1038/s41467-018-03502-7>
- Murthy, S. E., Dubin, A. E., Whitwam, T., Jojoa-Cruz, S., Cahalan, S. M., Mousavi, S. A. R., Ward, A. B., & Patapoutian, A. (2018). OSCA/TMEM63 are an evolutionarily conserved family of mechanically activated ion channels. *ELife*, *7*, 1–17. <https://doi.org/10.7554/eLife.41844>
- Murthy, S. E., Loud, M. C., Daou, I., Marshall, K. L., Schwaller, F., Kühnemund, J., Francisco, A. G., Keenan, W. T., Dubin, A. E., Lewin, G. R., & Patapoutian, A. (2018). The mechanosensitive ion channel Piezo2 mediates sensitivity to mechanical pain in mice. *Science Translational Medicine*, *10*(462), eaat9897. <https://doi.org/10.1126/scitranslmed.aat9897>
- Neubarth, N. L., Emanuel, A. J., Liu, Y., Springel, M. W., Handler, A., Zhang, Q., Lehnert, B. P., Guo, C., Orefice, L. L., Abdelaziz, A., DeLisle, M. M., Iskols, M., Rhyins, J., Kim, S. J., Cattel, S. J., Regehr, W., Harvey, C. D., Drugowitsch, J., & Ginty, D. D. (2020). Meissner corpuscles and their spatially intermingled afferents underlie gentle touch perception. *Science*, *368*(6497). <https://doi.org/10.1126/science.abb2751>
- Nonomura, K., Woo, S., Chang, R. B., Gillich, A., Qiu, Z., & Francisco, A. G. (2017). Piezo2 senses airway stretch and mediates lung inflation-induced apnoea. *Nature*, *541*(7636), 176–181. <https://doi.org/10.1038/nature20793>
- Nosyreva, E. D., Thompson, D., & Syeda, R. (2020). Identification and functional characterization of the Piezo1 channel pore domain. *Journal of Biological Chemistry*, jbc.RA120.015905. <https://doi.org/10.1074/jbc.RA120.015905>
- Okubo, M., Fujita, A., Saito, Y., Komaki, H., Ishiyama, A., Takeshita, E., Kojima, E., Koichihara, R., Saito, T., Nakagawa, E., Sugai, K., Yamazaki, H., Kusaka, K., Tanaka, H., Miyake, N., Matsumoto, N., & Sasaki, M. (2015). A family of distal arthrogyriposis type 5 due to a novel PIEZO2 mutation. *American Journal of Medical Genetics, Part A*, *167*(5), 1100–1106. <https://doi.org/10.1002/ajmg.a.36881>
- Pathak, M. M., Nourse, J. L., Tran, T., Hwe, J., Arulmoli, J., Le, D. T. T., Bernardis, E., Flanagan, L. A., & Tombola, F. (2014). Stretch-activated ion channel Piezo1 directs lineage choice in human neural stem cells. *Proceedings of the National Academy of Sciences of the United States of America*, *111*(45), 16148–16153. <https://doi.org/10.1073/pnas.1409802111>
- Patkunarajah, A., Stear, J. H., Moroni, M., Schroeter, L., Blaszkiewicz, J., Tearle, J. L. E., Cox, C. D., Fuerst, C., Sánchez-Carranza, O., Fernández, M. D. Á. O., Fleischer, R., Eravci, M., Weise, C., Martinac, B., Biro, M., Lewin, G. R., & Poole, K. (2020). TMEM87a/Elkin1, a

- component of a novel mechanoelectrical transduction pathway, modulates melanoma adhesion and migration. *ELife*, 9, 1–25. <https://doi.org/10.7554/eLife.53308>
- Poole, K., Herget, R., Lapatsina, L., Ngo, H.-D., & Lewin, G. R. (2014). Turning Piezo ion channels to detect molecular-scale movements relevant for fine touch. *Nature Communications*, 5. <https://doi.org/10.1038/ncomms4520>
- Poole, K., Moroni, M., & Lewin, G. R. (2015). Sensory mechanotransduction at membrane-matrix interfaces. *Pflügers Arch*, 467, 121–132. <https://doi.org/10.1007/s00424-014-1563-6>
- Proske, U., & Gandevia, S. C. (2012). The proprioceptive senses: Their roles in signaling body shape, body position and movement, and muscle force. *Physiological Reviews*, 92(4), 1651–1697. <https://doi.org/10.1152/physrev.00048.2011>
- Qi, Y., Andolfi, L., Frattini, F., Mayer, F., Lazzarino, M., & Hu, J. (2015). Membrane stiffening by STOML3 facilitates mechanosensation in sensory neurons. *Nature Communications*, 6, 1–13. <https://doi.org/10.1038/ncomms9512>
- Ranade, S. S., Qiu, Z., Woo, S., Sik, S., Murthy, S. E., Cahalan, S. M., Xu, J., Mathur, J., Bandell, M., Coste, B., Li, Y.-S. J., Chien, S., & Patapoutian, A. (2014). Piezo1, a mechanically activated ion channel, is required for vascular development in mice. *Proceedings of the National Academy of Sciences of the United States of America*, 111(28), 10347–10352. <https://doi.org/10.1073/pnas.1409233111>
- Ranade, S. S., Syeda, R., & Patapoutian, A. (2015). Mechanically Activated Ion Channels. *Neuron*, 87(6), 1162–1179. <https://doi.org/10.1016/j.neuron.2015.08.032>
- Ranade, S. S., Woo, S.-H., Dubin, A. E., Moshourab, R. A., Wetzel, C., Petrus, M., Mathur, J., Bégay, V., Coste, B., Mainquist, J., Wilson, A. J., Francisco, A. G., Reddy, K., Qiu, Z., Wood, J. N., Lewin, G. R., & Patapoutian, A. (2014). Piezo2 is the major transducer of mechanical forces for touch sensation in mice. *Nature*, 516, 121–125. <https://doi.org/10.1038/nature13980>
- Retailleau, K., Duprat, F., Arhatte, M., Ranade, S. S., Peyronnet, R., Martins, J. R., Jodar, M., Moro, C., Offermanns, S., Feng, Y., Demolombe, S., Patel, A., & Honoré, E. (2015). Piezo1 in Smooth Muscle Cells Is Involved in Hypertension-Dependent Arterial Remodeling. *Cell Reports*, 13(6), 1161–1171. <https://doi.org/10.1016/j.celrep.2015.09.072>
- Richner, M., Bjerrum, O. J., Nykjaer, A., & Vaegter, C. B. (2011). The spared nerve injury (SNI) model of induced mechanical allodynia in mice. *Journal of Visualized Experiments*, 54, 3–5. <https://doi.org/10.3791/3092>
- Ridone, P., Pandzic, E., Vassalli, M., Cox, C. D., Macmillan, A., Gottlieb, P. A., & Martinac, B. (2020). Disruption of membrane cholesterol organization impairs the activity of PIEZO1 channel clusters. *The Journal of General Physiology*, 152(8). <https://doi.org/10.1085/jgp.201912515>
- Robert, X., & Gouet, P. (2014). Deciphering key features in protein structures with the new ENDscript server. *Nucleic Acids Research*, 42(W1), W320–W324. <https://doi.org/10.1093/nar/gku316>
- Romero, L. O., Massey, A. E., Mata-Daboin, A. D., Sierra-Valdez, F. J., Chauhan, S. C., Cordero-Morales, J. F., & Vásquez, V. (2019). Dietary fatty acids fine-tune Piezo1 mechanical response. *Nature Communications*, 10(1), 1–14. <https://doi.org/10.1038/s41467-019-09055-7>

- Rose, R. D., Koerber, H. R., Sedivec, M. J., & Mendell, L. M. (1986). Somal action potential duration differs in identified primary afferents. *Neuroscience Letters*, *63*(3), 259–264. [https://doi.org/10.1016/0304-3940\(86\)90366-6](https://doi.org/10.1016/0304-3940(86)90366-6)
- Saotome, K., Murthy, S. E., Kefauver, J. M., Whitwam, T., Patapoutian, A., & Ward, A. B. (2018). Structure of the mechanically activated ion channel Piezo1. *Nature*, *554*(7693), 481–486. <https://doi.org/10.1038/nature25453>
- Schewe, M., Nematian-Ardestani, E., Sun, H., Musinszki, M., Cordeiro, S., Bucci, G., de Groot, B. L., Tucker, S. J., Rapedius, M., & Baukrowitz, T. (2016). A Non-canonical Voltage-Sensing Mechanism Controls Gating in K2P K⁺ Channels. *Cell*, *164*(5), 937–949. <https://doi.org/10.1016/j.cell.2016.02.002>
- Schwaller, F., Bégay, V., García-García, G., Taberner, F. J., Moshourab, R., McDonald, B., Docter, T., Kühnemund, J., Ojeda-Alonso, J., Paricio-Montesinos, R., Lechner, S. G., Poulet, J. F. A., Millan, J. M., & Lewin, G. R. (2021). USH2A is a Meissner's corpuscle protein necessary for normal vibration sensing in mice and humans. *Nature Neuroscience*, *24*(1), 74–81. <https://doi.org/10.1038/s41593-020-00751-y>
- Seidahmed, M. Z., Maddirevula, S., Miqdad, A. M., Faifi, A. A., Samadi, A. A., & Alkuraya, F. S. (2020). Confirming the involvement of PIEZO2 in the etiology of Marden–Walker syndrome. *Am J Med Genet A*, *4*. <https://doi.org/10.1002/ajmg.a.62052>
- Servin-Vences, M. R., Moroni, M., Lewin, G. R., & Poole, K. (2017). Direct measurement of TRPV4 and PIEZO1 activity reveals multiple mechanotransduction pathways in chondrocytes. *ELife*, *6*, 1–24. <https://doi.org/10.7554/eLife.21074>
- Sun, W., Chi, S., Li, Y., Ling, S., Tan, Y., Xu, Y., Jiang, F., Li, J., Liu, C., Zhong, G., Cao, D., Jin, X., Zhao, D., Gao, X., Liu, Z., Xiao, B., & Li, Y. (2019). The mechanosensitive Piezo1 channel is required for bone formation. *ELife*, *8*, 1–25. <https://doi.org/10.7554/eLife.47454>
- Syeda, R., Xu, J., Dubin, A. E., Coste, B., Mathur, J., Huynh, T., Matzen, J., Lao, J., Tully, D. C., Engels, I. H., Petrassi, H. M., Schumacher, A. M., Montal, M., Bandell, M., & Patapoutian, A. (2015). Chemical activation of the mechanotransduction channel Piezo1. *ELife*, 1–11. <https://doi.org/10.7554/eLife.07369>
- Szczot, M., Liljencrantz, J., Ghitani, N., Barik, A., Lam, R., Thompson, J. H., Bharucha-Goebel, D., Saade, D., Necaie, A., Donkervoort, S., Foley, A. R., Gordon, T., Case, L., Bushnell, M. C., Bönnemann, C. G., & Chesler, A. T. (2018). PIEZO2 mediates injury-induced tactile pain in mice and humans. *Science Translational Medicine*, *10*(462), 1–10. <https://doi.org/10.1126/scitranslmed.aat9892>
- Taberner, F. J., Prato, V., Schaefer, I., Schrenk-Siemens, K., Heppenstall, P. A., & Lechner, S. G. (2019). Structure-guided examination of the mechanogating mechanism of PIEZO2. *Proceedings of the National Academy of Sciences of the United States of America*, *116*(28), 14260–14269. <https://doi.org/10.1073/pnas.1905985116>
- Tohyama, S., Hattori, F., Sano, M., Hishiki, T., Nagahata, Y., Matsuura, T., Hashimoto, H., Suzuki, T., Yamashita, H., Satoh, Y., Egashira, T., Seki, T., Muraoka, N., Yamakawa, H., Ohgino, Y., Tanaka, T., Yoichi, M., Yuasa, S., Murata, M., ... Fukuda, K. (2013). Distinct metabolic flow enables large-scale purification of mouse and human pluripotent stem cell-derived cardiomyocytes. *Cell Stem Cell*, *12*(1), 127–137. <https://doi.org/10.1016/j.stem.2012.09.013>
- Usoskin, D., Furlan, A., Islam, S., Abdo, H., Lönnerberg, P., Lou, D., Hjerling-leffler, J., Haeggström, J., Kharchenko, O., Kharchenko, P. V., Linnarsson, S., & Ernfors, P. (2014).

- Unbiased classification of sensory neuron types by large-scale single-cell RNA sequencing. *Nature Publishing Group*, 18(1), 145–153. <https://doi.org/10.1038/nn.3881>
- Wang, F., Knutson, K., Alcaïno, C., Linden, D. R., Gibbons, S. J., Kashyap, P., Grover, M., Oeckler, R., Gottlieb, P. A., Li, H. J., Leiter, A. B., Farrugia, G., & Beyder, A. (2017). Mechanosensitive ion channel Piezo2 is important for enterochromaffin cell response to mechanical forces. *Journal of Physiology*, 595(1), 79–91. <https://doi.org/10.1113/JP272718>
- Wang, L., Zhou, H., Zhang, M., Liu, W., Deng, T., Zhao, Q., Li, Y., Lei, J., Li, X., & Xiao, B. (2019). Structure and mechanogating of the mammalian tactile channel PIEZO2. *Nature*, 573(7773), 225–229. <https://doi.org/10.1038/s41586-019-1505-8>
- Wetzelsch, C., Hu, J., Riethmacher, D., Benckendorff, A., Harder, L., Eilers, A., Moshourab, R., Kozlenkov, A., Labuz, D., Caspani, O., Erdmann, B., Machelka, H., Heppenstall, P. A., & Lewin, G. R. (2007). A stomatin-domain protein essential for touch sensation in the mouse. *Nature*, 445(January), 206–209. <https://doi.org/10.1038/nature05394>
- Wetzelsch, C., Pifferi, S., Picci, C., Gök, C., Hoffmann, D., Bali, K. K., Lampe, A., Lapatsina, L., Fleischer, R., Smith, E. S. J., Bégay, V., Moroni, M., Estebanez, L., Kühnemund, J., Walcher, J., Specker, E., Neuenschwander, M., Von Kries, J. P., Haucke, V., ... Lewin, G. R. (2017). Small-molecule inhibition of STOML3 oligomerization reverses pathological mechanical hypersensitivity. *Nature Neuroscience*, 20(2), 209–218. <https://doi.org/10.1038/nn.4454>
- Witschi, R., Morscher, G., Scheurer, L., Deschamps, J., & Zeilhofer, H. U. (2010). Hoxb8-Cre Mice: A Tool for Brain-Sparing Conditional Gene Deletion. *Genesis*, 602(July), 596–602. <https://doi.org/10.1002/dvg.20656>
- Wong, T.-Y., Juang, W.-C., Tsai, C.-T., Tseng, C.-J., Lee, W.-H., Chang, S.-N., & Cheng, P.-W. (2018). Mechanical Stretching Simulates Cardiac Physiology and Pathology through Mechanosensor Piezo1. *Journal of Clinical Medicine*, 7(11), 410. <https://doi.org/10.3390/jcm7110410>
- Woo, S., Lumpkin, E. A., & Patapoutian, A. (2014). Merkel cells and neurons keep in touch. *Trends in Cell Biology*, 25(2), 74–81. <https://doi.org/10.1016/j.tcb.2014.10.003>
- Woo, S., Ranade, S., Weyer, A. D., Dubin, A. E., Baba, Y., Qiu, Z., Petrus, M., Miyamoto, T., Reddy, K., Lumpkin, E. A., Stucky, C. L., & Patapoutian, A. (2014). Piezo2 is required for Merkel-cell mechanotransduction. *Nature*, 509(7502), 622–626. <https://doi.org/10.1038/nature13251>
- Woo, S.-H., Lukacs, V., Nooij, J. C. De, Zaytseva, D., Criddle, C. R., Francisco, A., Jessell, T. M., Wilkinson, K. A., & Patapoutian, A. (2015). Piezo2 is the principal mechanotransduction channel for proprioception. *Nature Neuroscience*, 18(12), 1756–1763. <https://doi.org/10.1038/nn.4162>
- Wu, J., Lewis, A. H., & Grandl, J. (2016). Touch, Tension, and Transduction – The Function and Regulation of Piezo Ion Channels. *Trends in Biochemical Sciences*, xx, 1–15. <https://doi.org/10.1016/j.tibs.2016.09.004>
- Wu, J., Young, M., Lewis, A. H., Martfeld, A. N., Kalmeta, B., & Grandl, J. (2017). Inactivation of Mechanically Activated Piezo1 Ion Channels Is Determined by the C-Terminal Extracellular Domain and the Inner Pore Helix. *Cell Reports*, 21(9), 2357–2366. <https://doi.org/10.1016/j.celrep.2017.10.120>
- Yamaguchi, T., Takano, K., Inaba, Y., Morikawa, M., Motobayashi, M., Kawamura, R., Wakui, K., Nishi, E., Hirabayashi, S. ichi, Fukushima, Y., Kato, H., Takahashi, J., & Kosho, T.

- (2019). PIEZO2 deficiency is a recognizable arthrogryposis syndrome: A new case and literature review. *American Journal of Medical Genetics, Part A*, 179(6), 948–957. <https://doi.org/10.1002/ajmg.a.61142>
- Zapata-Aldana, E., Al-Mobarak, S. B., Karp, N., & Campbell, C. (2019). Distal arthrogryposis type 5 and PIEZO2 novel variant in a Canadian family. *American Journal of Medical Genetics, Part A*, 179(6), 1034–1041. <https://doi.org/10.1002/ajmg.a.61143>
- Zarychanski, R., Schulz, V. P., Houston, B. L., Maksimova, Y., Houston, D. S., Smith, B., Rinehart, J., & Gallagher, P. G. (2012). Mutations in the mechanotransduction protein PIEZO1 are associated with hereditary xerocytosis. *Blood*, 120(9), 1908–1916. <https://doi.org/10.1182/blood-2012-04-422253>.The
- Zeng, W. Z., Marshall, K. L., Min, S., Daou, I., Chapleau, M. W., Abboud, F. M., Liberles, S. D., & Patapoutian, A. (2018). PIEZO2 mediates neuronal sensing of blood pressure and the baroreceptor reflex. *Science*, 362(6413), 464–467. <https://doi.org/10.1126/science.aau6324>
- Zhao, Q., Wu, K., Geng, J., Chi, S., Wang, Y., Zhi, P., Zhang, M., & Xiao, B. (2016). Ion Permeation and Mechanotransduction Mechanisms of Mechanosensitive Piezo Channels. *Neuron*, 89(6), 1248–1263. <https://doi.org/10.1016/j.neuron.2016.01.046>
- Zhao, Q., Zhou, H., Chi, S., Wang, Y., Wang, J., Geng, J., Wu, K., Liu, W., Zhang, T., Dong, M. Q., Wang, J., Li, X., & Xiao, B. (2018). Structure and mechanogating mechanism of the Piezo1 channel. *Nature*, 554(7693), 487–492. <https://doi.org/10.1038/nature25743>
- Zheng, W., Gracheva, E. O., & Bagriantsev, S. N. (2019). A hydrophobic gate in the inner pore helix is the major determinant of inactivation in mechanosensitive Piezo channels. *ELife*, 8, 1–18. <https://doi.org/10.7554/eLife.44003>
- Zheng, W., Nikolaev, Y. A., Gracheva, E. O., & Bagriantsev, S. N. (2019). Piezo2 integrates mechanical and thermal cues in vertebrate mechanoreceptors. *Proceedings of the National Academy of Sciences of the United States of America*, 116(35), 17547–17555. <https://doi.org/10.1073/pnas.1910213116>
- Zhou, T., Gao, B., Fan, Y., Liu, Y., Feng, S., Cong, Q., Zhang, X., Zhou, Y., Yadav, P. S., Lin, J., Wu, N., Zhao, L., Huang, D., Zhou, S., Su, P., & Yang, Y. (2020). Piezo1/2 mediate mechanotransduction essential for bone formation through concerted activation of NFAT-YAP1-β-catenin. *ELife*, 9, 1–38. <https://doi.org/10.7554/eLife.52779>

10. Acknowledgments

First of all, I would like to thank my supervisor Prof. Dr. Gary Lewin. He gave me the opportunity to work in a superb scientific environment and continuously supported me by giving me suggestions, comments and ideas that were crucial for the development of this thesis and very important for my training as a scientist.

Likewise, I would like to thank Mirko Moroni and Rocío Servin Vences who helped me experimentally and taught me the fundamental techniques to carry out this research. Thank you for your constructive scientific aid, but also for all the funny moments we shared.

Furthermore, I would like to thank Prof. Dr. Oliver Daumke for accepting to be my supervisor. Additionally, I want to thank Prof. Dr. James Poulet and Dr. Niccolo Zampieri for taking part of my committee meetings; thank you for your expertise, advice and constructive suggestions and comments.

I am also very grateful for the help of Fred Schwaller and Carina Fürst. Thanks for your helpful comments regarding this thesis. Additionally, I want to thank you for making the office environment a very cozy place. I am also very fond of our scientific discussions and all the good moments we shared.

I want to thank as well all the people in the lab who made this work possible. Especially to Karola Bach, Franziska Bartelt and Maria Braunschweig who helped me out in keeping the mice lines healthy and performing the genotyping; Valérie for taking care of the generation of the transgenic mice, as well as for her patience regarding animal reports.

In terms of funding, I would like to express my gratitude to the SFB 958 RTG for granting me a fellowship during the first year of my PhD. This includes also Simone Schlender for coordinating workshops and retreats that were very helpful for my scientific education.

I would like to thank my husband Pascal for all his support, love, patience and strength. Thanks for always being there for me.

That goes also to my family, without them this would not have been possible. My father Juan, mother Sandra, sister Ady and brother Chini, muchas gracias por tanto amor y apoyo.

Among my friends I would like to thank Chochis, Mayra, Eddie, Alexis, Pau, Wis, Pamela. Even though some of you were physically distant, I always felt your close support. That goes also to Elías, Wladi, Max, Kitty, Felix, Karlien, JY, Jan and Alice. Thanks for making my time as a PhD student a joyful experience.